ELSEVIER

Nuclear Physics A 695 (2001) 3–50

NUCLEAR PHYSICS A

www.elsevier.com/locate/npe

General properties of the $\pi h_{9/2}[541]1/2^-$ configuration and level scheme of ^{165}Tm

H.J. Jensen [a,1], R.A. Bark [a,b], P.O. Tjøm [c], G.B. Hagemann [a,*], I.G. Bearden [a], H. Carlsson [d], S. Leoni [e], T. Lönnroth [f], W. Reviol [g,2], L.L. Riedinger [g], H. Schnack-Petersen [a], T. Shizuma [a,3], X.Z. Wang [g], J. Wrzesinski [h]

[a] *Niels Bohr Institute, University of Copenhagen, Blegdamsvej 17, 2100 Copenhagen, Denmark*
[b] *Department of Nuclear Physics, Australian National University, Canberra, ACT 0200, Australia*
[c] *Department of Physics, University of Oslo, Oslo, Norway*
[d] *Department of Physics, University of Lund, Sweden*
[e] *Dipartemento di Fisica, Università di Milano, Via Celoria 16, 20133 Milano, Italy*
[f] *Department of Physics, Åbo akademi, Porthansgatan 3, 20500 Turku, Finland*
[g] *Department of Physics and Astronomy, University of Tennessee, Knoxville, TN 37996, USA*
[h] *Niewodniczański Institute of Nuclear Physics, PL-31-342 Cracow, Poland*

Received 16 January 2001; revised 5 April 2001; accepted 14 May 2001

Abstract

^{165}Tm has been studied through the reactions ^{150}Nd(^{19}F, 4n), $E_{\text{beam}} = 85$ MeV and ^{154}Sm (^{15}N, 4n), $E_{\text{beam}} = 70$ MeV. The level scheme has been extended to spin $71/2^- \hbar$, and four new bands have been added. Two are assigned to the $K = 17/2$, three-quasiparticle configurations, $\pi[523]7/2^- \otimes \nu[642]5/2^+ \otimes \nu[523]5/2^-$ and $\pi[404]7/2^+ \otimes \nu[642]5/2^+ \otimes \nu[523]5/2^-$, and the remaining two are assigned to γ-vibrations coupled to an $h_{9/2}$ proton. Lifetimes of high-spin states in the $[541]1/2^-$ and $[411]1/2^+$ bands have been measured using DSAM techniques, allowing transition quadrupole moments to be deduced. Furthermore, crossings between the $[541]1/2^-$ and $[523]7/2^-$ bands and between the $[411]1/2^+$ and $[404]7/2^+$ bands are analysed with a band-mixing calculation to obtain the quadrupole moments of the $[523]7/2^-$ and $[404]7/2^+$ bands. While the $[523]7/2^-$, $[411]1/2^+$ and $[404]7/2^+$ bands all have similar deformations, the $[541]1/2^-$ band has a quadrupole moment approximately 15% larger. The relative deformations are in good agreement with diabatic potential energy surface calculations performed using the code “Ultimate Cranker”. The experimental crossing frequency, due to the alignment of $i_{13/2}$ neutrons, is found to be delayed in the $[541]1/2^-$ band compared to the other bands. This is a universal feature in the rare-earth

* Corresponding author.
E-mail address: hagemann@alf.nbi.dk (G.B. Hagemann).

[1] Present address: Cyclotron and PET unit, Copenhagen University Hospital, Copenhagen, Denmark.
[2] Present address: Washington University, Chemistry Department, St. Louis, MO 63130, USA.
[3] Present address: Japan Atomic Energy Institute, Ibaraki 319-1195, Japan.

PII: S0375-9474(01)01111-3

region, and extensive systematic Cranked Shell Model calculations have been performed to predict deformations and crossing frequencies for nuclei in the region. The model is unable to reproduce the full delay in crossing frequency, confirming that deformation alone is not responsible for the shift.

PACS: 21.10.-k; 23.20.Ck; 23.20.Lv; 25.70.-z; 27.70.+q
Keywords: NUCLEAR REACTIONS ^{150}Nd(^{19}F, 4n), $E_{\text{beam}} = 85$ MeV; ^{154}Sm(^{15}N, 4n), $E_{\text{beam}} = 70$ MeV; Measured E_γ, I_γ; $\gamma\gamma$ coincidence, DSA; ^{165}Tm deduced levels; J, π rotational band structure; E2/M1 mixing ratios, transition quadrupole moments, configurations, alignments, $B(\text{M1})/B(\text{E2})$ and $B(\text{E1})/B(\text{E2})$ ratios; PES surface calculations, calculations of crossing frequency and aligned angular momenta

1. Introduction

The phenomenon of delayed alignment of $i_{13/2}$ neutrons in the $h_{9/2}$ bands of odd-proton nuclei in the rare-earth region is now well established. Shifts in crossing frequencies of up to 75 keV, when compared with even–even nuclei, have been reported [1–4]. It has been expected for some time that deformation changes would cause a shift in crossing frequency [5], but when deformations predicted from potential energy surface (PES) calculations are used to predict the shift using the Cranked Shell Model (CSM) [6], an underestimate is obtained [3,7,8]. Recent evidence suggests that proton–neutron interactions play an important role in contributing to the shift in crossing frequency [7,9]. However, a possibility is that the deformations are underestimated in the PESs, and therefore, it is important to have experimental measurements of the deformation associated with the $h_{9/2}$ bands. Until now, relatively few measurements of deformation for the $h_{9/2}$ bands in the rare-earth region have been made [10–13]. This work presents new results on the nucleus ^{165}Tm. High-spin states have been observed in order to determine the crossing frequency and gain in aligned angular momentum in the $h_{9/2}$ band, and quadrupole moments have been obtained using the DSAM technique. The results are compared with new, diabatic PES calculations, which are then applied in an extensive investigation of shapes and crossing frequencies in the rare-earth region. Partial results of these calculations have been presented in earlier reports [1,14].

2. Experimental details and data analysis

2.1. Experimental method

The two heaviest stable beams that can be used to produce ^{165}Tm in a heavy-ion, xn reaction, ^{19}F and ^{15}N, were used to study excited states in ^{165}Tm in two experiments, using the accelerator facility of the Tandem Accelerator Laboratory at the Niels Bohr Institute together with the Nordball spectrometer [15,16].

2.1.1. The first experiment

In the first experiment, ^{165}Tm was populated in the ^{150}Nd(^{19}F, 4n) reaction at a beam energy of 85 MeV. Two target combinations were used: (i) two thin stacked 0.73 mg/cm^2

^{150}Nd metallic foils and (ii) 1.35 mg/cm^2 ^{150}Nd evaporated onto a backing of 8.3 mg/cm^2 ^{197}Au. The target material was enriched to 97.84%. The Nordball detector system equipped with 20 Compton suppressed HPGe spectrometers and the full 60-element BaF^2 crystal inner ball was used to detect the emitted γ-radiation in the thin target experiment. More than 1.4×10^9 double- and higher-fold events in prompt coincidence with at least one γ ray detected in the inner ball were recorded. With the backed target, a total of 0.8×10^9 double- and higher-fold events in prompt coincidence with at least three γ rays detected in the inner ball were recorded. In the latter case, two of the HPGe detectors were replaced by planar Low-Energy Photon (LEP) Ge detectors. The high sensitivity for low-energy transitions of the LEP Ge detectors was important for the study of the neighbouring odd–odd nucleus ^{164}Tm, which was populated by the dominant 5n reaction channel. The results from the analysis for ^{164}Tm are published by Reviol et al. [17] in a separate article.

2.1.2. The second experiment

In the second experiment ^{165}Tm was populated in the ^{154}Sm(^{15}N, 4n) reaction at a beam energy of 70 MeV. Three target combinations were used: (i) two thin stacked 0.65 mg/cm^2 and 0.78 mg/cm^2 ^{154}Sm metallic foils, (ii) 1.0 mg/cm^2 ^{154}Sm with a 5.3 mg/cm^2 gold backing and (iii) 1.0 mg/cm^2 ^{154}Sm with a 5.0 mg/cm^2 lead backing. The target material was enriched to 98.69%. More than 0.5, 0.3 and 0.9×10^9 double- and higher-fold events, in prompt coincidence with two or more γ rays detected in the inner ball, were recorded in the three measurements, respectively.

In the first and the second experiment, ^{165}Tm was populated with approximately 20% and 80% of the total fusion cross section, respectively. The angular momentum input was slightly lower (by 4–6 $\hbar$) in the second experiment. The level scheme for ^{165}Tm was consequently built entirely on the basis of data from the second experiment, except for the high-spin part of the scheme, for which a better population was obtained in the first experiment.

2.2. Analysis methods

Energy and efficiency calibrations of the detectors were made with a mixed radioactive source (^{133}Ba, ^{134}Cs, ^{152}Eu) for both experiments. The relative γ-ray intensities for the sources were taken from Ref. [18]. Offline, the calibrated and checked events were written to new magnetic tapes in a compact event format by means of the sorting code *Juggler* by J. Wrzesinski [19].

2.2.1. Building the level scheme

Thin- and backed-target data from both experiments were sorted into symmetric two-dimensional E_γ–E_γ matrices for coincidences between any two Ge detectors and into one three-dimensional E_γ–E_γ–E_γ cube with an energy range of 60–1230 keV. Prompt coincidences between any of the Ge detectors were defined by a narrow energy dependent time gate, which excluded events caused by neutrons and ensured no degrading of the efficiency for the low-energy gamma rays, which were delayed due to their slower charge collection times. Additional software gates on both BaF_2 sum energy and fold were used to enhance the 4n channel. A nonlinear gain [20] was used for the sorting of the cube in order to save disk-space. Matrices and cubes were corrected for background, using a prescription similar to the one given by Palameta et al. [21].

Information from the E_γ–E_γ matrices was used to built the main part of the level scheme and to extract gamma-ray energies and relative intensities. The analysis of triple coincidences, accounting for approximately 10% of the total events, was important to establish complicated parts of the level scheme. For the construction of the level scheme, the analysis programs GF2, ESCL8R and LEVIT8R by D.C. Radford [20] were used.

2.2.2. *Analysis of DCO data*

A technique used frequently to determine multipolarities and multipole mixing ratios, δ, of transitions depopulating nuclear levels, using multidetector arrays, is to use Directional Correlations of γ rays deexciting oriented states (DCO) [22–24]. The 20 Nordball Ge detectors are grouped into four rings, at polar angles $\theta = 37.4°$, 79.2°, and the equivalent angles of 100.8° and 142.6° relative to the beam axis, with 5 detectors equidistantly placed in each. Information about multipolarities and mixing ratios were extracted from the DCO-ratio

$$R_{\mathrm{DCO}} = \frac{W(\text{“}37 \times 79\text{”})}{W(\text{“}79 \times 37\text{”})} \tag{1}$$

and information about the dealignment parameter, σ/I, was obtained from the ratio

$$\frac{W(\text{“}37 \times 37\text{”})}{W(\text{“}79 \times 79\text{”})}. \tag{2}$$

Three different DCO matrices were constructed: two symmetric matrices (“37 × 37”) and (“79 × 79”) for determining the dealignment parameter and one asymmetric matrix (“37 × 79”) for determining multipolarities and mixing ratios.

Examples of calculated ratios between the correlation function for the two symmetric matrices, $W(\text{“}37 \times 37\text{”})/W(\text{“}79 \times 79\text{”})$, are presented in Fig. 1(a) as a function of σ/I for selective stretched quadrupole–quadrupole cascades $I \to I-2 \to I-4$. An average value of 0.26 ± 0.04, with a negligible dependence on the initial spin I, was measured for the dealignment parameter for transitions from states with $I \leqslant 49/2$.

The DCO ratio (1) for a stretched quadrupole–quadrupole cascade has a value of 1.0, whereas the ratio for a quadrupole–dipole cascade, has a strong dependence on the E2/M1 mixing ratio, δ, and a somewhat weaker dependence on σ/I. Examples of calculated DCO ratios (1) for the geometry of Nordball, are presented in Fig. 1(b) as a function of arctan(δ) for appropriate values of σ/I. The ratio for a pure stretched quadrupole–dipole cascade, when gating on the stretched quadrupole, is, for the geometry of Nordball, expected to be $R_{\mathrm{DCO}} = 0.60 \pm 0.03$ for $\sigma/I = 0.26 \pm 0.04$.

DCO ratios were measured for most of the transitions in the established level scheme for ^{165}Tm, and were used to distinguish between quadrupole and dipole transitions. As gating transitions, lines known to be of stretched quadrupole type were chosen consistently. The

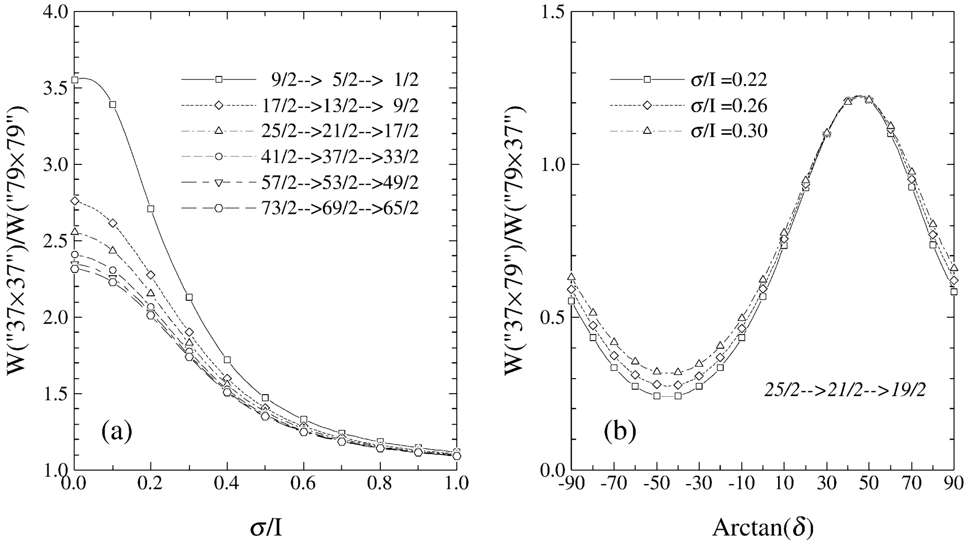

Fig. 1. (a) Calculated ratios, $W(\text{“}37\times 37\text{”})/W(\text{“}79\times 79\text{”})$, as a function of the dealignment parameter, σ/I, for selective examples of stretched quadrupole–quadrupole cascades $I \to I-2 \to I-4$, and (b) calculated DCO ratios, $R_{\mathrm{DCO}} = W(\text{“}37\times 79\text{”})/W(\text{“}79\times 37\text{”})$, as a function of arctan(δ) for representative values of σ/I. Gating is done at the stretched quadrupole transition.

DCO ratios were also used to determine mixing ratios for bands known to have mixing ratios significantly different from zero (i.e., the [541]1/2$^-$ and [404]7/2$^+$ bands), and for the transitions depopulating the newly observed γ-vibrational bands.

3. Experimental results

3.1. The level scheme

Prior to the present work the nucleus ^{165}Tm had been studied by in-beam γ-spectroscopy experiments using the reactions ^{165}Ho(α, 4nγ)^{165}Tm and ^{158}Gd(^{11}B, 4n)^{165}Tm [25–27]. Seven rotational band structures with intraband transitions and the assignments — $\pi h_{11/2}$[523]7/2$^-$ ($\alpha = \pm 1/2$), $\pi h_{9/2}$[541]1/2$^-$ ($\alpha = +1/2$), $\pi d_{3/2}$[411]1/2$^+$ ($\alpha = \pm 1/2$) and $\pi g_{7/2}$[404]7/2$^+$ ($\alpha = \pm 1/2$) — were established to maximum spins of 27/2–37/2 $\hbar$. Candidates for the lowest levels of the $\pi d_{5/2}$[402]5/2$^+$, $\pi d_{5/2}$[411]3/2$^+$ and $\pi h_{11/2}$[514]9/2$^-$ configurations, and the 3/2$^-\hbar$ band head of the $\pi h_{9/2}$[541]1/2$^-$ ($\alpha = -1/2$) band were established too [25–27].

The full level scheme of ^{165}Tm obtained in the present work, is presented in Fig. 2. The previously known bands are labeled according to the Nilsson orbital occupied by the odd-proton, whereas new bands are labeled numerically. A partial level scheme for ^{165}Tm showing details of the [541]1/2$^-$, [411]1/2$^+$ and [404]7/2$^+$ bands and the new bands 3 and 4, is shown in Fig. 3. Level and transition energies are listed in Table 1, together

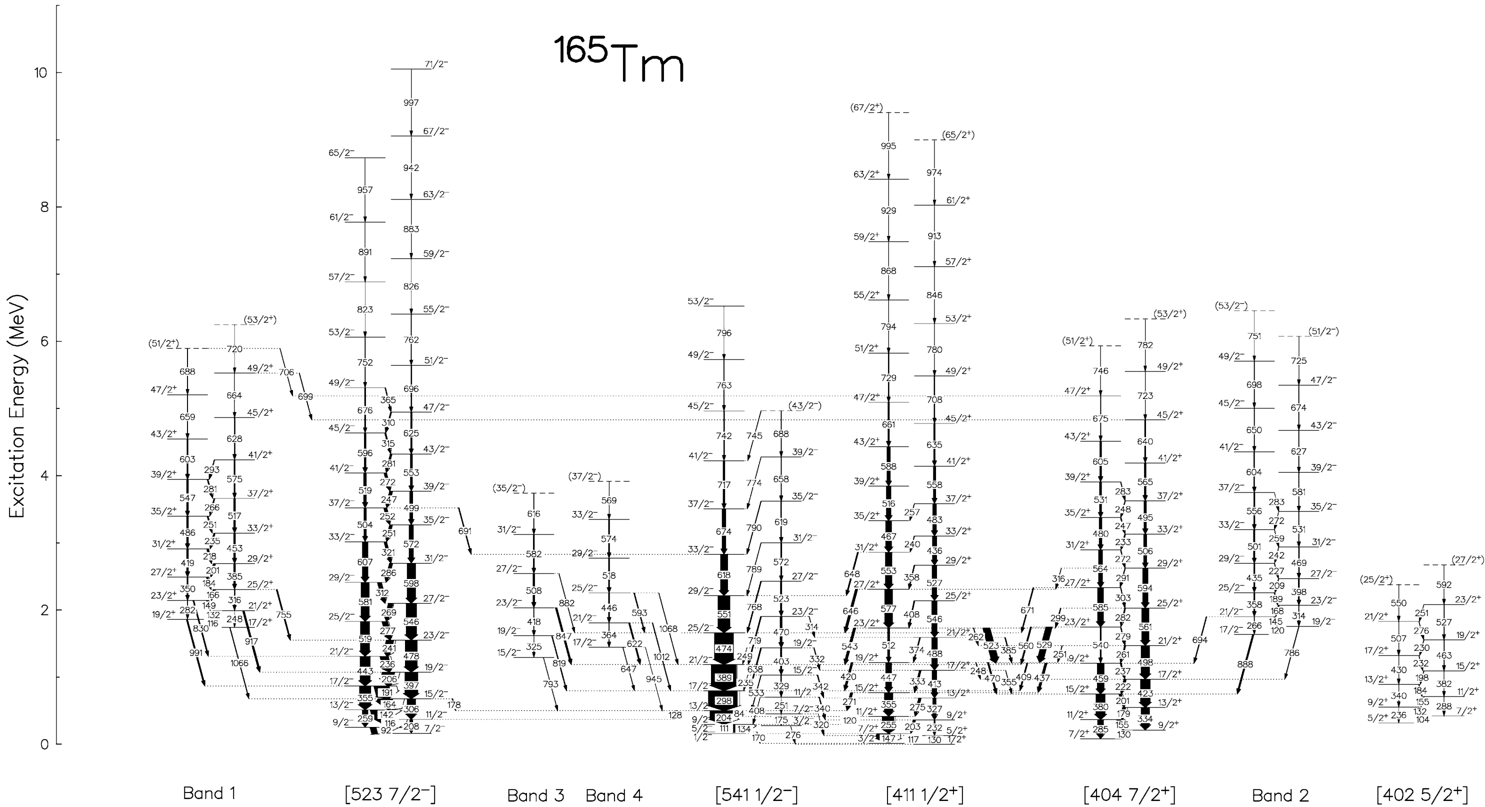

Fig. 2. The level scheme of ^{165}Tm, established in the present work. The thickness of the black part of the arrows represents measured relative γ-ray intensities and the white part represents the expected intensity due to internal conversion.

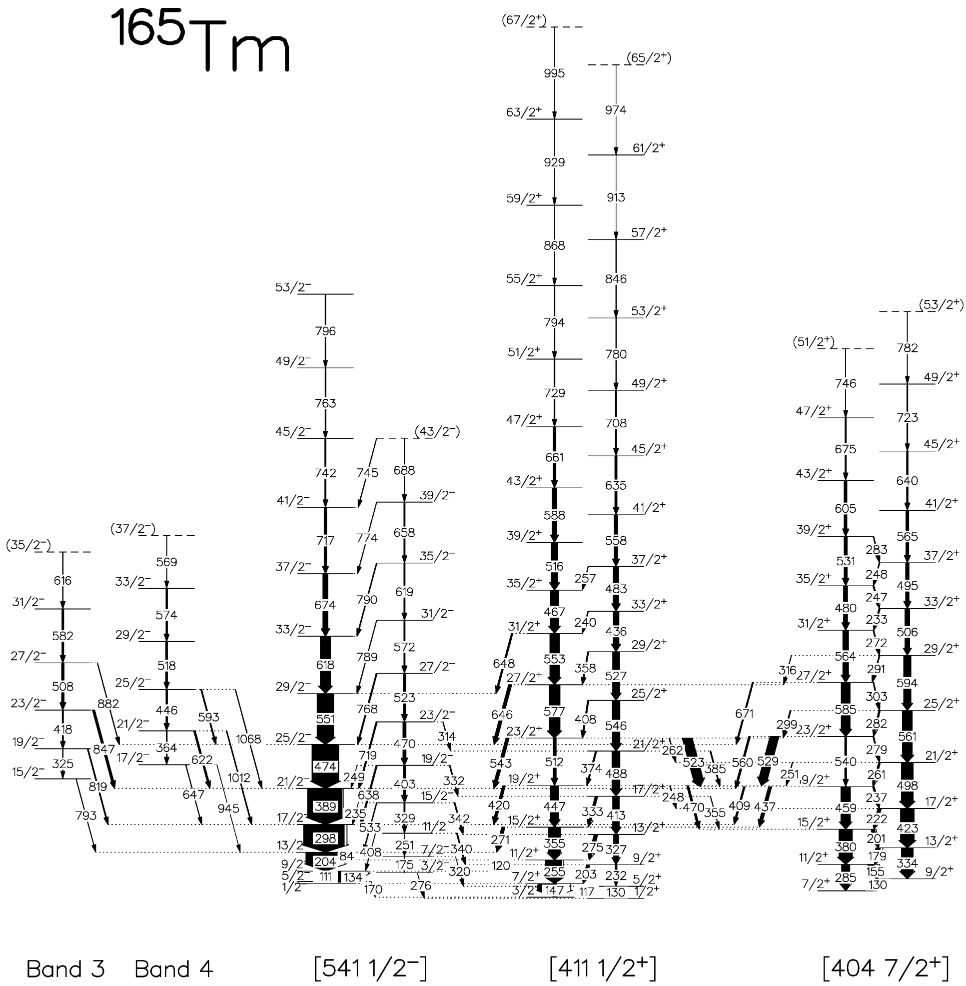

Fig. 3. Partial level scheme of ^{165}Tm showing details of transitions connecting the bands [541]1/2^{-}, [411]1/2^{+}, [404]7/2^{+} and the new bands 3 and 4.

with relative intensities, spin and configuration assignments, and in some cases DCO and E2/M1 mixing ratios.

3.1.1. [523]7/2^{-} band

The band built on the [523]7/2^{-} configuration, previously known to maximum spin 35/2$^{-}\hbar$, was fully confirmed in the present work. New transitions assigned to the [523]7/2^{-} band can be seen in Fig. 4, (a) and (b). The high-spin part of the level scheme is seen up to the maximum established spins of 65/2$^{-}\hbar$ and 71/2$^{-}\hbar$ for the positive and negative signature, respectively. Some contaminant lines due, for example, to the 882.0 keV transition depopulating band 3, are seen too.

Table 1
Configuration assignments, level energies, E_i, γ-ray energies, E_γ, relative intensities, $\mathcal{I}_\gamma^{rel}$, DCO-ratios, R_{DCO}, E2/M1 mixing ratios, δ, γ-branching ratios, λ, and electromagnetic branching ratios $B(M1)/B(E2)$, $B(E1)/B(E2)$ and $B(E2)/B(E2)$ for ^{165}Tm

$[Nn_3\Lambda]\Omega^\pi I_i^\pi \rightarrow [Nn_3\Lambda]\Omega^\pi I_f^\pi$	E_i [keV]	E_γ [keV]	$\mathcal{I}_\gamma^{rel}$	R_{DCO}	δ
[523]7/2⁻ 9/2⁻ → [523]7/2⁻ 7/2⁻	252.2(3)	91.7(2)	21.68(108)	0.90(4)	
[523]7/2⁻ 13/2⁻ → [523]7/2⁻ 11/2⁻	510.8(3)	142.2(2)	25.64(107)	0.87(6)	
→ [523]7/2⁻ 9/2⁻		258.7(2)	8.26(48)	1.05(15)	
λ(258.7, 142.2) = 0.32(2)		B(M1)/B(E2) = 0.867(62)			
[523]7/2⁻ 17/2⁻ → [523]7/2⁻ 15/2⁻	865.7(3)	190.8(2)	43.34(175)	0.83(3)	
→ [523]7/2⁻ 13/2⁻		355.0(2)	30.53(124)	0.97(5)	
λ(355.0, 190.8) = 0.70(4)		B(M1)/B(E2) = 0.798(46)			
[523]7/2⁻ 21/2⁻ → [523]7/2⁻ 19/2⁻	1308.3(3)	236.2(2)	30.41(123)	0.80(3)	
→ [523]7/2⁻ 17/2⁻		442.5(2)	37.05(150)	1.02(6)	
λ(442.5, 236.2) = 1.22(7)		B(M1)/B(E2) = 0.733(42)			
[523]7/2⁻ 25/2⁻ → [523]7/2⁻ 23/2⁻	1827.1(4)	277.3(2)	20.45(83)	0.78(3)	
→ [523]7/2⁻ 21/2⁻		518.8(2)	33.23(135)	0.98(4)	
λ(518.8, 277.3) = 1.62(9)		B(M1)/B(E2) = 0.752(43)			
[523]7/2⁻ 29/2⁻ → [523]7/2⁻ 27/2⁻	2408.3(4)	312.1(2)	13.17(54)	0.79(10)	
→ [523]7/2⁻ 25/2⁻		581.2(2)	30.30(123)	1.01(6)	
λ(581.2, 312.1) = 2.30(13)		B(M1)/B(E2) = 0.657(38)			
[523]7/2⁻ 33/2⁻ → [523]7/2⁻ 31/2⁻	3015.3(4)	320.8(2)	8.78(36)	0.70(3)	
→ [523]7/2⁻ 29/2⁻		607.0(2)	20.91(85)	0.99(10)	
λ(607.0, 320.8) = 2.38(14)		B(M1)/B(E2) = 0.726(42)			
[523]7/2⁻ 37/2⁻ → [523]7/2⁻ 35/2⁻	3518.9(4)	252.1(2)	9.22(38)	0.69(4)	
→ [523]7/2⁻ 33/2⁻		503.7(2)	9.22(38)	0.96(6)	
→ [541]1/2⁻ 33/2⁻		690.8(2)	2.60(35)		
λ(503.7, 252.1) = 1.00(6)		B(M1)/B(E2) = 1.403(82)			
λ(690.8, 252.1) = 0.28(4)		B(M1)/B(E2) = 24.142(3399)			
λ(690.8, 503.7) = 0.28(4)		B(E2)/B(E2) = 0.058(8)			
[523]7/2⁻ 41/2⁻ → [523]7/2⁻ 39/2⁻	4037.9(5)	271.8(2)	8.08(33)	0.70(5)	
→ [523]7/2⁻ 37/2⁻		519.0(2)	9.93(44)	1.01(7)	
λ(519.0, 271.8) = 1.23(7)		B(M1)/B(E2) = 1.058(64)			
[523]7/2⁻ 45/2⁻ → [523]7/2⁻ 43/2⁻	4633.6(5)	314.9(2)	3.97(18)	0.70(23)	
→ [523]7/2⁻ 41/2⁻		595.6(2)	7.52(32)	1.02(23)	
λ(595.6, 314.9) = 1.89(12)		B(M1)/B(E2) = 0.878(55)			
[523]7/2⁻ 49/2⁻ → [523]7/2⁻ 47/2⁻	5308.8(5)	364.8(2)	2.07(31)		
→ [523]7/2⁻ 45/2⁻		675.5(2)	3.31(17)	0.94(13)	
λ(675.5, 364.8) = 1.60(25)		B(M1)/B(E2) = 1.256(199)			
[523]7/2⁻ 53/2⁻ → [523]7/2⁻ 49/2⁻	6060.4(6)	751.6(2)	1.70(10)		
[523]7/2⁻ 57/2⁻ → [523]7/2⁻ 53/2⁻	6883.3(7)	822.9(2)	0.72(7)		
[523]7/2⁻ 61/2⁻ → [523]7/2⁻ 57/2⁻	7774.1(8)	890.6(2)	0.44(6)		
[523]7/2⁻ 65/2⁻ → [523]7/2⁻ 61/2⁻	8730.9(15)	956.8(3)	0.20(10)		
[523]7/2⁻ 11/2⁻ → [523]7/2⁻ 9/2⁻	368.5(3)	116.1(2)	23.66(118)	0.88(4)	
→ [523]7/2⁻ 7/2⁻		208.0(2)	4.26(26)	1.00(5)	
λ(208.0, 116.1) = 0.18(1)		B(M1)/B(E2) = 0.958(76)			
[523]7/2⁻ 15/2⁻ → [523]7/2⁻ 13/2⁻	674.8(3)	163.9(2)	37.25(152)	0.85(3)	
→ [541]1/2⁻ 13/2⁻		177.5(2)	0.80(6)		
→ [523]7/2⁻ 11/2⁻		306.3(2)	22.13(92)	1.04(4)	
λ(306.3, 163.9) = 0.59(3)		B(M1)/B(E2) = 0.715(42)			
λ(306.3, 177.5) = 27.66(237)		B(M1)/B(E2) = 0.012(1)			
[523]7/2⁻ 19/2⁻ → [523]7/2⁻ 17/2⁻	1072.0(3)	206.0(2)	37.14(150)	0.80(3)	
→ [523]7/2⁻ 15/2⁻		397.1(2)	38.80(157)	1.00(4)	
λ(397.1, 206.0) = 1.04(6)		B(M1)/B(E2) = 0.750(43)			

Table 1 —continued

$[Nn_3\Lambda]\Omega^\pi\ I_i^\pi \rightarrow [Nn_3\Lambda]\Omega^\pi\ I_f^\pi$	E_i [keV]	E_γ [keV]	$\mathcal{I}_\gamma^{\mathrm{rel}}$	R_{DCO}	δ
$[523]7/2^-\ 23/2^- \rightarrow [523]7/2^-\ 21/2^-$	1549.7(4)	241.1(2)	27.29(110)	0.78(4)	
$\rightarrow [523]7/2^-\ 19/2^-$		477.6(2)	43.86(177)	0.97(5)	
$\lambda(477.6, 241.1) = 1.61(9)$		$B(\mathrm{M1})/B(\mathrm{E2}) = 0.765(44)$			
$[523]7/2^-\ 27/2^- \rightarrow [523]7/2^-\ 25/2^-$	2096.0(4)	268.8(2)	16.53(67)	0.75(3)	
$\rightarrow [523]7/2^-\ 23/2^-$		546.4(2)	38.29(155)	1.01(5)	
$\lambda(546.4, 268.8) = 2.32(13)$		$B(\mathrm{M1})/B(\mathrm{E2}) = 0.751(43)$			
$[523]7/2^-\ 31/2^- \rightarrow [523]7/2^-\ 29/2^-$	2694.3(4)	285.8(2)	10.04(41)	0.73(4)	
$\rightarrow [523]7/2^-\ 27/2^-$		598.3(2)	31.58(128)	0.98(5)	
$\lambda(598.3, 285.8) = 3.15(18)$		$B(\mathrm{M1})/B(\mathrm{E2}) = 0.723(42)$			
$[523]7/2^-\ 35/2^- \rightarrow [523]7/2^-\ 33/2^-$	3266.7(4)	251.2(2)	8.68(37)	0.71(3)	
$\rightarrow [523]7/2^-\ 31/2^-$		572.5(2)	16.50(67)	0.99(7)	
$\lambda(572.5, 251.2) = 1.90(11)$		$B(\mathrm{M1})/B(\mathrm{E2}) = 1.414(83)$			
$[523]7/2^-\ 39/2^- \rightarrow [523]7/2^-\ 37/2^-$	3766.0(4)	247.0(2)	9.04(37)	0.74(8)	
$\rightarrow [523]7/2^-\ 35/2^-$		499.4(2)	11.04(46)	0.99(6)	
$\lambda(499.4, 247.0) = 1.22(7)$		$B(\mathrm{M1})/B(\mathrm{E2}) = 1.170(68)$			
$[523]7/2^-\ 43/2^- \rightarrow [523]7/2^-\ 41/2^-$	4318.6(5)	280.7(2)	5.65(24)	0.70(11)	
$\rightarrow [523]7/2^-\ 39/2^-$		552.8(2)	7.73(33)	1.03(16)	
$\lambda(552.8, 280.7) = 1.37(8)$		$B(\mathrm{M1})/B(\mathrm{E2}) = 1.183(71)$			
$[523]7/2^-\ 47/2^- \rightarrow [523]7/2^-\ 45/2^-$	4943.8(5)	309.8(2)	3.41(15)	0.69(20)	
$\rightarrow [523]7/2^-\ 43/2^-$		625.3(2)	6.04(26)	0.95(15)	
$\lambda(625.3, 309.8) = 1.77(11)$		$B(\mathrm{M1})/B(\mathrm{E2}) = 1.258(77)$			
$[523]7/2^-\ 51/2^- \rightarrow [523]7/2^-\ 47/2^-$	5640.0(6)	696.2(2)	3.21(15)	0.82(16)	
$[523]7/2^-\ 55/2^- \rightarrow [523]7/2^-\ 51/2^-$	6402.3(7)	762.3(2)	1.67(9)		
$[523]7/2^-\ 59/2^- \rightarrow [523]7/2^-\ 55/2^-$	7228.6(8)	826.3(2)	0.58(6)		
$[523]7/2^-\ 63/2^- \rightarrow [523]7/2^-\ 59/2^-$	8111.8(9)	883.2(3)	0.29(4)		
$[523]7/2^-\ 67/2^- \rightarrow [523]7/2^-\ 63/2^-$	9053.3(11)	941.5(4)	0.10(4)		
$[523]7/2^-\ 71/2^- \rightarrow [523]7/2^-\ 67/2^-$	10050.8(19)	997.4(10)	0.05(4)		
$[404]7/2^+\ 9/2^+ \rightarrow [404]7/2^+\ 7/2^+$	210.4(3)	130.0(2)	8.34(191)	1.27(3)	$1.00^{+0.12}_{-0.12}$
$[404]7/2^+\ 13/2^+ \rightarrow [404]7/2^+\ 11/2^+$	544.7(3)	178.9(2)	11.86(50)	1.23(5)	$1.00^{+0.14}_{-0.14}$
$\rightarrow [404]7/2^+\ 9/2^+$		334.3(2)	29.76(125)	1.04(5)	
$\lambda(334.3, 178.9) = 2.51(15)$		$B(\mathrm{M1})/B(\mathrm{E2}) = 0.101(28)$			
$[404]7/2^+\ 17/2^+ \rightarrow [404]7/2^+\ 15/2^+$	967.3(3)	221.6(2)	6.74(28)	1.10(4)	$0.57^{+0.06}_{-0.06}$
$\rightarrow [404]7/2^+\ 13/2^+$		422.8(2)	35.29(144)	1.01(4)	
$\lambda(422.8, 221.6) = 5.24(30)$		$B(\mathrm{M1})/B(\mathrm{E2}) = 0.124(11)$			
$[404]7/2^+\ 21/2^+ \rightarrow [411]1/2^+\ 19/2^+$	1465.8(3)	250.6(10)	1.20(15)		
$\rightarrow [404]7/2^+\ 19/2^+$		260.9(2)	3.81(17)	1.02(12)	$0.46^{+0.19}_{-0.13}$
$\rightarrow [404]7/2^+\ 17/2^+$		498.5(2)	31.50(129)	1.01(3)	
$\lambda(498.5, 260.9) = 8.27(50)$		$B(\mathrm{M1})/B(\mathrm{E2}) = 0.120(19)$			
$\lambda(498.5, 250.6) = 26.25(345)$		$B(\mathrm{M1})/B(\mathrm{E2}) = 0.052(7)$			
$[404]7/2^+\ 25/2^+ \rightarrow [404]7/2^+\ 23/2^+$	2026.7(3)	281.9(2)	3.17(15)	0.85(7)	$0.27^{+0.08}_{-0.08}$
$\rightarrow [411]1/2^+\ 23/2^+$		298.7(2)	2.17(20)		
$\rightarrow [404]7/2^+\ 21/2^+$		560.8(2)	26.05(106)	0.98(5)	
$\lambda(560.8, 281.9) = 8.22(51)$		$B(\mathrm{M1})/B(\mathrm{E2}) = 0.195(15)$			
$\lambda(560.8, 298.7) = 12.00(121)$		$B(\mathrm{M1})/B(\mathrm{E2}) = 0.120(12)$			
$[404]7/2^+\ 29/2^+ \rightarrow [404]7/2^+\ 27/2^+$	2620.9(4)	291.1(2)	1.85(10)	0.85(30)	$0.27^{+0.37}_{-0.37}$
$\rightarrow [411]1/2^+\ 27/2^+$		315.8(2)	0.65(7)		
$\rightarrow [404]7/2^+\ 25/2^+$		594.3(2)	19.84(82)	0.99(4)	
$\lambda(594.3, 315.8) = 30.52(352)$		$B(\mathrm{M1})/B(\mathrm{E2}) = 0.053(6)$			
$\lambda(594.3, 291.1) = 10.72(73)$		$B(\mathrm{M1})/B(\mathrm{E2}) = 0.181(34)$			

Table 1 —continued

$[Nn_3\Lambda]\Omega^\pi I_i^\pi$	$\rightarrow [Nn_3\Lambda]\Omega^\pi I_f^\pi$	E_i [keV]	E_γ [keV]	$\mathcal{I}_\gamma^{\mathrm{rel}}$	R_{DCO}	δ
$[404]7/2^+$ $33/2^+$	$\rightarrow [404]7/2^+$ $31/2^+$	3126.6(4)	233.0(2)	2.59(12)	0.89(10)	$0.32^{+0.12}_{-0.12}$
	$\rightarrow [404]7/2^+$ $29/2^+$		505.9(2)	11.88(50)	0.99(4)	
	$\lambda(505.9, 233.0) = 4.59(29)$		$B(\mathrm{M1})/B(\mathrm{E2}) = 0.359(35)$			
$[404]7/2^+$ $37/2^+$	$\rightarrow [404]7/2^+$ $35/2^+$	3621.9(5)	248.4(2)	1.60(9)	0.82(8)	$0.25^{+0.10}_{-0.10}$
	$\rightarrow [404]7/2^+$ $33/2^+$		495.3(2)	9.70(41)	1.01(5)	
	$\lambda(495.3, 248.4) = 6.06(43)$		$B(\mathrm{M1})/B(\mathrm{E2}) = 0.209(18)$			
$[404]7/2^+$ $41/2^+$	$\rightarrow [404]7/2^+$ $37/2^+$	4187.3(6)	565.4(2)	6.94(30)	0.94(7)	
$[404]7/2^+$ $45/2^+$	$\rightarrow [404]7/2^+$ $41/2^+$	4827.1(6)	639.9(2)	4.20(19)	0.94(4)	
$[404]7/2^+$ $49/2^+$	$\rightarrow [404]7/2^+$ $45/2^+$	5550.6(7)	723.4(2)	1.19(8)		
$[404]7/2^+$ $(53/2^+)$	$\rightarrow [404]7/2^+$ $49/2^+$	6332.1(8)	781.5(2)	0.45(6)		
$[404]7/2^+$ $11/2^+$	$\rightarrow [404]7/2^+$ $9/2^+$	365.7(3)	155.2(2)	16.33(74)	1.24(6)	$1.00^{+0.16}_{-0.16}$
	$\rightarrow [404]7/2^+$ $7/2^+$		285.3(2)	20.79(96)	1.04(3)	
	$\lambda(285.3, 155.2) = 1.27(8)$		$B(\mathrm{M1})/B(\mathrm{E2}) = 0.138(44)$			
$[404]7/2^+$ $15/2^+$	$\rightarrow [404]7/2^+$ $13/2^+$	745.6(3)	200.8(2)	9.15(39)	1.15(6)	$0.67^{+0.17}_{-0.11}$
	$\rightarrow [404]7/2^+$ $11/2^+$		380.0(2)	34.04(140)	1.00(6)	
	$\lambda(380.0, 200.8) = 3.72(22)$		$B(\mathrm{M1})/B(\mathrm{E2}) = 0.126(24)$			
$[404]7/2^+$ $19/2^+$	$\rightarrow [404]7/2^+$ $17/2^+$	1204.8(3)	237.4(2)	3.45(16)	1.01(12)	$0.45^{+0.19}_{-0.14}$
	$\rightarrow [541]1/2^-$ $17/2^-$		409.4(2)	3.95(18)	0.56(4)	
	$\rightarrow [411]1/2^+$ $15/2^+$		436.9(2)	8.12(35)	0.98(6)	
	$\rightarrow [404]7/2^+$ $15/2^+$		459.4(2)	24.87(102)	1.00(3)	
	$\lambda(459.4, 237.4) = 7.21(45)$		$B(\mathrm{M1})/B(\mathrm{E2}) = 0.122(19)$			
	$\lambda(436.9, 237.4) = 2.35(15)$		$B(\mathrm{M1})/B(\mathrm{E2}) = 0.291(46)$			
	$\lambda(459.4, 436.9) = 3.06(18)$		$B(\mathrm{E2})/B(\mathrm{E2}) = 2.381(142)$			
	$\lambda(459.4, 409.4) = 6.296(386)$		$B(\mathrm{E1})/B(\mathrm{E2}) = 0.036(2)$			
	$\lambda(436.9, 409.4) = 2.056(129)$		$B(\mathrm{E1})/B(\mathrm{E2}) = 0.087(5)$			
$[404]7/2^+$ $23/2^+$	$\rightarrow [404]7/2^+$ $21/2^+$	1744.7(3)	278.7(2)	2.25(11)	0.83(11)	$0.26^{+0.12}_{-0.11}$
	$\rightarrow [411]1/2^+$ $19/2^+$		529.5(2)	22.74(94)	1.02(6)	
	$\rightarrow [404]7/2^+$ $19/2^+$		539.8(2)	4.19(20)	0.99(10)	
	$\rightarrow [541]1/2^-$ $21/2^-$		560.1(2)	4.46(20)	0.59(13)	
	$\lambda(529.5, 278.7) = 10.11(65)$		$B(\mathrm{M1})/B(\mathrm{E2}) = 0.123(11)$			
	$\lambda(539.8, 278.7) = 1.86(13)$		$B(\mathrm{M1})/B(\mathrm{E2}) = 0.738(67)$			
	$\lambda(539.8, 529.5) = 0.18(1)$		$B(\mathrm{E2})/B(\mathrm{E2}) = 0.167(11)$			
	$\lambda(529.5, 560.1) = 5.099(311)$		$B(\mathrm{E1})/B(\mathrm{E2}) = 0.036(2)$			
	$\lambda(539.8, 560.1) = 0.939(62)$		$B(\mathrm{E1})/B(\mathrm{E2}) = 0.213(14)$			
$[404]7/2^+$ $27/2^+$	$\rightarrow [404]7/2^+$ $25/2^+$	2329.7(3)	302.9(2)	1.75(9)	0.86(16)	$0.29^{+0.18}_{-0.18}$
	$\rightarrow [404]7/2^+$ $23/2^+$		585.0(2)	22.62(93)	1.00(3)	
	$\rightarrow [541]1/2^-$ $25/2^-$		670.8(2)	3.17(15)	0.75(16)	
	$\lambda(585.0, 302.9) = 12.93(85)$		$B(\mathrm{M1})/B(\mathrm{E2}) = 0.122(15)$			
	$\lambda(585.0, 670.8) = 7.136(447)$		$B(\mathrm{E1})/B(\mathrm{E2}) = 0.024(2)$			
$[404]7/2^+$ $31/2^+$	$\rightarrow [404]7/2^+$ $29/2^+$	2893.3(4)	272.3(2)	1.97(10)	0.70(9)	$0.11^{+0.10}_{-0.10}$
	$\rightarrow [404]7/2^+$ $27/2^+$		563.7(2)	14.83(62)	1.00(4)	
	$\lambda(563.7, 272.3) = 7.53(50)$		$B(\mathrm{M1})/B(\mathrm{E2}) = 0.256(18)$			
$[404]7/2^+$ $35/2^+$	$\rightarrow [404]7/2^+$ $33/2^+$	3373.5(4)	246.8(2)	2.30(11)	0.79(10)	$0.21^{+0.13}_{-0.13}$
	$\rightarrow [404]7/2^+$ $31/2^+$		480.3(2)	10.43(43)	1.03(4)	
	$\lambda(480.3, 246.8) = 4.53(29)$		$B(\mathrm{M1})/B(\mathrm{E2}) = 0.249(21)$			
$[404]7/2^+$ $39/2^+$	$\rightarrow [404]7/2^+$ $37/2^+$	3904.9(5)	283.0(2)	1.48(8)	0.84(11)	$0.27^{+0.13}_{-0.13}$
	$\rightarrow [404]7/2^+$ $35/2^+$		531.5(2)	7.87(34)	1.01(6)	
	$\lambda(531.5, 283.0) = 5.32(37)$		$B(\mathrm{M1})/B(\mathrm{E2}) = 0.227(22)$			

Table 1 —continued

$[Nn_3\Lambda]\Omega^\pi I_i^\pi \to [Nn_3\Lambda]\Omega^\pi I_f^\pi$	E_i [keV]	E_γ [keV]	$\mathcal{I}_\gamma^{rel}$	R_{DCO}	δ
$[404]7/2^+\ 43/2^+ \to [404]7/2^+\ 39/2^+$	4510.4(6)	605.5(2)	6.76(30)	0.98(7)	
$[404]7/2^+\ 47/2^+ \to [404]7/2^+\ 43/2^+$	5185.3(7)	674.9(2)	2.19(13)	1.09(11)	
$[404]7/2^+\ (51/2^+) \to [404]7/2^+\ 47/2^+$	5931.3(7)	746.0(2)	0.55(6)		
$[404]7/2^+ \otimes$ AE $17/2^- \to [404]7/2^+\ 15/2^+$	1633.3(3)	887.7(2)	5.30(60)	0.61(6)	
$[404]7/2^+ \otimes$ AE $21/2^- \to [404]7/2^+ \otimes$ AE $19/2^-$	1899.0(3)	145.5(2)	2.11(26)	1.40(26)	
$\to [404]7/2^+ \otimes$ AE $17/2^-$		265.8(2)	1.04(18)	0.81(15)	
$\to [404]7/2^+\ 19/2^+$		694.1(2)	2.39(36)	0.65(14)	
$\lambda(265.8, 145.5) = 0.49(10)$		$B(M1)/B(E2) = 0.606(129)$			
$\lambda(265.8, 694.1) = 0.435(100)$		$B(E1)/B(E2) = 0.007(2)$			
$[404]7/2^+ \otimes$ AE $25/2^- \to [404]7/2^+ \otimes$ AE $23/2^-$	2256.8(4)	189.3(2)	2.00(28)	1.38(39)	
$\to [404]7/2^+ \otimes$ AE $21/2^-$		357.8(2)	4.15(52)	1.05(17)	
$\lambda(357.8, 189.3) = 2.08(39)$		$B(M1)/B(E2) = 0.289(54)$			
$[404]7/2^+ \otimes$ AE $29/2^- \to [404]7/2^+ \otimes$ AE $27/2^-$	2692.1(4)	226.5(2)	1.05(18)	1.51(49)	
$\to [404]7/2^+ \otimes$ AE $25/2^-$		435.3(2)	4.35(58)	1.11(17)	
$\lambda(435.3, 226.5) = 4.14(90)$		$B(M1)/B(E2) = 0.225(49)$			
$[404]7/2^+ \otimes$ AE $33/2^- \to [404]7/2^+ \otimes$ AE $31/2^-$	3193.0(5)	258.7(2)	0.70(16)		
$\to [404]7/2^+ \otimes$ AE $29/2^-$		500.9(2)	5.20(72)	0.94(11)	
$\lambda(500.9, 258.7) = 7.43(199)$		$B(M1)/B(E2) = 0.170(45)$			
$[404]7/2^+ \otimes$ AE $37/2^- \to [404]7/2^+ \otimes$ AE $35/2^-$	3748.7(5)	283.4(2)	0.31(14)		
$\to [404]7/2^+ \otimes$ AE $33/2^-$		556.0(2)	4.57(70)	0.95(12)	
$\lambda(556.0, 283.4) = 14.74(703)$		$B(M1)/B(E2) = 0.110(52)$			
$[404]7/2^+ \otimes$ AE $41/2^- \to [404]7/2^+ \otimes$ AE $37/2^-$	4352.7(6)	604.1(2)	3.62(62)		
$[404]7/2^+ \otimes$ AE $45/2^- \to [404]7/2^+ \otimes$ AE $41/2^-$	5003.1(7)	650.3(2)	1.70(32)		
$[404]7/2^+ \otimes$ AE $49/2^- \to [404]7/2^+ \otimes$ AE $45/2^-$	5701.0(8)	697.9(2)	0.91(26)		
$[404]7/2^+ \otimes$ AE $(53/2^-) \to [404]7/2^+ \otimes$ AE $49/2^-$	6452.3(8)	751.3(2)	0.45(24)		
$[404]7/2^+ \otimes$ AE $19/2^- \to [404]7/2^+ \otimes$ AE $17/2^-$	1753.5(3)	120.3(2)	1.26(20)		
$\to [404]7/2^+\ 17/2^+$		786.1(2)	1.53(24)	0.59(21)	
$[404]7/2^+ \otimes$ AE $23/2^- \to [404]7/2^+ \otimes$ AE $21/2^-$	2067.4(4)	168.4(2)	2.25(30)		
$\to [404]7/2^+ \otimes$ AE $19/2^-$		314.0(2)	2.07(32)	0.96(17)	
$\lambda(314.0, 168.4) = 0.92(19)$		$B(M1)/B(E2) = 0.482(98)$			
$[404]7/2^+ \otimes$ AE $27/2^- \to [404]7/2^+ \otimes$ AE $25/2^-$	2465.5(4)	208.6(2)	1.28(22)	1.36(24)	
$\to [404]7/2^+ \otimes$ AE $23/2^-$		398.0(2)	4.25(56)	1.05(14)	
$\lambda(398.0, 208.6) = 3.32(72)$		$B(M1)/B(E2) = 0.230(50)$			
$[404]7/2^+ \otimes$ AE $31/2^- \to [404]7/2^+ \otimes$ AE $29/2^-$	2934.3(5)	242.1(2)	0.83(22)		
$\to [404]7/2^+ \otimes$ AE $27/2^-$		468.8(2)	3.27(48)	0.99(11)	
$\lambda(468.8, 242.1) = 3.94(119)$		$B(M1)/B(E2) = 0.281(85)$			
$[404]7/2^+ \otimes$ AE $35/2^- \to [404]7/2^+ \otimes$ AE $33/2^-$	3464.9(5)	271.8(2)	0.48(12)		
$\to [404]7/2^+ \otimes$ AE $31/2^-$		530.6(2)	2.47(44)	0.96(14)	
$\lambda(530.6, 271.8) = 5.15(158)$		$B(M1)/B(E2) = 0.282(87)$			
$[404]7/2^+ \otimes$ AE $39/2^- \to [404]7/2^+ \otimes$ AE $35/2^-$	4045.9(6)	580.9(2)	2.50(48)		
$[404]7/2^+ \otimes$ AE $43/2^- \to [404]7/2^+ \otimes$ AE $39/2^-$	4673.3(7)	627.5(2)	1.60(36)		
$[404]7/2^+ \otimes$ AE $47/2^- \to [404]7/2^+ \otimes$ AE $43/2^-$	5347.0(7)	673.7(2)	1.03(34)		
$[404]7/2^+ \otimes$ AE $(51/2^-) \to [404]7/2^+ \otimes$ AE $47/2^-$	6071.6(8)	724.6(2)	0.81(28)		

Table 1 —continued

$[Nn_3\Lambda]\Omega^\pi I_i^\pi$	$\to [Nn_3\Lambda]\Omega^\pi I_f^\pi$	E_i [keV]	E_γ [keV]	$\mathcal{I}_\gamma^{\text{rel}}$	R_{DCO}	δ
[411]1/2+ 5/2+	→ [411]1/2+ 3/2+	129.3(2)	116.9(2)	8.21(36)	0.73(6)	
	→ [411]1/2+ 1/2+		129.8(2)	1.00(40)	1.40(24)	
	λ(129.8, 116.9) = 0.12(5)		B(M1)/B(E2) = 0.131(53)			
[411]1/2+ 9/2+	→ [411]1/2+ 7/2+	361.6(2)	202.9(2)	6.22(41)	0.57(5)	
	→ [411]1/2+ 5/2+		232.2(2)	4.44(28)	1.06(5)	
	λ(232.2, 202.9) = 0.71(7)		B(M1)/B(E2) = 0.078(7)			
[411]1/2+ 13/2+	→ [411]1/2+ 11/2+	688.5(3)	275.3(2)	7.89(34)	0.47(4)	
	→ [411]1/2+ 9/2+		327.0(2)	12.45(53)	1.02(6)	
	λ(327.0, 275.3) = 1.58(10)		B(M1)/B(E2) = 0.079(5)			
[411]1/2+ 17/2+	→ [411]1/2+ 15/2+	1101.2(3)	333.3(2)	6.01(26)	0.51(5)	
	→ [404]7/2+ 15/2+		354.8(2)	0.88(9)		
	→ [411]1/2+ 13/2+		412.8(2)	16.91(70)	1.00(3)	
	λ(412.8, 333.3) = 2.81(17)		B(M1)/B(E2) = 0.080(5)			
	λ(412.8, 354.8) = 19.22(212)		B(M1)/B(E2) = 0.010(1)			
[411]1/2+ 21/2+	→ [411]1/2+ 19/2+	1589.4(3)	374.3(2)	3.02(14)	0.43(3)	
	→ [404]7/2+ 19/2+		384.5(2)	2.51(13)	0.54(14)	
	→ [411]1/2+ 17/2+		488.1(2)	20.34(83)	0.99(4)	
	λ(488.1, 374.3) = 6.74(42)		B(M1)/B(E2) = 0.054(3)			
	λ(488.1, 384.5) = 8.10(53)		B(M1)/B(E2) = 0.042(3)			
[411]1/2+ 25/2+	→ [411]1/2+ 23/2+	2135.6(3)	407.7(2)	3.28(15)	0.46(8)	
	→ [411]1/2+ 21/2+		546.3(2)	19.76(82)	0.99(5)	
	λ(546.3, 407.7) = 6.02(37)		B(M1)/B(E2) = 0.083(5)			
[411]1/2+ 29/2+	→ [411]1/2+ 27/2+	2662.6(4)	357.6(2)	2.79(14)	0.73(14)	
	→ [411]1/2+ 25/2+		526.9(2)	17.91(74)	0.99(3)	
	λ(526.9, 357.6) = 6.42(42)		B(M1)/B(E2) = 0.096(6)			
[411]1/2+ 33/2+	→ [411]1/2+ 31/2+	3098.5(4)	240.2(2)	1.46(8)	0.65(13)	
	→ [411]1/2+ 29/2+		435.8(2)	15.11(63)	1.01(4)	
	λ(435.8, 240.2) = 10.35(71)		B(M1)/B(E2) = 0.076(5)			
[411]1/2+ 37/2+	→ [411]1/2+ 35/2+	3581.8(4)	256.8(2)	1.03(6)	0.50(14)	
	→ [411]1/2+ 33/2+		483.3(2)	13.55(56)	1.03(8)	
	λ(483.3, 256.8) = 13.16(94)		B(M1)/B(E2) = 0.082(6)			
[411]1/2+ 41/2+	→ [411]1/2+ 37/2+	4140.2(5)	558.4(2)	9.11(38)	0.95(9)	
[411]1/2+ 45/2+	→ [411]1/2+ 41/2+	4775.0(6)	634.8(2)	5.87(26)	0.89(9)	
[411]1/2+ 49/2+	→ [411]1/2+ 45/2+	5483.4(7)	708.4(2)	2.94(14)	0.96(13)	
[411]1/2+ 53/2+	→ [411]1/2+ 49/2+	6263.3(8)	779.9(2)	1.29(8)	1.09(45)	
[411]1/2+ 57/2+	→ [411]1/2+ 53/2+	7109.6(8)	846.3(2)	0.50(8)		
[411]1/2+ 61/2+	→ [411]1/2+ 57/2+	8023.0(10)	913.4(3)	0.17(4)		
[411]1/2+ (65/2+)	→ [411]1/2+ 61/2+	8997.3(12)	974.3(5)	0.08(4)		
[411]1/2+ 7/2+	→ [411]1/2+ 3/2+	158.8(2)	147.0(2)	71.98(308)	1.00(26)	
[411]1/2+ 11/2+	→ [541]1/2− 9/2−	413.2(2)	119.9(2)	6.58(51)	0.72(5)	
	→ [411]1/2+ 7/2+		254.6(2)	43.80(181)	1.04(7)	
	λ(254.6, 119.9) = 6.657(585)		B(E1)/B(E2) = 0.071(6)			
[411]1/2+ 15/2+	→ [541]1/2− 13/2−	767.9(3)	270.8(2)	8.28(71)	0.59(3)	
	→ [411]1/2+ 11/2+		354.8(2)	29.60(121)	1.01(7)	
	λ(354.8, 270.8) = 3.575(340)		B(E1)/B(E2) = 0.061(6)			

Table 1 —continued

$[Nn_3\Lambda]\Omega^\pi I_i^\pi \to [Nn_3\Lambda]\Omega^\pi I_f^\pi$	E_i [keV]	E_γ [keV]	$\mathcal{I}_\gamma^{rel}$	R_{DCO}	δ
$[411]1/2^+\ 19/2^+ \to [404]7/2^+\ 17/2^+$	1215.2(3)	247.6(2)	1.50(10)		
$\to [541]1/2^-\ 17/2^-$		419.7(2)	7.08(60)	0.55(3)	
$\to [411]1/2^+\ 15/2^+$		447.1(2)	20.43(168)	0.99(3)	
$\to [404]7/2^+\ 15/2^+$		469.9(2)	5.12(23)	1.03(6)	
$\lambda(447.1, 247.6) = 13.62(144)$		$B(\mathrm{M1})/B(\mathrm{E2}) = 0.060(6)$			
$\lambda(469.9, 247.6) = 3.41(27)$		$B(\mathrm{M1})/B(\mathrm{E2}) = 0.306(25)$			
$\lambda(469.9, 447.1) = 0.25(2)$		$B(\mathrm{E2})/B(\mathrm{E2}) = 0.196(18)$			
$\lambda(447.1, 419.7) = 2.886(341)$		$B(\mathrm{E1})/B(\mathrm{E2}) = 0.064(8)$			
$\lambda(469.9, 419.7) = 0.723(69)$		$B(\mathrm{E1})/B(\mathrm{E2}) = 0.329(32)$			
$[411]1/2^+\ 23/2^+ \to [404]7/2^+\ 21/2^+$	1727.8(3)	262.1(10)	1.34(15)		
$\to [411]1/2^+\ 19/2^+$		512.4(2)	8.19(35)	0.95(6)	
$\to [404]7/2^+\ 19/2^+$		523.1(2)	25.68(210)	0.98(4)	
$\to [541]1/2^-\ 21/2^-$		543.2(2)	8.45(70)	0.52(3)	
$\lambda(523.1, 262.1) = 19.16(266)$		$B(\mathrm{M1})/B(\mathrm{E2}) = 0.079(11)$			
$\lambda(512.4, 262.1) = 6.11(73)$		$B(\mathrm{M1})/B(\mathrm{E2}) = 0.222(27)$			
$\lambda(523.1, 512.4) = 3.14(29)$		$B(\mathrm{E2})/B(\mathrm{E2}) = 2.827(261)$			
$\lambda(523.1, 543.2) = 3.039(354)$		$B(\mathrm{E1})/B(\mathrm{E2}) = 0.062(7)$			
$\lambda(512.4, 543.2) = 0.969(90)$		$B(\mathrm{E1})/B(\mathrm{E2}) = 0.174(16)$			
$[411]1/2^+\ 27/2^+ \to [411]1/2^+\ 23/2^+$	2305.0(3)	577.2(2)	28.81(195)	0.99(3)	
$\to [541]1/2^-\ 25/2^-$		646.1(2)	8.37(60)	0.54(3)	
$\lambda(577.2, 646.1) = 3.442(339)$		$B(\mathrm{E1})/B(\mathrm{E2}) = 0.053(5)$			
$[411]1/2^+\ 31/2^+ \to [411]1/2^+\ 27/2^+$	2858.3(4)	553.3(2)	25.22(103)	1.02(4)	
$\to [541]1/2^-\ 29/2^-$		648.4(2)	3.97(73)	0.50(4)	
$\lambda(553.3, 648.4) = 6.353(1197)$		$B(\mathrm{E1})/B(\mathrm{E2}) = 0.023(4)$			
$[411]1/2^+\ 35/2^+ \to [411]1/2^+\ 31/2^+$	3325.1(4)	466.8(2)	21.84(89)	1.00(4)	
$[411]1/2^+\ 39/2^+ \to [411]1/2^+\ 35/2^+$	3840.8(5)	515.7(2)	17.08(70)	0.99(4)	
$[411]1/2^+\ 43/2^+ \to [411]1/2^+\ 39/2^+$	4429.1(6)	588.3(2)	12.00(49)	0.92(10)	
$[411]1/2^+\ 47/2^+ \to [411]1/2^+\ 43/2^+$	5089.9(7)	660.8(2)	6.76(29)	0.89(5)	
$[411]1/2^+\ 51/2^+ \to [411]1/2^+\ 47/2^+$	5819.3(8)	729.4(2)	2.61(13)	1.11(14)	
$[411]1/2^+\ 55/2^+ \to [411]1/2^+\ 51/2^+$	6613.2(8)	793.9(2)	1.22(8)		
$[411]1/2^+\ 59/2^+ \to [411]1/2^+\ 55/2^+$	7481.0(9)	867.8(2)	0.36(4)		
$[411]1/2^+\ 63/2^+ \to [411]1/2^+\ 59/2^+$	8409.9(11)	928.9(4)	0.12(4)		
$[411]1/2^+\ (67/2^+) \to [411]1/2^+\ 63/2^+$	9405.3(11)	995.4(6)	0.02(1)		
$[541]1/2^-\ 5/2^- \to [411]1/2^+\ 3/2^+$	181.6(2)	169.9(2)	0.50(40)	0.63(3)	
$[541]1/2^-\ 9/2^- \to [541]1/2^-\ 5/2^-$	293.1(2)	111.4(2)	5.83(45)	1.07(7)	
$\to [411]1/2^+\ 7/2^+$		134.4(2)	72.95(298)	0.66(3)	
$\lambda(111.4, 134.4) = 0.080(7)$		$B(\mathrm{E1})/B(\mathrm{E2}) = 0.068(6)$			
$[541]1/2^-\ 13/2^- \to [411]1/2^+\ 11/2^+$	497.0(2)	83.9(2)	13.91(57)	0.70(4)	
$\to [523]7/2^-\ 11/2^-$		128.4(2)	3.39(19)		
$\to [541]1/2^-\ 9/2^-$		204.0(2)	84.68(341)	1.08(5)	
$\lambda(204.0, 128.4) = 24.98(172)$		$B(\mathrm{M1})/B(\mathrm{E2}) = 0.005(0)$			
$\lambda(204.0, 83.9) = 6.088(350)$		$B(\mathrm{E1})/B(\mathrm{E2}) = 0.075(4)$			
$[541]1/2^-\ 17/2^- \to [541]1/2^-\ 13/2^-$	795.3(3)	298.3(2)	108.47(436)	1.00(7)	
$[541]1/2^-\ 21/2^- \to [541]1/2^-\ 17/2^-$	1184.7(3)	389.3(2)	92.73(372)	0.98(6)	
$[541]1/2^-\ 25/2^- \to [541]1/2^-\ 21/2^-$	1659.0(3)	474.3(2)	70.77(284)	0.99(5)	
$[541]1/2^-\ 29/2^- \to [541]1/2^-\ 25/2^-$	2209.9(3)	551.1(2)	43.45(175)	1.01(7)	
$[541]1/2^-\ 33/2^- \to [541]1/2^-\ 29/2^-$	2828.2(4)	618.3(2)	27.26(112)	0.98(4)	

Table 1 —continued

$[Nn_3\Lambda]\Omega^\pi I_i^\pi \to [Nn_3\Lambda]\Omega^\pi I_f^\pi$		E_i [keV]	E_γ [keV]	$\mathcal{I}_\gamma^{rel}$	R_{DCO}	δ
$[541]1/2^-$ $37/2^-$	$\to [541]1/2^-$ $33/2^-$	3502.4(4)	674.3(2)	13.41(55)	0.98(6)	
$[541]1/2^-$ $41/2^-$	$\to [541]1/2^-$ $37/2^-$	4219.7(5)	717.3(2)	6.58(28)	0.98(10)	
$[541]1/2^-$ $45/2^-$	$\to [541]1/2^-$ $41/2^-$	4961.6(6)	741.9(2)	2.96(14)	1.06(31)	
$[541]1/2^-$ $49/2^-$	$\to [541]1/2^-$ $45/2^-$	5724.4(7)	762.8(2)	1.68(9)	0.90(33)	
$[541]1/2^-$ $53/2^-$	$\to [541]1/2^-$ $49/2^-$	6520.7(7)	796.3(2)	0.75(5)		
$[541]1/2^-$ $3/2^-$	$\to [411]1/2^+$ $1/2^+$	275.6(3)	276.2(2)	0.03(2)		
$[541]1/2^-$ $7/2^-$	$\to [541]1/2^-$ $3/2^-$	449.9(3)	174.9(2)	0.03(2)		
	$\to [411]1/2^+$ $5/2^+$		319.9(3)	0.43(40)	0.64(13)	
	$\lambda(174.9, 319.9) = 0.070(80)$		$B(E1)/B(E2) = 0.055(63)$			
$[541]1/2^-$ $11/2^-$	$\to [541]1/2^-$ $7/2^-$	701.2(2)	251.4(2)	0.81(12)	1.03(14)	
	$\to [411]1/2^+$ $9/2^+$		339.6(2)	2.52(26)	0.59(4)	
	$\to [541]1/2^-$ $9/2^-$		408.0(2)	0.47(6)	0.58(12)	$-0.03^{+0.16}_{-0.23}$
	$\lambda(251.4, 408.0) = 1.72(34)$		$B(M1)/B(E2) = 0.006(1)$			
	$\lambda(251.4, 339.6) = 0.321(58)$		$B(E1)/B(E2) = 0.061(11)$			
$[541]1/2^-$ $15/2^-$	$\to [541]1/2^-$ $17/2^-$	1030.1(3)	234.8(5)	0.14(8)		
	$\to [541]1/2^-$ $11/2^-$		328.9(2)	2.89(20)	1.02(8)	
	$\to [411]1/2^+$ $13/2^+$		341.5(2)	2.60(19)	0.62(4)	
	$\to [541]1/2^-$ $13/2^-$		533.3(2)	1.58(10)	0.44(17)	$-0.22^{+0.24}_{-0.78}$
	$\lambda(328.9, 533.3) = 1.83(17)$		$B(M1)/B(E2) = 0.009(2)$			
	$\lambda(328.9, 234.8) = 20.64(1188)$		$B(M1)/B(E2) = 0.010(6)$			
	$\lambda(328.9, 341.5) = 1.112(112)$		$B(E1)/B(E2) = 0.067(7)$			
$[541]1/2^-$ $19/2^-$	$\to [541]1/2^-$ $21/2^-$	1433.5(3)	248.9(10)	0.27(16)		
	$\to [411]1/2^+$ $17/2^+$		332.1(2)	2.04(20)	0.61(10)	
	$\to [541]1/2^-$ $15/2^-$		403.5(2)	5.76(26)	0.99(5)	
	$\to [541]1/2^-$ $17/2^-$		638.1(2)	3.53(17)	0.37(9)	$-0.36^{+0.16}_{-0.38}$
	$\lambda(403.5, 638.1) = 1.63(11)$		$B(M1)/B(E2) = 0.015(3)$			
	$\lambda(403.5, 248.9) = 21.33(1268)$		$B(M1)/B(E2) = 0.023(13)$			
	$\lambda(403.5, 332.1) = 2.824(305)$		$B(E1)/B(E2) = 0.079(9)$			
$[541]1/2^-$ $23/2^-$	$\to [411]1/2^+$ $21/2^+$	1903.7(3)	314.1(2)	1.13(10)	0.65(13)	
	$\to [541]1/2^-$ $19/2^-$		469.9(2)	8.10(35)	1.04(10)	
	$\to [541]1/2^-$ $21/2^-$		719.4(2)	3.33(18)	0.24(8)	$-1.00^{+0.47}_{-0.86}$
	$\lambda(469.9, 719.4) = 2.43(17)$		$B(M1)/B(E2) = 0.009(8)$			
	$\lambda(469.9, 314.1) = 7.168(706)$		$B(E1)/B(E2) = 0.079(8)$			
$[541]1/2^-$ $27/2^-$	$\to [541]1/2^-$ $23/2^-$	2427.1(3)	523.4(2)	5.88(27)	0.97(10)	
	$\to [541]1/2^-$ $25/2^-$		768.1(2)	2.99(16)	0.31(8)	$-1.68^{+0.68}_{-2.19}$
	$\lambda(523.4, 768.1) = 1.97(14)$		$B(M1)/B(E2) = 0.008(13)$			
$[541]1/2^-$ $31/2^-$	$\to [541]1/2^-$ $27/2^-$	2999.2(4)	572.1(2)	5.10(27)	0.99(11)	
	$\to [541]1/2^-$ $29/2^-$		789.5(3)	1.33(25)	0.34(8)	$-2.11^{+0.61}_{-1.57}$
	$\lambda(572.1, 789.5) = 3.83(75)$		$B(M1)/B(E2) = 0.004(9)$			
$[541]1/2^-$ $35/2^-$	$\to [541]1/2^-$ $31/2^-$	3618.1(4)	618.9(2)	3.35(22)	0.99(12)	
	$\to [541]1/2^-$ $33/2^-$		789.7(2)	1.77(19)	0.34(8)	$-2.11^{+0.61}_{-1.57}$
	$\lambda(618.9, 789.7) = 1.89(24)$		$B(M1)/B(E2) = 0.012(26)$			
$[541]1/2^-$ $39/2^-$	$\to [541]1/2^-$ $35/2^-$	4276.1(5)	658.0(2)	2.40(100)	1.01(28)	
	$\to [541]1/2^-$ $37/2^-$		773.8(2)	0.75(7)		
	$\lambda(658.0, 773.8) = 3.20(137)$		$B(M1)/B(E2) = 0.058(25)$			
$[541]1/2^-$ $(43/2^-)$	$\to [541]1/2^-$ $39/2^-$	4964.3(5)	688.1(2)	1.49(10)		
	$\to [541]1/2^-$ $41/2^-$		744.6(2)	0.92(7)		
	$\lambda(688.1, 744.6) = 1.62(16)$		$B(M1)/B(E2) = 0.160(16)$			

Table 1 —continued

$[Nn_3\Lambda]\Omega^\pi I_i^\pi \to [Nn_3\Lambda]\Omega^\pi I_f^\pi$	E_i [keV]	E_γ [keV]	$\mathcal{I}_\gamma^{\text{rel}}$	R_{DCO}	δ
$\{[541]1/2^-; K\pm2\}$ $15/2^-$ → $[541]1/2^-$ $13/2^-$	1289.7(3)	792.8(2)	0.74(16)	0.35(14)	
$\{[541]1/2^-; K\pm2\}$ $19/2^-$ → $\{[541]1/2^-; K\pm2\}$ $15/2^-$	1614.5(3)	324.9(2)	0.56(6)		
→ $[541]1/2^-$ $17/2^-$		819.2(2)	2.47(17)	0.36(11)	
λ(324.9, 819.2) = 0.23(3)		B(M1)/B(E2) = 0.020(3)			
$\{[541]1/2^-; K\pm2\}$ $23/2^-$ → $\{[541]1/2^-; K\pm2\}$ $19/2^-$	2032.0(3)	417.5(2)	2.89(14)	0.91(10)	
→ $[541]1/2^-$ $21/2^-$		847.0(2)	5.86(27)	0.40(6)	
λ(417.5, 847.0) = 0.49(3)		B(M1)/B(E2) = 0.029(2)			
$\{[541]1/2^-; K\pm2\}$ $27/2^-$ → $\{[541]1/2^-; K\pm2\}$ $23/2^-$	2540.7(4)	508.5(2)	6.24(28)	0.98(12)	
→ $[541]1/2^-$ $25/2^-$		882.0(2)	1.02(9)	0.26(16)	
λ(508.5, 882.0) = 6.12(61)		B(M1)/B(E2) = 0.006(1)			
$\{[541]1/2^-; K\pm2\}$ $31/2^-$ → $\{[541]1/2^-; K\pm2\}$ $27/2^-$	3123.1(5)	582.4(2)	4.16(21)	0.94(6)	
$\{[541]1/2^-; K\pm2\}$ $(35/2^-)$ → $\{[541]1/2^-; K\pm2\}$ $31/2^-$	3738.6(6)	615.5(2)	2.07(13)	0.90(15)	
$\{[541]1/2^-; K\pm2\}$ $17/2^-$ → $[541]1/2^-$ $17/2^-$	1442.4(3)	646.9(2)	0.92(16)	0.74(18)	
→ $[541]1/2^-$ $13/2^-$		945.5(2)	0.39(8)		
λ(945.5, 646.9) = 0.42(11)		B(M1)/B(E2) = 4.562(1227)			
$\{[541]1/2^-; K\pm2\}$ $21/2^-$ → $\{[541]1/2^-; K\pm2\}$ $17/2^-$	1806.9(3)	364.4(2)	2.35(12)	0.91(17)	
→ $[541]1/2^-$ $21/2^-$		621.9(2)	4.39(21)	0.88(18)	
→ $[541]1/2^-$ $17/2^-$		1012.4(2)	1.92(13)	0.77(14)	
λ(364.4, 621.9) = 0.54(4)		B(M1)/B(E2) = 0.035(2)			
λ(1012.4, 621.9) = 0.44(4)		B(M1)/B(E2) = 7.007(581)			
λ(1012.4, 364.4) = 0.82(7)		B(E2)/B(E2) = 0.005(0)			
$\{[541]1/2^-; K\pm2\}$ $25/2^-$ → $\{[541]1/2^-; K\pm2\}$ $21/2^-$	2252.2(3)	445.6(2)	4.09(19)	0.98(17)	
→ $[541]1/2^-$ $25/2^-$		592.7(2)	2.69(15)		
→ $[541]1/2^-$ $21/2^-$		1067.6(2)	1.11(9)	0.76(25)	
λ(445.6, 592.7) = 1.52(11)		B(M1)/B(E2) = 0.038(3)			
λ(1067.6, 592.7) = 0.41(4)		B(M1)/B(E2) = 11.186(1101)			
λ(1067.6, 445.6) = 0.27(3)		B(E2)/B(E2) = 0.003(0)			
$\{[541]1/2^-; K\pm2\}$ $29/2^-$ → $\{[541]1/2^-; K\pm2\}$ $25/2^-$	2770.5(4)	518.4(2)	4.77(24)	0.99(8)	
$\{[541]1/2^-; K\pm2\}$ $33/2^-$ → $\{[541]1/2^-; K\pm2\}$ $29/2^-$	3344.8(5)	574.2(2)	3.60(19)		
$\{[541]1/2^-; K\pm2\}$ $(37/2^-)$ → $\{[541]1/2^-; K\pm2\}$ $33/2^-$	3914.3(6)	569.5(2)	1.23(9)		
$[402]5/2^+$ $9/2^+$ → $[402]5/2^+$ $7/2^+$	551.8(3)	131.9(2)	0.51(8)		
→ $[402]5/2^+$ $5/2^+$		236.3(2)	0.38(6)		
λ(236.3, 131.9) = 0.75(17)		B(M1)/B(E2) = 0.298(66)			
$[402]5/2^+$ $13/2^+$ → $[402]5/2^+$ $11/2^+$	891.7(3)	184.4(2)	1.05(7)		
→ $[402]5/2^+$ $9/2^+$		340.0(2)	0.61(6)		
λ(340.0, 184.4) = 0.58(7)		B(M1)/B(E2) = 0.865(103)			
$[402]5/2^+$ $17/2^+$ → $[402]5/2^+$ $15/2^+$	1322.0(4)	232.5(2)	0.96(7)		
→ $[402]5/2^+$ $13/2^+$		430.4(2)	1.01(7)		
λ(430.4, 232.5) = 1.05(11)		B(M1)/B(E2) = 0.775(78)			
$[402]5/2^+$ $21/2^+$ → $[402]5/2^+$ $19/2^+$	1828.4(4)	275.8(2)	0.88(7)		
→ $[402]5/2^+$ $17/2^+$		506.6(2)	1.50(10)		
λ(506.6, 275.8) = 1.70(18)		B(M1)/B(E2) = 0.647(67)			
$[402]5/2^+$ $(25/2^+)$ → $[402]5/2^+$ $21/2^+$	2378.4(6)	550.0(2)	0.90(9)		
$[402]5/2^+$ $7/2^+$ → $[402]5/2^+$ $5/2^+$	419.7(3)	104.1(2)	0.50(8)		
$[402]5/2^+$ $11/2^+$ → $[402]5/2^+$ $9/2^+$	707.3(3)	155.4(2)	0.90(9)		
→ $[402]5/2^+$ $7/2^+$		287.8(2)	0.57(6)		
λ(287.8, 155.4) = 0.63(9)		B(M1)/B(E2) = 0.575(84)			

Table 1 —continued

$[Nn_3\Lambda]\Omega^\pi I_i^\pi \to [Nn_3\Lambda]\Omega^\pi I_f^\pi$		E_i [keV]	E_γ [keV]	$\mathcal{I}_\gamma^{rel}$	R_{DCO}	δ
$[402]5/2^+$ $15/2^+$	$\to [402]5/2^+$ $13/2^+$	1089.5(4)	197.7(2)	1.03(7)		
	$\to [402]5/2^+$ $11/2^+$		382.2(2)	0.94(7)		
	$\lambda(382.2, 197.7) = 0.91(9)$		$B(M1)/B(E2) = 0.802(81)$			
$[402]5/2^+$ $19/2^+$	$\to [402]5/2^+$ $17/2^+$	1552.3(4)	230.0(2)	0.89(5)		
	$\to [402]5/2^+$ $15/2^+$		462.7(2)	1.58(10)		
	$\lambda(462.7, 230.0) = 1.78(15)$		$B(M1)/B(E2) = 0.680(58)$			
$[402]5/2^+$ $23/2^+$	$\to [402]5/2^+$ $21/2^+$	2079.2(5)	250.6(2)	0.49(6)		
	$\to [402]5/2^+$ $19/2^+$		527.1(2)	1.78(11)		
	$\lambda(527.1, 250.6) = 3.63(50)$		$B(M1)/B(E2) = 0.493(68)$			
$[402]5/2^+$ $(27/2^+)$	$\to [402]5/2^+$ $23/2^+$	2671.0(6)	591.8(2)	1.13(9)		
$[523]7/2^- \otimes$ AE $17/2^+$	$\to [523]7/2^-$ $15/2^-$	1740.8(3)	1066.0(3)	1.83(70)	0.51(23)	
$[523]7/2^- \otimes$ AE $21/2^+$	$\to [523]7/2^- \otimes$ AE $19/2^+$	1989.3(4)	132.2(2)	1.52(14)		
	$\to [523]7/2^- \otimes$ AE $17/2^+$		248.4(2)	0.30(15)		
	$\to [523]7/2^-$ $19/2^-$		917.4(2)	6.12(56)	0.60(5)	
	$\lambda(248.4, 132.2) = 0.20(10)$		$B(M1)/B(E2) = 1.436(730)$			
	$\lambda(248.4, 917.4) = 0.049(25)$		$B(E1)/B(E2) = 0.019(10)$			
$[523]7/2^- \otimes$ AE $25/2^+$	$\to [523]7/2^- \otimes$ AE $23/2^+$	2304.7(4)	166.0(2)	5.56(48)	1.06(12)	
	$\to [523]7/2^- \otimes$ AE $21/2^+$		315.5(2)	3.04(30)	1.13(23)	
	$\to [523]7/2^-$ $23/2^-$		754.9(2)	4.00(38)	0.74(14)	
	$\lambda(315.5, 166.0) = 0.55(7)$		$B(M1)/B(E2) = 0.866(114)$			
	$\lambda(315.5, 754.9) = 0.760(104)$		$B(E1)/B(E2) = 0.007(1)$			
$[523]7/2^- \otimes$ AE $29/2^+$	$\to [523]7/2^- \otimes$ AE $27/2^+$	2689.3(4)	200.9(2)	5.53(48)	0.97(13)	
	$\to [523]7/2^- \otimes$ AE $25/2^+$		384.7(2)	5.83(50)	1.02(8)	
	$\lambda(384.7, 200.9) = 1.05(13)$		$B(M1)/B(E2) = 0.682(83)$			
$[523]7/2^- \otimes$ AE $33/2^+$	$\to [523]7/2^- \otimes$ AE $31/2^+$	3142.2(5)	234.7(2)	4.13(36)	0.88(8)	
	$\to [523]7/2^- \otimes$ AE $29/2^+$		453.0(2)	6.01(50)	0.96(11)	
	$\lambda(453.0, 234.7) = 1.46(18)$		$B(M1)/B(E2) = 0.702(85)$			
$[523]7/2^- \otimes$ AE $37/2^+$	$\to [523]7/2^- \otimes$ AE $35/2^+$	3658.9(5)	265.7(2)	2.86(26)		
	$\to [523]7/2^- \otimes$ AE $33/2^+$		516.8(2)	6.23(54)	1.06(12)	
	$\lambda(516.8, 265.7) = 2.18(27)$		$B(M1)/B(E2) = 0.625(79)$			
$[523]7/2^- \otimes$ AE $41/2^+$	$\to [523]7/2^- \otimes$ AE $39/2^+$	4233.9(6)	293.4(2)	1.40(18)		
	$\to [523]7/2^- \otimes$ AE $37/2^+$		575.2(2)	4.09(38)	0.97(19)	
	$\lambda(575.2, 293.4) = 2.92(46)$		$B(M1)/B(E2) = 0.591(94)$			
$[523]7/2^- \otimes$ AE $45/2^+$	$\to [523]7/2^- \otimes$ AE $41/2^+$	4861.6(6)	627.7(2)	3.08(30)		
$[523]7/2^- \otimes$ AE $49/2^+$	$\to [523]7/2^- \otimes$ AE $45/2^+$	5525.3(7)	663.7(2)	0.92(18)		
	$\to [404]7/2^+$ $45/2^+$	5526.0(7)	698.9(2)	1.39(10)		
	$\lambda(698.9, 663.7) = 1.51(31)$		$B(E2)/B(E2) = 1.17(24)$			
$[523]7/2^- \otimes$ AE $(53/2^+)$	$\to [523]7/2^- \otimes$ AE $49/2^+$	6244.8(8)	719.6(2)	0.41(6)		
$[523]7/2^- \otimes$ AE $19/2^+$	$\to [523]7/2^- \otimes$ AE $17/2^+$	1857.1(4)	116.2(2)	0.27(20)		
	$\to [523]7/2^-$ $17/2^-$		991.4(2)	4.65(50)	0.54(5)	
$[523]7/2^- \otimes$ AE $23/2^+$	$\to [523]7/2^- \otimes$ AE $21/2^+$	2138.5(4)	149.0(2)	4.30(38)	1.00(11)	
	$\to [523]7/2^- \otimes$ AE $19/2^+$		281.5(2)	1.09(20)	1.07(14)	
	$\to [523]7/2^-$ $21/2^-$		830.2(2)	3.65(34)	0.56(6)	
	$\lambda(281.5, 149.0) = 0.25(5)$		$B(M1)/B(E2) = 1.460(297)$			
	$\lambda(281.5, 830.2) = 0.299(61)$		$B(E1)/B(E2) = 0.008(2)$			
$[523]7/2^- \otimes$ AE $27/2^+$	$\to [523]7/2^- \otimes$ AE $25/2^+$	2488.3(4)	183.5(2)	6.20(52)	0.96(10)	
	$\to [523]7/2^- \otimes$ AE $23/2^+$		349.8(2)	4.53(40)	0.98(12)	
	$\lambda(349.8, 183.5) = 0.73(9)$		$B(M1)/B(E2) = 0.804(98)$			

Table 1 —continued

$[Nn_3\Lambda]\Omega^\pi I_i^\pi \to [Nn_3\Lambda]\Omega^\pi I_f^\pi$	E_i [keV]	E_γ [keV]	$\mathcal{I}_\gamma^{\rm rel}$	$R_{\rm DCO}$	δ
$[523]7/2^- \otimes$ AE $31/2^+ \to [523]7/2^- \otimes$ AE $29/2^+$	2907.3(5)	217.9(2)	5.10(42)	0.96(16)	
$\to [523]7/2^- \otimes$ AE $27/2^+$		419.1(2)	6.37(54)	1.04(9)	
$\lambda(419.1, 217.9) = 1.25(15)$		B(M1)/B(E2) = 0.693(82)			
$[523]7/2^- \otimes$ AE $35/2^+ \to [523]7/2^- \otimes$ AE $33/2^+$	3393.0(5)	250.6(2)	3.18(28)	0.87(10)	
$\to [523]7/2^- \otimes$ AE $31/2^+$		485.8(2)	6.60(56)	1.00(12)	
$\lambda(485.8, 250.6) = 2.08(25)$		B(M1)/B(E2) = 0.574(70)			
$[523]7/2^- \otimes$ AE $39/2^+ \to [523]7/2^- \otimes$ AE $37/2^+$	3940.3(5)	281.2(2)	2.25(30)		
$\to [523]7/2^- \otimes$ AE $35/2^+$		547.4(2)	5.99(54)		
$\lambda(547.4, 281.2) = 2.66(43)$		B(M1)/B(E2) = 0.575(93)			
$[523]7/2^- \otimes$ AE $43/2^+ \to [523]7/2^- \otimes$ AE $39/2^+$	4543.8(6)	603.5(2)	4.94(44)		
$[523]7/2^- \otimes$ AE $47/2^+ \to [523]7/2^- \otimes$ AE $43/2^+$	5202.9(7)	659.1(2)	1.86(22)		
$[523]7/2^- \otimes$ AE $(51/2^+) \to [523]7/2^- \otimes$ AE $47/2^+$	5890.7(8)	687.8(2)	0.77(20)		
$\to [404]7/2^+$ $47/2^+$	5891.3(7)	705.9(2)	0.87(6)		
$\lambda(705.9, 687.8) = 1.13(30)$		B(E2)/B(E2) = 0.99(26)			

Spectra illustrating the crossings and the weak interband transitions between the $[523]7/2^-$ and $[541]1/2^-$ bands around spin $13/2^-\hbar$ and between the $[523]7/2^- \otimes$ AB and $[541]1/2^-$ bands around $37/2^-\hbar$, both established in this work, are shown in Fig. 4, (c) and (d).

3.1.2. Band 1

Two new strongly coupled sequences, feeding into the $[523]7/2^-$ band between spin $15/2^-\hbar$ and $23/2^-\hbar$ via five transitions of energies 754.9, 830.2, 917.4, 991.4 and 1066.0 keV, and with DCO ratios consistent with pure stretched dipole character, have been established. The pure dipole character of the depopulating transitions supports our assignment of a bandhead spin of $17/2\hbar$, and positive parity is suggested, after considering possible configurations in Section 4.2.1.

A gate on the 917.4 keV dipole transition is shown in Fig. 4(e). All transitions below spin $19/2^-\hbar$ of band $[523]7/2^-$ and above spin $21/2^+\hbar$ in the new band are seen in agreement with the proposed level scheme. A few contaminant lines are seen too, but these can all be explained by a 916 keV transition [4] populating band $[541]1/2^-$ at spin $25/2^-\hbar$. Fig. 4(f) shows a gate on 349.8 keV, suggested to be the $27/2^+ \to 23/2^+$ transition of the new band. The E2 transitions in coincidence with the 349.8 keV line and the four strongest transitions depopulating the new bands are seen in agreement with the proposed level scheme.

3.1.3. [541]1/2⁻ band

The favoured signature ($\alpha_f = +1/2$) of the $[541]1/2^-$ band, which was known previously to spin $37/2^-\hbar$, has been confirmed and extended with four new E2 transitions to spin $53/2^-\hbar$. A double gate between the previously highest known transition energy,

[4] Since it has not been possible to connect unambiguously a band to this transition, it is neither included in the level scheme nor in Table 1.

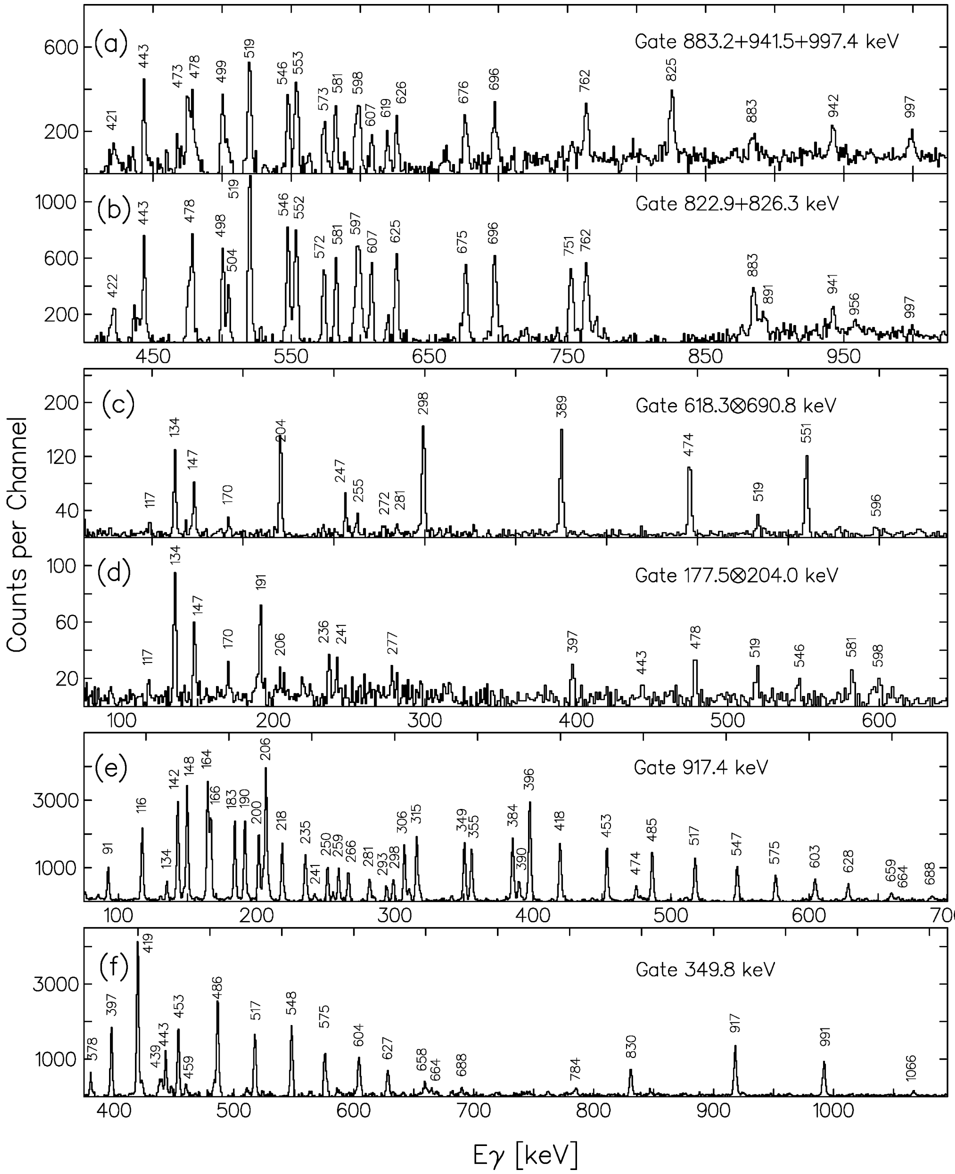

Fig. 4. ((a) and (b)) Coincidence spectra (from the first experiment) obtained by gating on a sum of transitions placed in the high-spin part of band [523]7/2$^-$. ((c) and (d)) Double gated spectra illustrating interband transitions between bands [523]7/2$^-$ and [541]1/2$^-$. ((e) and (f)) Coincidence spectra showing the two signatures of band 1 and the dipole transitions depopulating the band.

674.3 keV, and a sum of transitions below spin $29/2^-\hbar$ (134.4, 204.0, 298.3, 389.3, 474.3 and 551.1 keV) is shown in Fig. 5(a).

The unfavoured signature, [541]1/2$^-$ ($\alpha_u = -1/2$), has been extended from spin $3/2^-\hbar$ to $39/2^-\hbar$ ($43/2^-\hbar$). A double gate between the 572.1 keV transition and the 719.4 keV

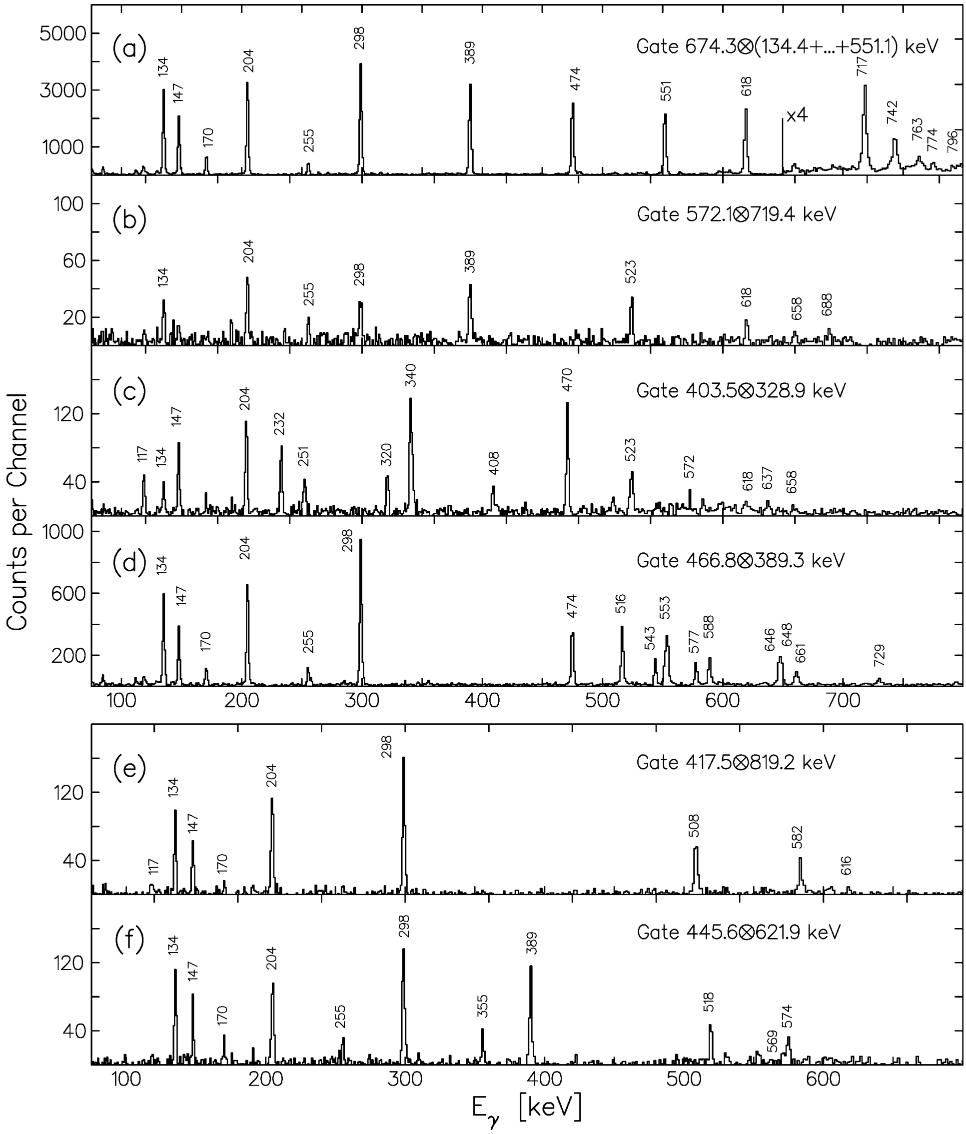

Fig. 5. (a) Sum of double gated spectra showing band [541]$1/2^-$ ($\alpha = +1/2$). ((b) and (c)) Double gated spectra showing band [541]$1/2^-$ ($\alpha = -1/2$). (d) Double gated spectrum illustrating the low-spin part of band [541]$1/2^-$ ($\alpha = +1/2$) and interband E1 transitions between bands [411]$1/2^+$ and [541]$1/2^-$. ((e) and (f)) Double gated spectra showing the new bands 3 and 4.

M1 transition depopulating the unfavoured signature is shown in Fig. 5(b). The three transitions above $31/2^-\hbar$, and part of the favoured signature, is seen in agreement with the proposed level scheme. The complicated structure of the level scheme, with the three doublets 717.3, 719.4, 618.3, 618.9, 789.5 and 789.7 keV, could be solved only by means of the cube. Fig. 5(c) illustrates the lower part of the level scheme, the decay to the favoured signature via the weak 408.0 keV transition and the decay to band $[411]1/2^+$ ($\alpha = +1/2$) via the two E1 transitions of energy 319.9 and 339.6 keV. A double gate between the 466.8 keV $35/2^+\hbar \to 31/2^+$ transition of the $[411]1/2^+$ band and the 389.3 keV transition of the $[541]1/2^-$ ($\alpha = +1/2$) band, shown in Fig. 5(d) illustrates the low-spin part of $[541]1/2^-$ ($\alpha = +1/2$) and the interband E1 transitions between the two bands.

Interband transitions between the $[541]1/2^-$ and $[411]1/2^+$ bands all have DCO ratios close to 0.6 in agreement with a pure dipole (E1) character, whereas the intense $I \to I-1$ transitions between the unfavoured and favoured signatures of $[541]1/2^-$ have ratios smaller than 0.6 and values decreasing with increasing spin. Large negative mixing ratios in the range from ≈ 0 to ≈ -2.1 (for spins $11/2^-\hbar$ to $35/2^-\hbar$) have been extracted for the latter transitions, indicating a strong E2 mixing.

3.1.4. Bands 3 and 4

Two new decoupled rotational band structures which decay to band $[541]1/2^-$ have been established — bands 3 and 4. Fig. 5, (e) and (f) show examples of coincidence spectra for bands 3 and 4, respectively. It should be mentioned that in gate (f) some contaminants come in via an unresolved coincidence between a 621.9 keV transition and the 447.1 keV $19/2 \to 15/2$ transition of the $[411]1/2^+$ band.

DCO ratios for four out of five inband transitions for band 3 are consistent with stretched E2 multipolarity. The weighted average of the DCO ratios for the four interband transitions from band 3 to the $[541]1/2^-$ ($\alpha = +1/2$) band is 0.36 ± 0.05. Hence it is suggested that they have mixed E2/M1 multipolarity and that band 3 has negative parity. The most likely spin for the lowest level is therefore $15/2^-\hbar$. The average DCO ratio corresponds to two possible values for the mixing ratio $\bar{\delta}_w = -0.38^{+0.11}_{-0.19}$ and $\bar{\delta}_w = -2.49^{+0.77}_{-1.14}$, which both indicate a considerable E2 mixing.

DCO ratios for the three lowest inband transitions of band 4 unambiguously confirm that they are stretched quadrupole transitions. Due to low intensities, the determination of the multipolarity for the out of band transitions of band 4 is difficult. However, a weighted average of DCO ratios of 0.81 ± 0.13 was found for the 646.9 and 621.9 keV $I \to I$ transitions, which gives two possible values for the mixing ratio $\bar{\delta}_w = -0.65^{+0.38}_{-0.88}$ and $\bar{\delta}_w = 1.64^{+4.34}_{-0.79}$. The three lowest levels of band 4, decay to levels of band $[541]1/2^-$ ($\alpha = +1/2$) with both spin I and $I-2$. This gives only three possibilities [5] for the spin of the lowest level; $13/2\hbar$, $15/2\hbar$ and $17/2\hbar$. Spin $17/2\hbar$ is suggested, as with this choice band 3 and 4 resemble signature partners, but without transitions connecting them. This implies that band 4 has negative parity, too. Further arguments for this assignment will be given in Section 4.2.3.

3.1.5. $[411]1/2^+$ and $[404]7/2^+$ bands

The $[411]1/2^+$ and $[404]7/2^+$ bands were previously reported to spins $29/2\hbar$ and $33/2\hbar$, respectively. These have now been extended to spins $67/2\hbar$ and $53/2\hbar$. Near spin $19/2\hbar$, the $\alpha = -1/2$ signatures of the two bands come close in energy and interact, caus-

[5] If multipoles higher than quadrupoles are excluded.

ing numerous cross-over transitions between the bands. To obtain a smooth progression of the moments-of-inertia for these bands, it has been necessary to change the previous assignment above spin $19/2^+\hbar$ and interchange levels between the bands in the interacting region. In this way it is ensured that the two signatures of the [404]$7/2^+$ band behave as normal signature partners with no signature splitting before and after the alignment of $i_{13/2}$ neutrons. The two bands are given a detailed band-mixing analysis in Section 5.1.

Spectra illustrating the high-spin part of the [411]$1/2^+$ band are shown in Fig. 6, (a), (b), and Fig. 5(d), while the double gated spectra of Fig. 6, (c) and (d), emphasize the [404]$7/2^+$ band and its link to the [411]$1/2^+$ band. Note that the E1 transition between the [404]$7/2^+$ and [541]$1/2^-$ bands are a consequence of the mixing between the [411]$1/2^+$ and [404]$7/2^+$ bands as they would otherwise be K-forbidden. Measured DCO ratios support the pure stretched dipole structure of these transitions. This interpretation is at variance with Ref. [27].

3.1.6. Band 2

A new strongly coupled band, labeled 2, which decays to the [404]$7/2^+$ band between spin $15/2^+\hbar$ and $19/2^+\hbar$ via transitions of 694, 786 and 888 keV, has been found. Spectra illustrating the coincidence relations for the established level scheme are shown in Fig. 6, (e) and (f). DCO ratios for the 694, 786 and 888 keV interband transitions strongly indicate stretched dipole character.

3.1.7. [402]$5/2^+$, [514]$9/2^-$ and [411]$3/2^+$ bands

New levels have been added to the [402]$5/2^+$ band, see Fig. 2, and the band has been extended from spin $9/2^+\hbar$ to spin $27/2^+\hbar$. The previously reported transitions linking the [402]$5/2^+$ band to the [404]$7/2^+$ band, have not been observed, and neither have any of previously reported transitions associated with the [514]$9/2^-$ and [411]$3/2^+$ bands. Presumably, these bands are too far from the yrast line to be populated with sufficient strength with the present reactions.

3.2. DSAM analysis of transitions in the [541]$1/2^-$ and [411]$1/2^+$ bands

The Doppler Shift Attenuation Method was used to obtain lifetimes of high-spin states in the [541]$1/2^-$ and [411]$1/2^+$ bands. The method is discussed in detail by Gascon et al. [11], and only an outline is given here.

The stopping process of the recoiling ions in the target and backing is first dominated by electronic stopping and then, at lower energies, nuclear stopping, which involves collisions between nuclei of the host material and the recoiling nuclei. The velocity distributions of the recoiling ions are calculated in a Monte Carlo approach developed by W.M. Currie [28], using empirical electronic stopping powers [29], corrected for shell effects [30,31], and nuclear stopping described by the differential Lindhardt cross section [32]. The simulation code, by J.C. Bacelar [33], is used to calculate lineshapes as a function of time, in steps of 5 fs. By solving the Bateman's equations for the yield emitted in the same time steps, the lineshapes for each step are weighted by the yield and added together to form the

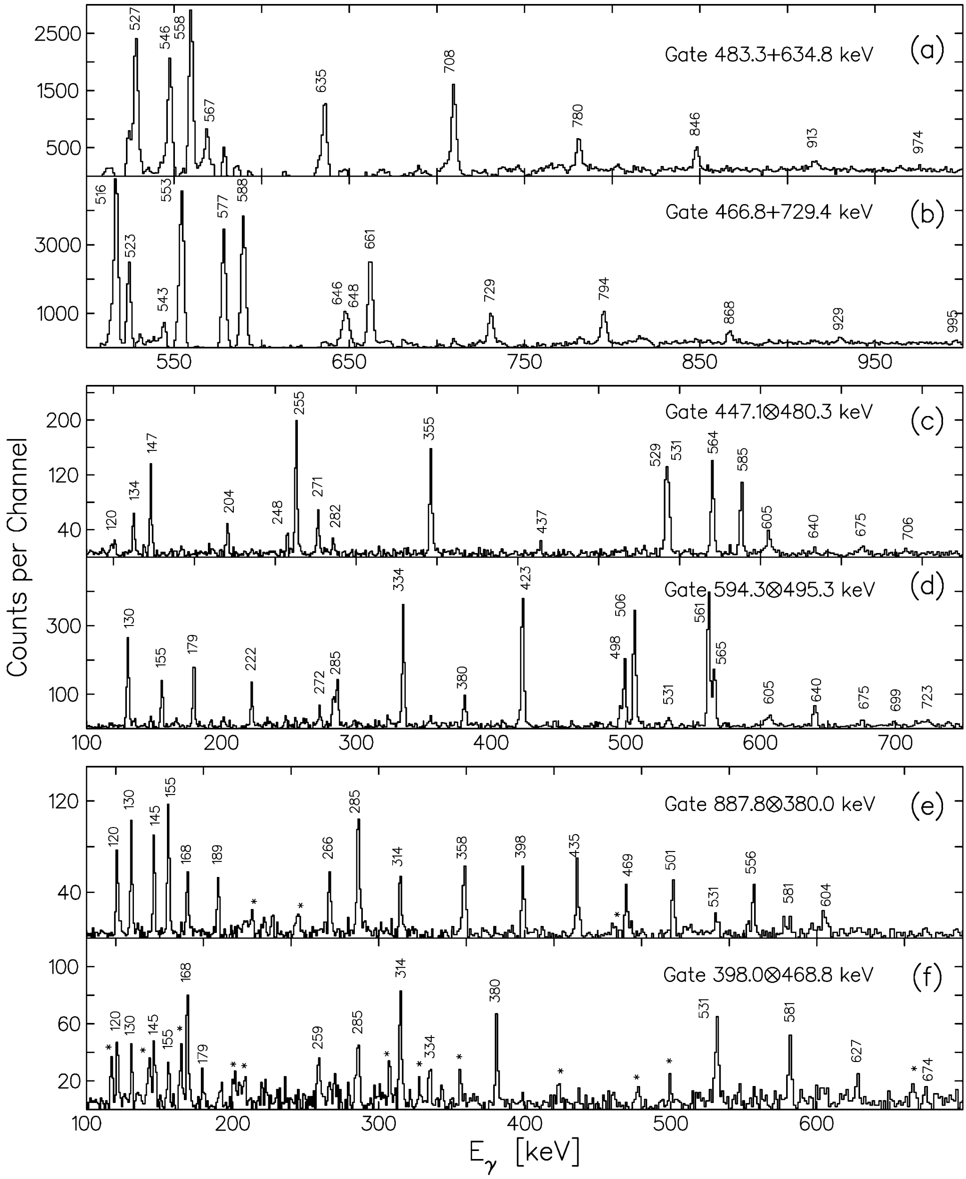

Fig. 6. ((a) and (b)) Coincidence spectra illustrating the high-spin part of band [411]1/2$^+$. ((c) and (d)) Double gated spectra illustrating the high-spin part of band [404]7/2$^+$, and the crossing between bands [411]1/2$^+$ and [404]7/2$^+$. ((e) and (f)) Double gated spectra showing the new band 2.

simulated lineshape for a given set of lifetimes of all states involved in the cascade and its feeding. A least-squares fitting procedure finds the optimal lifetimes for states involved in the cascade [11,33].

For each of the two backing materials (Au and Pb), four $\gamma\gamma$-matrices — one for each polar angle $\theta = 37°$, $79°$, $101°$ and $143°$, versus the sum of all angles — were used in the DSAM analysis. Gates on transitions in all bands were inspected to find suitable spectra, free of contaminating lines, for the analysis of the Doppler broadened lineshapes of E2 cascade transitions down the bands. It was not possible to gate above any transitions of interest (and consequently eliminate the uncertainty connected to the simulation of the time-structure in the side-feeding) due largely to a lack of statistics, but suitable gates below were found for both signatures of the $[411]1/2^+$ band and for the favoured signature of the $[541]1/2^-$ band. They were the 483 keV $37/2^+ \to 33/2^+$ and 527 keV $29/2^+ \to 25/2^+$ transitions of the positive signature of the $[411]1/2^+$ band and the 516 keV $39/2^+ \to 35/2^+$ and 467 keV $35/2^+ \to 31/2^+$ transitions of the negative signature, and the 474 keV $25/2^- \to 21/2^-$ transition of the $[541]1/2^-$ band.

The decay times of the states were successively determined from above. The side-feeding intensities were fitted by modeling the time structure of the side-feeding intensities as a cascade of three transitions all sharing the same effective transition quadrupole moment, Q_s, and a fixed $J^{(2)}$ moment of inertia of $65.0\,\hbar^2$ MeV^{-1}. Examples of fitted spectra are shown in Fig. 7.

Transition quadrupole moments were extracted from lifetimes using the rigid rotational model formula. The lifetimes and quadrupole moments obtained from the Pb-backed data are listed in Table 2 and presented in Fig. 8. The statistics for the Au-backed data are less than a third of that collected with the Pb backing. The quadrupole moments are identical, within the uncertainties, for both backings. An additional 5% systematic error has been added to the uncertainties listed in Table 2 to account for uncertainties in the electronic stopping powers.

Table 2
Level lifetimes and quadrupole moments of the $\Delta I = 2$ transitions of the $[541]1/2^-$ and $[411]1/2^+$ bands in ^{165}Tm

$[Nn_3\Lambda]\Omega^\pi$	$I_i \to I_f$	E_γ (keV)	τ (ps)	Q_t (b)	Q_s (b)
$[541]1/2^-$	$33/2^- \to 29/2^-$	618.3(2)	$0.27^{+0.05}_{-0.05}$	$9.8^{+0.9}_{-0.9}$	$6.40^{+0.25}_{-0.25}$
	$37/2^- \to 33/2^-$	674.3(2)	$0.26^{+0.04}_{-0.04}$	$7.9^{+0.6}_{-0.6}$	$6.40^{+0.25}_{-0.25}$
	$41/2^- \to 37/2^-$	717.3(2)	$0.22^{+0.03}_{-0.03}$	$7.3^{+0.5}_{-0.5}$	$6.40^{+0.25}_{-0.25}$
	$45/2^- \to 41/2^-$	741.9(2)	$0.15^{+0.02}_{-0.02}$	$8.1^{+0.6}_{-0.6}$	$6.40^{+0.25}_{-0.25}$
	$49/2^- \to 45/2^-$	762.8(2)	$0.10^{+0.03}_{-0.04}$	$9.3^{+1.6}_{-1.5}$	$6.40^{+0.25}_{-0.25}$
	Weighted average $Q_t = 8.3 \pm 0.5$ b, $\beta_2 = 0.33 \pm 0.02$				
$[411]1/2^+$	$45/2^+ \to 41/2^+$	634.8(2)	$0.27^{+0.05}_{-0.06}$	$9.0^{+1.0}_{-0.9}$	$7.55^{+0.50}_{-0.60}$
	$47/2^+ \to 43/2^+$	660.8(2)	$0.29^{+0.05}_{-0.04}$	$8.0^{+0.6}_{-0.7}$	$7.45^{+0.30}_{-0.30}$
	$49/2^+ \to 45/2^+$	708.4(2)	$0.20^{+0.04}_{-0.05}$	$8.1^{+1.0}_{-0.8}$	$7.55^{+0.50}_{-0.60}$
	$51/2^+ \to 47/2^+$	729.4(2)	$0.18^{+0.03}_{-0.02}$	$7.9^{+0.5}_{-0.6}$	$7.45^{+0.30}_{-0.30}$
	$53/2^+ \to 49/2^+$	779.9(2)	$0.20^{+0.07}_{-0.05}$	$6.2^{+0.8}_{-1.1}$	$7.55^{+0.50}_{-0.60}$
	$55/2^+ \to 51/2^+$	793.9(2)	$0.21^{+0.07}_{-0.04}$	$5.8^{+0.5}_{-1.0}$	$7.45^{+0.30}_{-0.30}$
	Weighted average $Q_t = 7.4 \pm 0.5$ b, $\beta_2 = 0.30 \pm 0.02$				

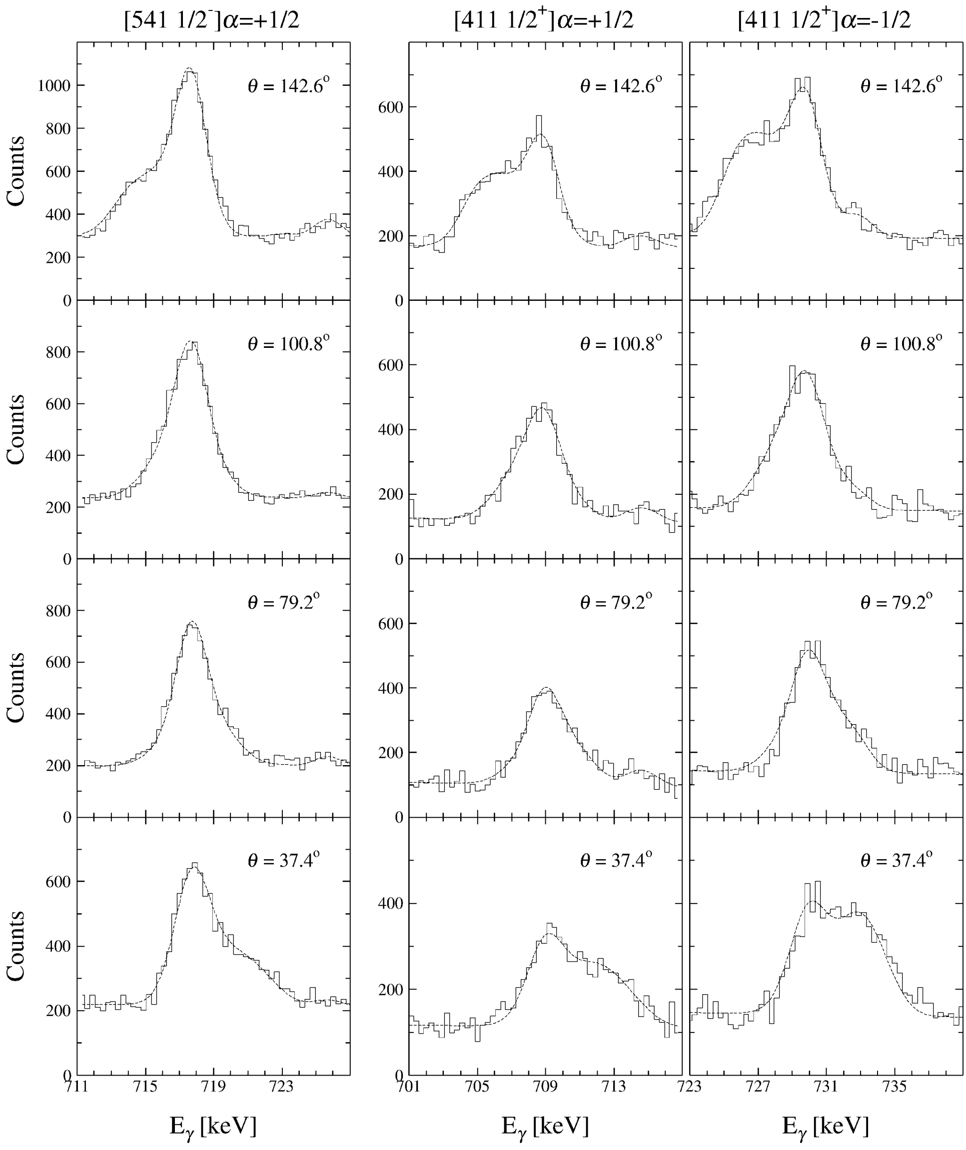

Fig. 7. Examples of observed and fitted peak shapes at the four detector angles, $\theta = 142.6°$, 100.8°, 79.2°, and 37.4°, for the 717.3 keV $I = 41/2^- \to 37/2^-$ transition of the [541]$1/2^-$ ($\alpha = +1/2$) band (left column), 708.4 keV $I = 49/2^+ \to 45/2^+$ transition of the [411]$1/2^+$ ($\alpha = +1/2$) band (middle column), and the 729.4 keV $I = 51/2^+ \to 47/2^+$ transition of the [541]$1/2^-$ ($\alpha = -1/2$) band (right column). Data from the experiment with lead backing are shown as histograms and the fitted shapes as dashed lines.

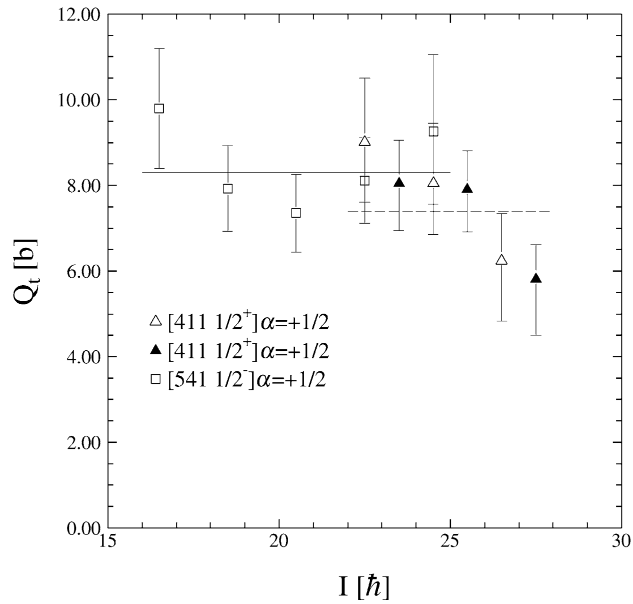

Fig. 8. Measured quadrupole moments for band [541]1/2$^-$ ($\alpha = +1/2$) (squares) and [411]1/2$^+$ ($\alpha = \pm 1/2$) (triangles). The weighted average is shown with solid (8.3 $\pm$ 0.5 b) and dashed (7.4 $\pm$ 0.5 b) lines for the [541]1/2$^-$ and [411]1/2$^+$ bands, respectively.

4. Interpretation of band structures

Figs. 9, (a) and (b), show experimental aligned angular momenta, i_x, while Figs. 10, (a) and (b), show the corresponding Routhians. Backbends (or upbends) in the alignment plots are understood as being due to band crossings. In the rare-earth region, the first backbend is attributed to the alignment of $i_{13/2}$ neutrons, which in the CSM terminology is denoted as the AB crossing [6]. Crossing frequencies, $\hbar\omega_c$, and gain in aligned angular momenta, Δi_x, for the crossings observed in the various bands are listed in Table 3 together with the corresponding values for the neighbouring even–even nuclei.

The new bands in ^{165}Tm are assigned configurations by examining properties such as aligned angular momenta, crossing frequencies and B(M1)/B(E2) ratios.

4.1. B(M1)/B(E2) values

Experimental ratios of B(M1)/B(E2) for the high-K bands ($K \geqslant 5/2$) are shown in Fig. 11, where they are compared with theoretical estimates based on an extension of the semiclassical formula by Dönau and Frauendorf [36,37]. The experimental values were obtained from the data according to:

$$\frac{B(\mathrm{M1}, I \to I-1)}{B(\mathrm{E2}, I \to I-2)} = 0.6967 \frac{E_2^5(I \to I-2)}{E_1^3(I \to I-1)} \frac{1}{\lambda(1+\delta^2)}. \tag{3}$$

In addition to the branching ratio λ, the E2/M1 mixing ratio, δ, is required. Of the bands in Fig. 11 the mixing ratio has only been determined from the DCO analysis for the [404]7/2$^+$

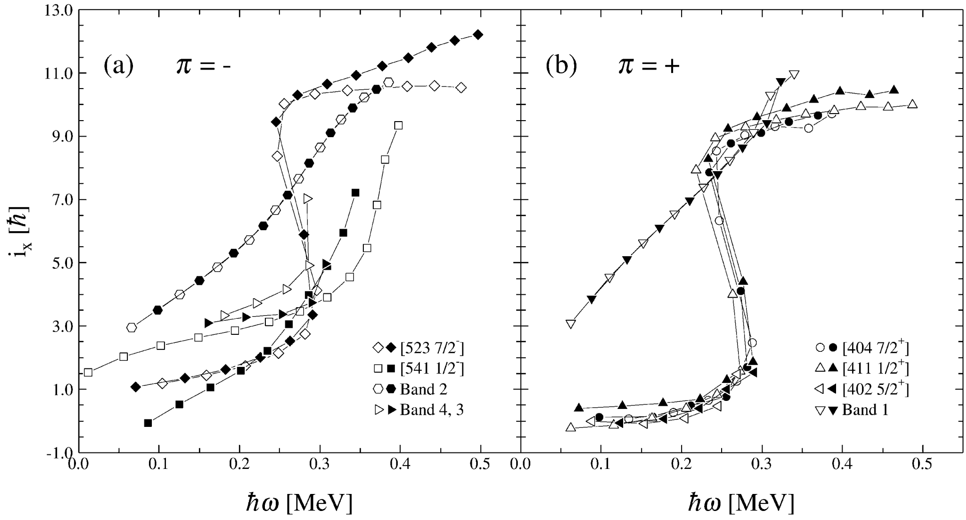

Fig. 9. Aligned angular momenta for bands in ^{165}Tm with (a) negative and (b) positive parity versus rotational frequency $\hbar\omega$. Data are shown relative to a reference configuration with a moment of inertia parameterized by the Harris parameters $\mathcal{J}_0 = 35.0\ \hbar^2/\text{MeV}$ and $\mathcal{J}_1 = 43.0\ \hbar^4/\text{MeV}^3$.

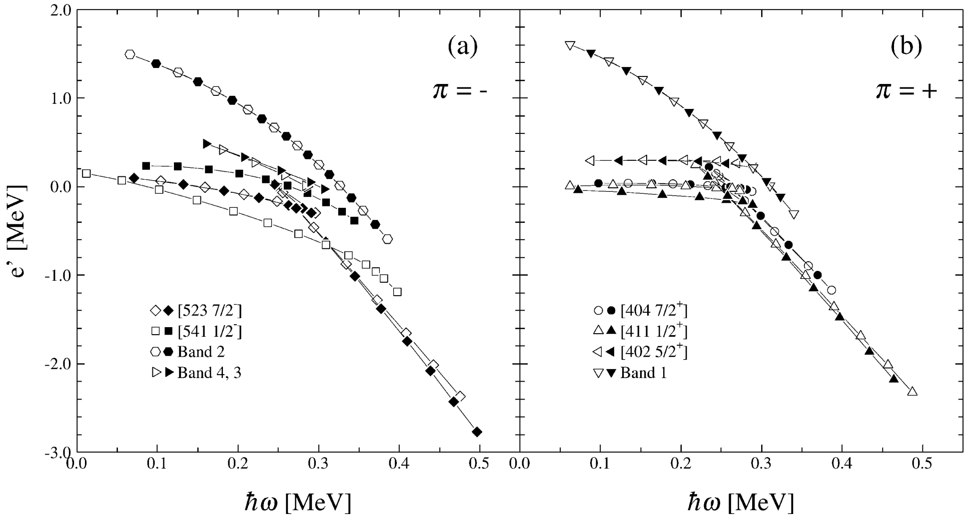

Fig. 10. Experimental Routhians for bands in ^{165}Tm with (a) negative and (b) positive parity versus rotational frequency $\hbar\omega$. Data are shown relative to a reference configuration with a moment of inertia parameterized by the Harris parameters $\mathcal{J}_0 = 35.0\ \hbar^2/\text{MeV}$ and $\mathcal{J}_1 = 43.0\ \hbar^4/\text{MeV}^3$.

band. For the remaining bands, δ was taken to be zero, and since δ is expected to have a magnitude of less than 0.3, the experimental $B(\text{M1})/B(\text{E2})$ ratios may be overestimated by up to 10%. Levels that are mixed due to known band-crossings (e.g. the $[404]7/2^+$ and $[411]1/2^+$ crossing near spin $19/2\hbar$) were corrected to obtain pure branching ratios λ.

Table 3
Rotational frequencies, $\hbar\omega_c$ and gain in aligned angular momentum, Δi_x, at the AB-band crossing for rotational bands in ^{165}Tm, and for the yrast band in the neighbouring even–even nuclei ^{164}Er [34] and ^{166}Yb [35]

Nucleus	$[Nn_3\Lambda]\Omega^\pi$	α	$\hbar\omega_c$ (keV)	Δi_x ($\hbar$)	$\Delta e'$ (keV)[a]
^{165}Tm	[523]7/2$^-$	+1/2	270^{+2}_{-4}	$7.9^{+0.3}_{-0.3}$	< 5
		−1/2	272^{+2}_{-4}	$7.9^{+0.3}_{-0.3}$	
	[541]1/2$^-$	+1/2	355^{+15}_{-5}	> 5.3	442 ± 3
		−1/2	$\sim 300^{+20}_{-20}$	?	
	Band 2	+1/2	Blocked	–	< 1
		−1/2	Blocked	–	
	Band 4	+1/2	> 280	?	$\sim 8 \pm 2$
	Band 3	−1/2	> 290	?	
	[404]7/2$^+$	+1/2	261^{+2}_{-4}	$8.1^{+0.3}_{-0.3}$	< 3
		−1/2	261^{+2}_{-4}	$8.1^{+0.3}_{-0.3}$	
	[411]1/2$^+$	+1/2	247^{+4}_{-4}	$8.2^{+0.3}_{-0.3}$	113 ± 3
		−1/2	262^{+4}_{-4}	$8.2^{+0.3}_{-0.3}$	
	[402]5/2$^+$	+1/2	?	?	8 ± 2
		−1/2	?	?	
	Band 1	+1/2	Blocked	–	< 3
		−1/2	Blocked	–	
^{164}Er	Yrast band	0	281 ± 2	$7.0^{+0.5}_{-0.5}$	
^{166}Yb	Yrast band	0	269 ± 2	$7.9^{+0.5}_{-0.5}$	

[a] Signature splitting, $\Delta e'$, extracted at $\hbar\omega = 200$ keV.

The measured $B(\mathrm{M1})/B(\mathrm{E2})$ values are in good agreement with the semiclassical estimates for the [404]7/2$^+$, [402]5/2$^+$ and [523]7/2$^-$ bands. In these calculations, g_R was taken to be 0.32, the g_K values were obtained from Ref. [38] and Q_0 taken to be 7.2 e b, an average of the measured values (see Sections 3.2 and 6.2.1). The alignments i_x were obtained from Fig. 9 and similar plots for ^{164}Er and ^{166}Yb.

4.2. New bands: configuration assignments

4.2.1. Band 1

The excitation energy of the head of band 1, around 2 MeV, is compatible with a three-quasiparticle excitation. Considering its decay to the [523]7/2$^-$ band, a candidate configuration would be a [523]7/2$^-$ proton coupled to the negative-parity configuration ν[642]5/2$^+$ $\otimes$ ν[523]5/2$^-$ (or AE and AF in CSM terminology) observed in the even–even neighbours. The band has a large value of aligned angular momentum at low rotational frequencies, which increases gradually to around 10$\hbar$ at the highest frequency, see Fig. 9. The large aligned angular momentum at low frequency is consistent with a contribution from an aligned $i_{13/2}$ neutron, in which case the gradual upbend would be due to the development of a BC alignment with a strong interaction. This is consistent with the CSM,

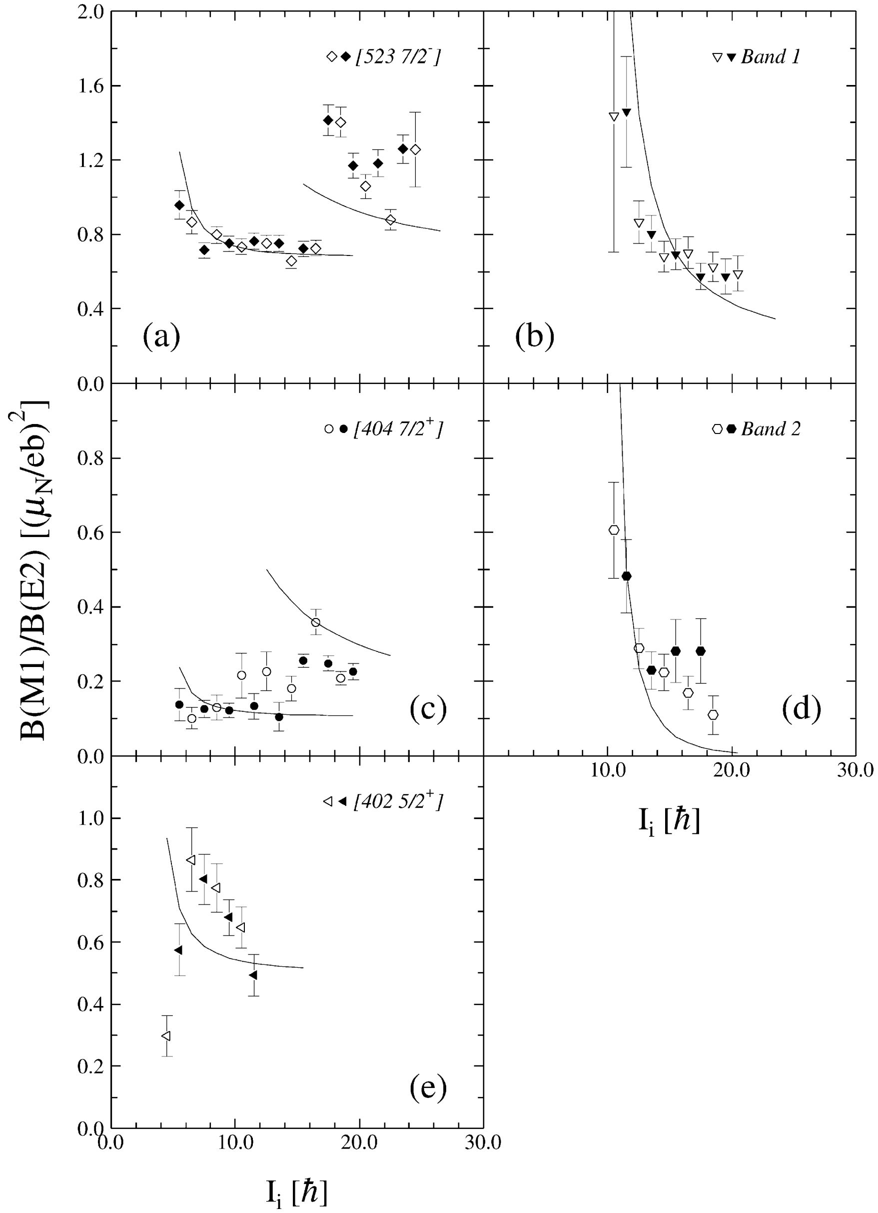

Fig. 11. Experimental and calculated $B(\mathrm{M1})/B(\mathrm{E2})$ ratios for band $[523]7/2^{-}$, bands 1, $[404]7/2^{+}$, bands 2 and $[402]5/2^{+}$. See text for further details.

which predicts that the BC crossing has a much larger interaction strength ($\sim$ 200 keV) than the AB crossing ($\sim$ 50 keV). This prediction is also qualitatively confirmed by observations in the neighbouring even–even isotopes.

The proposed configuration, $\pi[523]7/2^{-} \otimes \nu[642]5/2^{+} \otimes \nu[523]5/2^{-}$, would have a bandhead with $K^{\pi} = 17/2^{+}$, consistent with the data, and has $B(\mathrm{M1})/B(\mathrm{E2})$ values which are in good agreement with the experimental values, see Fig. 11(b). The most obvious alternative at higher excitation, the $[523]7/2^-$ proton coupled to the negative-parity configuration $\nu[642]5/2^+ \otimes \nu[521]3/2^-$ (AG or AH), could easily be excluded due to large deviations (typically more than 0.4 $(\mu_N/e\,\mathrm{b})^2$) between the experimental $B(\mathrm{M1})/B(\mathrm{E2})$ values and the semiclassical estimate.

4.2.2. Band 2

Band 2 has similar excitation energy and alignment to band 1, and thus similar arguments apply to its configuration assignment. The negative parity and the decay to the $[404]7/2^+$ band argues for a $\pi[404]7/2^+ \otimes \nu[642]5/2^+ \otimes \nu[523]5/2^-$ configuration assignment. This assignment implies a value of $K^\pi = 17/2^-$, which is compatible with the observed bandhead, and has $B(\mathrm{M1})/B(\mathrm{E2})$ values in good agreement with the measured values, see Fig. 11(d). The most obvious alternative, the $[404]7/2^+$ proton coupled to the negative-parity configuration $\nu[642]5/2^+ \otimes \nu[521]3/2^-$ (AG or AH), could be excluded with the same arguments given for band 1.

4.2.3. Bands 3 and 4

At low frequencies, the aligned angular momentum of bands 3 and 4 is consistent with one aligned quasiparticle, which is unlikely to be an $i_{13/2}$ neutron as the band evidently does not show a strongly interacting BC crossing, as do bands 1 and 2. Instead they show a crossing at the same frequency as the (unblocked) AB crossing in the $[523]7/2^-$ band. The decay to the $[541]1/2^-$ band suggests the aligned particle to be an $h_{9/2}$ proton. The energies for the spin 15/2 and 17/2 levels, 1289.7 and 1442.4 keV, respectively, while low, do not completely exclude a three-quasiparticle structure. However, due to the loss of intensity to the $[541]1/2^-$ band, it is likely that the bandheads have not been observed. In the even–even neighbours ^{164}Er and ^{166}Yb, γ-vibrational bands based on levels at 860 and 932 keV (similar to the difference in excitation energy at low spins for band $[541]1/2^-$ and bands 3, 4) have been reported [34,35], opening the possibility that bands 3 and 4 are members of a γ band coupled to an $h_{9/2}$ proton.

This interpretation is supported by similarities to ^{164}Er for the ratio between the decay strength out of the γ band, $B(\mathrm{E2})_{\mathrm{out}}$, and the inband strength, $B(\mathrm{E2})_{\mathrm{in}}$. The average values for the ratios

$$\frac{B(\mathrm{E2};\, I \to I)_{\mathrm{out}}}{B(\mathrm{E2};\, I \to I-2)_{\mathrm{in}}} \quad \text{and} \quad \frac{B(\mathrm{E2};\, I \to I-2)_{\mathrm{out}}}{B(\mathrm{E2};\, I \to I-2)_{\mathrm{in}}}$$

are 0.03(2) and 0.0017(12), respectively, for even spins in ^{164}Er. The corresponding values for band 4 are 0.14(2) and 0.0042(11), respectively. The average values for the ratios

$$\frac{B(\mathrm{E2};\, I \to I+1)_{\mathrm{out}}}{B(\mathrm{E2};\, I \to I-2)_{\mathrm{in}}} \quad \text{and} \quad \frac{B(\mathrm{E2};\, I \to I-1)_{\mathrm{out}}}{B(\mathrm{E2};\, I \to I-2)_{\mathrm{in}}}$$

are 0.08(4) and 0.020(9), respectively, for odd spins in ^{164}Er. Only the $I \to I-1$ transitions were observed for band 3, and with an average ratio of 0.03(2). The expected $B(\mathrm{E2};\, I \to I+1)_{\mathrm{out}}/B(\mathrm{E2};\, I \to I-2)_{\mathrm{in}}$ ratio for band 3 implies intensities for the missing $I \to I+1$ transitions below the detectable limit in the present experiments. The $B(\mathrm{E2})_{\mathrm{out}}/B(\mathrm{E2})_{\mathrm{in}}$

decay strength ratios for bands 3 and 4 in ^{165}Tm are all slightly larger than found for the γ-vibrational band in ^{164}Er, which indicate vibrational rather than single-particle strength for $B(\mathrm{E2})_{\mathrm{out}}$ in ^{165}Tm.

M1 decay strength is not expected for $\Delta K = 2$ transitions form a γ-vibrational band, but can occur, presumably caused by mixing. Some examples of admixed M1 strength are found for the decay between bands 3 and 4 and the $[541]1/2^-$ band (see Section 3.1.4). Mixing ratios of similar magnitude and sign are also measured in the decay from the γ-vibrational band to the ground band in ^{164}Er. Furthermore, gamma bands of similar excitation energy have been suggested [39] in ^{167}Tm.

5. Band mixing and relative deformations

In Fig. 12, the energies of the positive and negative-parity bands, relative to a rigid rotor reference, are plotted as a function of spin. A close inspection of Fig. 12, and the level scheme, reveals many examples of bandcrossings. In Table 4, all pairs of bands that have a minimum level separation of less than 40 keV are listed. The minimum separation energy gives an estimate of the maximum interaction strength. When interband transitions are also observed, it is possible to deduce relative quadrupole moments by means of a two-band (or two-level) mixing analysis. Such crossings occur between the $[411]1/2^+$ and $[404]7/2^+$ bands, and the $[541]1/2^-$ and $[523]7/2^-$ bands.

5.1. $[411]1/2^+$ and $[404]7/2^+$ bands

To obtain the relative transition quadrupole moments between the $[411]1/2^+$ and $[404]7/2^+$ bands, a two-band mixing analysis was performed using the model described in

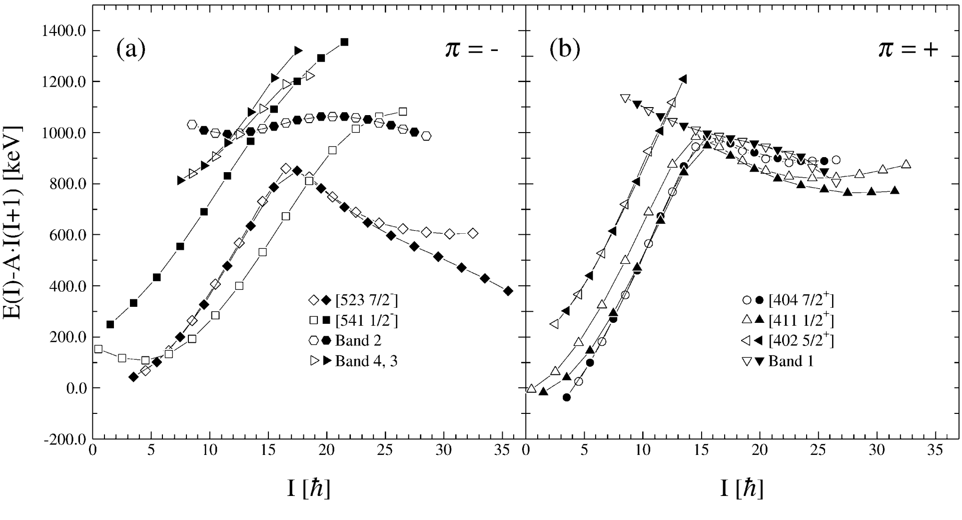

Fig. 12. Excitation energy versus spin for the negative (a) and positive (b) parity bands of ^{165}Tm relative to a rigid rotor with a moment of inertia $\mathcal{J}_{\mathrm{rig}} = 67.0\ \hbar^2/\mathrm{MeV}$.

Table 4
Minimum level distances between rotational bands of ^{165}Tm

		α	ΔE [keV]	I [$\hbar$]
[523]7/2$^-$	[541]1/2$^-$	+1/2	13.8(4)	13/2
[523]7/2$^-$	[541]1/2$^-$	−1/2	16.5(6)	37/2
[541]1/2$^-$	Band 2	+1/2	23.4(11)	49/2
[541]1/2$^-$	Band 2	−1/2	38.4(5)	27/2
Band 4	Band 2	+1/2	4.6(5)	25/2
Band 3	Band 2	−1/2	35.4(5)	23/2
[404]7/2$^+$	[411]1/2$^+$	+1/2	28.1(6)	33/2
[404]7/2$^+$	[411]1/2$^+$	−1/2	10.4(4)	19/2
Band 1	[404]7/2$^+$	+1/2	15.6(7)	33/2
Band 1	[404]7/2$^+$	−1/2	14.0(6)	31/2
Band 1	[411]1/2$^+$	+1/2	18.5(11)	53/2

Energy distance, ΔE, and spin, I, is given for "crossings" if the separation is less than 40.0 keV.

Table 5
Parameters determined from two band-mixing calculations for band [411]1/2$^+$ and [404]7/2$^+$

Band	$\Im_{0i}$ (10^{-2} keV^{-1})	C_i (10^6 keV^3)	i_{xi} ($\hbar$)	K_i ($\hbar$)	E_{0i} (keV)	Q_{0i} (b)	V_{int} (keV)
[404]7/2$^+$	3.37	4.32	0.0	≡ 3.5	28.9	7.1(6)	5.0(5)
[411]1/2$^+$	3.77	7.88	0.0	≡ 0.5	−46.2	≡ 7.4	

I ($\hbar$)	Wave-function amplitudes				Excitation energy (keV)			
	"[404]7/2$^+$"		"[411]1/2$^+$"		"[404]7/2$^+$"		"[411]1/2$^+$"	
	[404]7/2$^+$	[411]1/2$^+$	[404]7/2$^+$	[411]1/2$^+$	E_{exp}	E_{calc}[a]	E_{exp}	E_{calc}[a]
3.5	0.9979	−0.0643	0.0643	0.9979	80.3(2)	80.16	158.8(2)	157.75
5.5	0.9950	−0.1003	0.1003	0.9950	365.7(3)	365.82	413.2(2)	415.68
7.5	0.9773	−0.2118	0.2118	0.9773	745.6(3)	744.78	767.9(3)	768.81
9.5	0.7460	−0.6660	0.6660	0.7460	1204.8(3)	1203.13	1215.2(3)	1213.14
11.5	0.9274	0.3741	−0.3741	0.9274	1744.7(3)	1743.98	1727.8(3)	1729.64
13.5	0.9323	0.3618	−0.3618	0.9323	2329.7(3)	2343.32	2305.0(3)	2328.57

A labeling "$[Nn_3\Lambda]\Omega^\pi$" and $[Nn_3\Lambda]\Omega^\pi$ for perturbed and unperturbed bands respectively, is used.
≡ Denotes value kept fixed in the fit.
[a] E_{calc} is the calculated perturbed energy.

Ref. [40]. Briefly, two unperturbed bands are parameterized using a VMI [41] expression and allowed to interact with a spin-independent interaction, V_{int}. The parameters describing the unperturbed bands, the interaction, and the relative quadrupole moments of the unperturbed bands, are varied to obtain a best fit to the level energies and inband/outband branching ratios. The resulting parameters are listed in Table 5, and the quality of the fit can be judged in Fig. 13, where calculated energies and branching ratios, according to the best

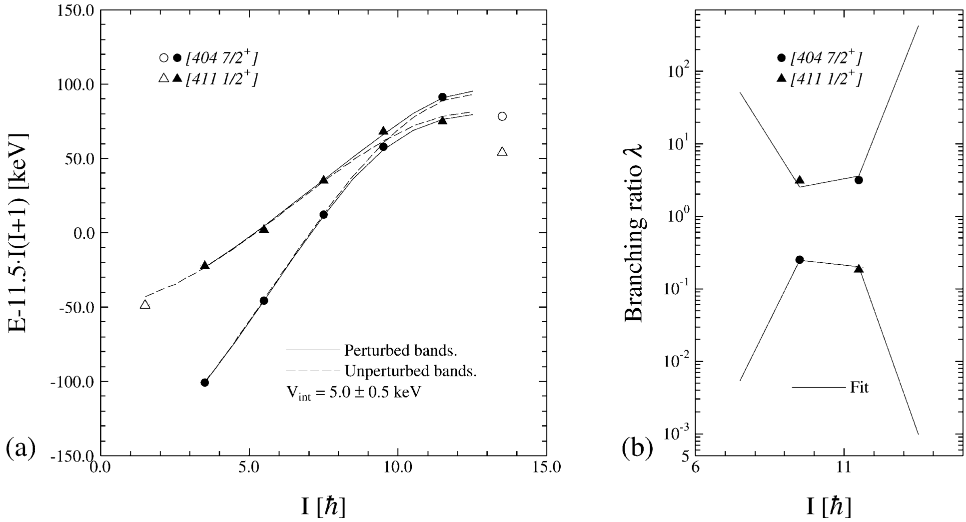

Fig. 13. Results of two-band mixing calculations for bands [411]1/2+ and [404]7/2+. Filled symbols are included in the fit. Solid and dashed lines for the calculated perturbed and unperturbed bands, respectively.

fit, are compared with the experimental quantities. An interaction strength of 5.0(5) keV and a value of 0.96(5) is found for the ratio $Q([404]7/2^+)/Q([411]1/2^+)$. If it can be assumed that the quadrupole moment of the [411]1/2+ band is constant as a function of spin, then the average values of Q_t measured for the [411]1/2+ band imply a value for the [404]7/2+ band of 7.1(6) e b. Consequently, within uncertainties, the two bands have the same deformation.

5.2. [541]1/2− and [523]7/2− bands

The crossing between the [541]1/2− and [523]7/2− bands, at spin 13/2−, is illustrated in Fig. 14. Because no E2 transitions between the bands are observed at this crossing, a different approach, which compares the strength of the inband E2 transitions with that of the $\Delta I = 1$ transitions linking the two bands, is employed. In this analysis, it is assumed that the two bands are only mixed in the vicinity of the crossing at the 13/2 levels. This assumption is justified by the observation that the interaction strength must be less than 6.9 keV, and that the level separation at the adjacent spins are considerably larger, see Fig. 12(a). Then writing the wave-functions of the perturbed levels in terms of the unperturbed levels at $I = 13/2$ as

$$\begin{aligned} \left|\text{“}[541]1/2^-\text{”}\right\rangle &:= \alpha \cdot \left|[523]7/2^-\right\rangle + \beta \cdot \left|[541]1/2^-\right\rangle, \\ \left|\text{“}[523]7/2^-\text{”}\right\rangle &:= -\beta \cdot \left|[523]7/2^-\right\rangle + \alpha \cdot \left|[541]1/2^-\right\rangle, \end{aligned} \tag{4}$$

a mixing angle θ can be defined and related to the interaction strength V_{int} and the perturbed energy difference $\Delta E = E_{ye} - E_{yr}$ via the amplitudes α and β

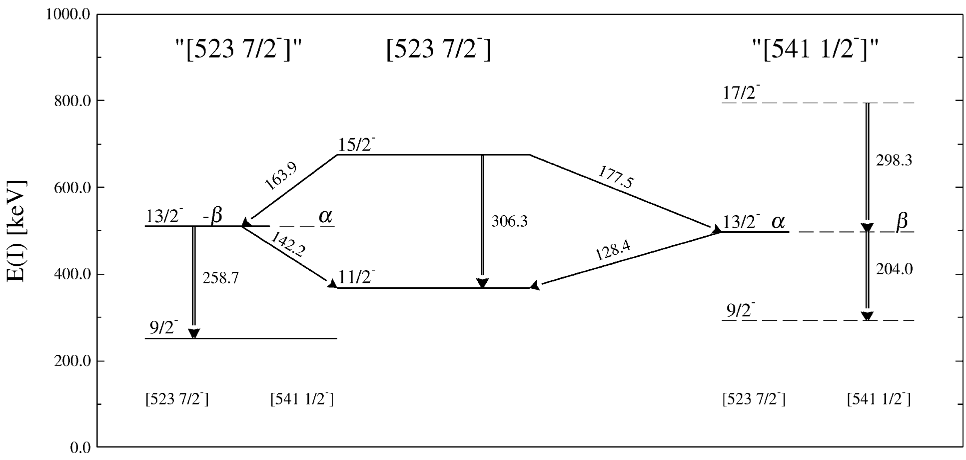

Fig. 14. Illustration of mixing between the $[541]1/2^-$ and $[523]7/2^-$ near the spin $13/2^-$ levels.

$$\alpha = \cos(\theta/2), \qquad \beta = \sin(\theta/2) = \sqrt{1-\alpha^2} \quad \text{and} \quad \sin(\theta) = \frac{2 \cdot V_{\text{int}}}{\Delta E}.$$

With no off diagonal matrix elements the M1 branching ratio from the $I = 15/2$ state in band $[523]7/2^-$ can be written

$$\frac{T_\gamma(163.9)}{T_\gamma(177.5)} = \left(\frac{0.1639}{0.1775}\right)^3 \cdot \left(\frac{\beta}{\alpha}\right)^2.$$

Similarly, the ratio of M1/E2 branching ratios from the two $I = 13/2$ states can be expressed as

$$\begin{aligned}\frac{\lambda_{13/2}(\text{“}[523]7/2^-\text{”})}{\lambda_{13/2}(\text{“}[541]1/2^-\text{”})} &= \frac{T_\gamma(258.7)/T_\gamma(142.2)}{T_\gamma(204.0)/T_\gamma(128.4)} \\ &= \left(\frac{0.2587}{0.2040}\right)^5 \cdot \left(\frac{0.1284}{0.1422}\right)^3 \cdot \left(\frac{\alpha}{\beta}\right)^2 \cdot \left(\frac{\langle \frac{13}{2}\frac{7}{2}20|\frac{9}{2}\frac{7}{2}\rangle}{\langle \frac{13}{2}\frac{1}{2}20|\frac{9}{2}\frac{1}{2}\rangle}\right)^2 \\ &\quad \times \left(\frac{Q_t([523]7/2^-)}{Q_t([541]1/2^-)}\right)^2, \end{aligned} \tag{5}$$

where the decay pattern, notation for admixed amplitudes and transition energies, are explained in Fig. 14.

With these equations it is possible to solve for the mixing amplitudes and obtain the interaction strength, $V_{\text{int}} = 1.75(18)$ keV, and deduce the relative quadrupole moments: $Q([541]1/2^-)/Q([523]7/2^-) = 1.16(9)$. The wave-function for the $[541]1/2^-$ configuration is known to be mixed with $\Omega \geqslant 3/2$ states. In the evaluation of the uncertainty for the relative quadrupole moments a possible 50% $\Omega = 3/2$ mixing was included in Eq. (5). If the average experimental value, $Q_t = 8.3(5)$ eb is used for the $[541]1/2^-$ band, then a quadrupole moment of $Q([523]7/2^-) = 7.2(7)$ eb is deduced.

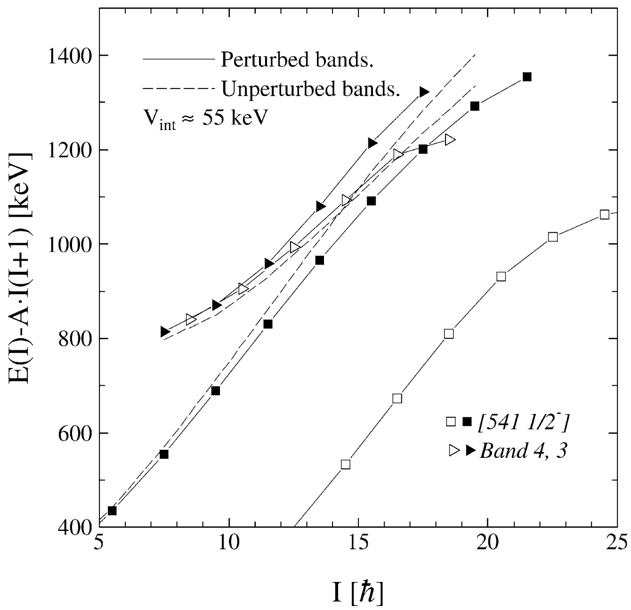

Fig. 15. Excitation energy versus spin relative to a rigid rotor with a moment of inertia $\mathcal{J}_{\rm rig} = 67.0\ \hbar^2/$ MeV, for bands [541]1/2$^-$, 3 and 4. Solid lines for the empirical bands, and dashed lines for the calculated unperturbed bands with $\alpha = -1/2$.

5.3. γ-band–[541]1/2⁻ crossing

A small signature splitting between bands 3 and 4 develops above spin 25/2, which can be seen in Fig. 12. The figure also suggests that the splitting could be due to an interaction of band 3 with the unfavoured signature of the [541]1/2$^-$ band. This possibility was tested using a two-band mixing calculation with the model described in Section 5.1. The results are illustrated in Fig. 15. The interaction was found to be 55 keV. Thus, in this model band 4 is unperturbed by the favoured signature of the [541]1/2$^-$ band due to a large energy separation of ≈ 600 keV, and the unperturbed levels of band 3 are found to have a negligible signature splitting relative to band 4. No signature splitting has been observed in the γ-vibrational bands of the neighbouring even–even nuclei at low spins. It is therefore expected (as a first approximation) that the γ-vibrational band built on the [541]1/2$^-$ configuration in ^{165}Tm has no signature splitting.

6. Crossing frequencies and alignments

Some pronounced similarities and differences can be seen in the alignment curves shown in Fig. 9. The three positive-parity bands, [404]7/2$^+$, [411]1/2$^+$ and [402]5/2$^+$ have a similar alignment pattern with almost identical AB band-crossing frequencies, $\hbar\omega_c$, and gain in aligned angular momentum, Δi_x. Likewise, the negative-parity [523]7/2$^-$ band has a crossing at the same frequency as that associated with the positive-parity one-quasiparticle bands. They all have $\hbar\omega_c$'s and Δi_x's which are close to the values observed in the neighbouring even nuclei ^{164}Er and ^{166}Yb. However, the AB crossing associated with the other negative-parity band, based on the $[541]1/2^-$ configuration, occurs at a much higher frequency, 0.355 MeV, compared with 0.275 MeV for the positive-parity bands. The crossing frequency is shifted up by about 80 keV. Such shifts in $\hbar\omega_c$ are now a well recognized feature of the $[541]1/2^-$ bands in the rare-earth region, with systematics documented in, e.g., Refs. [1,2,14].

In the CSM, a change in crossing frequency and alignment can be generated by a change in quadrupole deformation. This is because both the neutron pairing gap, Δ_ν, and the degree of Coriolis mixing depend on the position of the neutron Fermi level, λ_ν. The pairing depends upon the level density and the Coriolis mixing is stronger near low-Ω components of the $\nu i_{13/2}$ intruder shell. Since λ_ν depends on the shape parameters an early explanation put forward for the shift in crossing frequency was that the $[541]1/2^-$ proton polarized the core, and the resulting change in deformation caused the shift. Indeed the present and previous measurements of Q_t confirm the core polarization effect, but CSM calculations [6,42] using frequency adiabatic configurations based on both experimentally determined [10,11] and expected changes in equilibrium deformations [43] were only able to explain a fraction of the observed shift in $\hbar\omega_c$, varying from 20–60%, in the cases where these shifts are large [3,8,10,11]. A major drawback of the former *adiabatic* calculations is that constant deformation parameters and pairing gaps were used. These could be expected to be different for the one-quasiparticle bands and the three-quasiparticle S-bands, formed by the alignment of $i_{13/2}$ neutrons. Furthermore, the calculations did not address how well the CSM describes a second quantity observed in experiment, namely Δi_x, and no *systematic* comparisons between data and predictions, for either quantity, have been made.

6.1. CSM calculations

To obtain a systematic understanding of the shifts and alignment gain in the rare-earth region, calculations have been performed for the $[541]1/2^-$ bands of all odd-proton nuclei in the rare-earth region with $68 \leqslant Z \leqslant 77$ and $94 \leqslant N \leqslant 102$, and for the yrast bands of all even–even nuclei in the same region. Potential energy surfaces were calculated using the cranked Nilsson–Strutinsky code “Ultimate Cranker” [44–46]. The calculations were fully diabatic [44,45,47,48] up to a rotational frequency of 0.35 MeV, so that configurations such as the $h_{9/2}$ and $h_{11/2}$ orbitals could be separated unambiguously. The diabaticity enabled the energies and deformations of both the one-quasiparticle, and corresponding three-quasiparticle bands, to be calculated independently, free of mixing at the crossing, by minimizing the potential energy surfaces. Frequency independent monopole pairing was used at each mesh point of the potential energy surface, expressed as a fraction of the BCS pairing gap at $\hbar\omega = 0$, for the proton one-quasiparticle configuration, and the neutron zero- and two-quasiparticle configurations. These fractions were calculated self-consistently at deformations appropriate for the band crossing [45]. Particle number projection was performed. Further details of the calculations have been given in [14], where the results for $N = 98$ isotones are presented.

6.2. Comparison of measured and calculated deformations

6.2.1. Deformations in ^{165}Tm

The quadrupole moments measured for the four bands are summarized in Table 6, where they are compared with the results of calculations. According to the calculations, the alignment of $i_{13/2}$ neutrons does not change the deformation of the bands significantly, and the bands maintain a constant quadrupole moment (typically changing by less than 0.2 e b) over the calculated frequency interval. This is the justification for the use of average quadrupole moments to deduce the values for the [404]7/2$^+$ and [523]7/2$^-$ bands. However, the calculated deformations are in general lower than the experimentally measured values by 1–8%. The largest deviation is for the [541]1/2$^-$ band, but even there the calculated value is just outside the range allowed by the uncertainties. Since there may be systematic errors in the stopping powers used in the DSAM analysis, it is also interesting to compare relative deformations. In Table 6, both the measured and calculated values, normalized to the quadrupole moment of the [541]1/2$^-$ S-band, are compared and found to be in good agreement. The [541]1/2$^-$ intruder orbital stands out with a quadrupole moment approximately 12% higher than the [411]1/2$^+$, [404]7/2$^+$ and [523]7/2$^-$ bands, confirming the core polarization.

6.2.2. Deformations in the rare-earth region

In Table 7, a complete set of calculated deformations for the mass region is listed. The core-polarizing effect of the [541]1/2$^-$ proton on the deformation is predicted as a general feature. This prediction is in qualitative agreement with previous measurements of Q_t's for the [541]1/2$^-$ band in ^{157}Ho, ^{161}Tm, ^{167}Lu and ^{169}Lu, [10–13], and with calculated deformations in the rare-earth region using the Woods–Saxon potential [43]. The [541]1/2$^-$ proton is found to drive the shape towards slightly positive γ-deformations, and generally ε_2 increases by around 0.04, compared with the even–even neighbours. However, the alignment of $i_{13/2}$ neutrons is predicted to have a smaller effect on the deformation, reducing the ε_2 deformation by typically less than 0.01 and driving to slightly negative γ-values.

Table 6
Calculated and experimentally deduced transition quadrupole moments and ratios of quadrupole moments, R

Band	Q_t (e b)	R^a	Q_{calc} (e b)	Q_{calc}(S-band) (e b)	$R_{calc}{}^b$
[541]1/2$^-$	8.3(5)	1.00	7.6	7.7	1.00
[411]1/2$^+$	7.4(5)	0.89(8)	7.3	7.1	0.92
[404]7/2$^+$	7.1(6)	0.86(9)	6.8	6.8	0.88
[523]7/2$^-$	7.2(7)	0.87(10)	6.9	6.8	0.90

[a] Normalized to experimental Q_t of [541]1/2$^-$ band.

[b] Normalized to theoretical Q_t of [541]1/2$^-$ S-band, using S-band Q_t for [411]1/2$^+$ band and one-quasiparticle Q_t for [404]7/2$^+$ and [523]7/2$^-$ bands.

Table 7

Predicted shape parameters, ε_2, ε_4 and γ, for the $[541]1/2^-$ (g-) and $[541]1/2^- \otimes$ AB (S-) band in isotopes of Tm, Lu, Ta, Re and Ir, and for the $(0,+)$ yrast (g-) and (S-) bands in the neighbouring even–even isotopes

Nucleus		$N=94$		$N=96$		$N=98$		$N=100$		$N=102$	
		g-band	S-band	g-band	S-band	g-band	S-band	g-band	S-band	g-band	S-band
Ir[a]	ε_2	–	–	0.209	0.205	0.221	0.208	0.229	0.214	0.229	0.217
	ε_4[b]	–	–	$\equiv 0.00$	$\equiv 0.00$	$\equiv 0.01$	$\equiv 0.01$	$\equiv 0.02$	$\equiv 0.02$	$\equiv 0.02$	$\equiv 0.02$
	γ°	–	–	5	−1	5	−1	2	−2	2	−2
	$\hbar\omega_c$ / Δi_x	–		220 keV / 10.9 $\hbar$		244 keV / 10.2 $\hbar$		252 keV / 10.1 $\hbar$		253 keV / 9.1 $\hbar$	
Re[a]	ε_2	–	–	0.232	0.227	0.241	0.234	0.252	0.245	0.251	0.241
	ε_4[b]	–	–	$\equiv 0.00$	$\equiv 0.00$	$\equiv 0.01$	$\equiv 0.01$	$\equiv 0.02$	$\equiv 0.02$	$\equiv 0.02$	$\equiv 0.02$
	γ°	–	–	3	−2	5	1	1	0	1	0
	$\hbar\omega_c$ / Δi_x	–		226 keV / 9.9 $\hbar$		263 keV / 9.4 $\hbar$		260 keV / 8.4 $\hbar$		274 keV / 8.4 $\hbar$	
W	ε_2	0.197	(0.186)[c]	0.220	0.216	0.228	0.216	0.240	0.233	0.244	0.233
	ε_4	0.001	(0.013)[c]	0.003	0.008	0.010	0.018	0.020	0.027	0.029	0.034
	γ°	−7	(9)[c]	−2	−6	−1	−5	−2	−4	−2	−5
	$\hbar\omega_c$ / Δi_x	193 keV / 10.8 $\hbar$		204 keV / 10.7 $\hbar$		232 keV / 10.1 $\hbar$		245 keV / 9.4 $\hbar$		249 keV / 9.1 $\hbar$	
Ta	ε_2	0.242	0.228	0.250	0.242	0.263	0.254	0.277	0.272	0.278	0.262
	ε_4	-0.004	0.003	0.004	0.008	0.013	0.019	0.024	0.028	0.032	0.034
	γ°	1	3	4	−2	2	−1	1	0	1	−1
	$\hbar\omega_c/\Delta i_x$	231 keV / 9.4 $\hbar$		234 keV / 9.5 $\hbar$		276 keV / 8.9 $\hbar$		275 keV / 7.8 $\hbar$		298 keV / 7.4 $\hbar$	
Hf	ε_2	0.214	0.205	0.236	0.231	0.252	0.237	0.264	0.253	0.266	0.250
	ε_4	−0.001	0.008	0.004	0.011	0.013	0.019	0.024	0.028	0.033	0.036
	γ°	−4	3	−3	−5	−1	−4	−2	-2	−1	−3
	$\hbar\omega_c/\Delta i_x$	201 keV / 10.0 $\hbar$		210 keV / 10.1 $\hbar$		251 keV / 9.5 $\hbar$		259 keV / 8.6 $\hbar$		271 keV / 8.2 $\hbar$	
Lu	ε_2	0.270	0.255	0.271	0.264	0.281	0.275	0.295	0.290	0.302	0.273
	ε_4	0.006	0.008	0.012	0.016	0.020	0.024	0.030	0.033	0.041	0.045
	γ°	1	0	2	−1	1	−1	1	0	1	−1
	$\hbar\omega_c/\Delta i_x$	255 keV / 9.4 $\hbar$		245 keV / 9.3 $\hbar$		295 keV / 8.0 $\hbar$		283 keV / 7.7 $\hbar$		354 keV / 5.9 $\hbar$	
Yb	ε_2	0.241	0.217	0.250	0.240	0.268	0.258	0.278	0.271	0.285	0.258
	ε_4	−0.002	0.010	0.007	0.012	0.019	0.027	0.031	0.035	0.039	0.043
	γ°	−5	4	−2	−5	−1	−3	−1	−1	−1	−3
	$\hbar\omega_c/\Delta i_x$	218 keV / 9.7 $\hbar$		217 keV / 9.8 $\hbar$		264 keV / 9.0 $\hbar$		270 keV / 7.7 $\hbar$		296 keV / 7.2 $\hbar$	
Tm	ε_2	0.279	0.257	0.271	0.262	0.280	0.275	0.289	0.288	0.297	0.272
	ε_4	−0.001	−0.001	0.003	0.007	0.008	0.015	0.019	0.023	0.030	0.031
	γ°	1	−1	1	−4	1	−1	1	0	1	−2
	$\hbar\omega_c/\Delta i_x$	263 keV / 9.0 $\hbar$		255 keV / 9.5 $\hbar$		298 keV / 7.6 $\hbar$		288 keV / 7.3 $\hbar$		363 keV / 5.6 $\hbar$	
Er	ε_2	0.245	0.237	0.254	0.249	0.267	0.259	0.276	0.274	0.286	0.263
	ε_4	−0.005	0.001	0.004	0.009	0.010	0.017	0.022	0.026	0.032	0.034
	γ°	−3	-3	−3	−6	−4	−5	−1	−2	−2	−4
	$\hbar\omega_c/\Delta i_x$	235 keV / 9.4 $\hbar$		225 keV / 9.4 $\hbar$		270 keV / 8.6 $\hbar$		274 keV / 7.8 $\hbar$		309 keV / 7.1 $\hbar$	

Values are given for spin values just before and after the crossing, respectively. Predicted rotational frequencies, $\hbar\omega_c$, and gain in aligned angular momenta, Δi_x, at the AB-band crossing are given too.

[a] Values for Re and Ir are from [47].

[b] ε_4 was fixed in the calculations for Re and Ir isotopes.

[c] Values for the S-band in ^{168}W are uncertain.

A comparison between predicted and measured quadrupole deformations for the $[541]1/2^-$ band, with available data in the rare-earth region, reveals that the typical deviations are of the same relative size as for ^{165}Tm. For ^{169}Lu [10] and ^{179}Ir [49] the predicted values are, for example, higher by 5 and 7%, respectively. For the even–even nucleus ^{168}W [50] they are higher by 6% and lower by 9% for the g- and S-band, respectively.

6.3. *Comparison of measured and calculated crossing frequencies and alignments*

The crossing frequencies and gain in aligned angular momentum of the even–even nuclei are considered first. The experimental values are listed in Table 8 and plotted in Fig. 16, where they are compared with the experimental quantities. The crossing frequencies and alignment gain for the even–even nuclei are, respectively, under- and overestimated by the calculations. The reason for the discrepancy is not understood, but may be related to pairing. Note that in the CSM calculations of Bengtsson and Frauendorf [6], empirical values of the pairing gap parameter Δ were employed, which are larger than those calculated self-consistently here. An increase in pairing would increase the crossing frequency and decrease the gain in aligned angular momentum. Thus the present discrepancy could indicate that the pairing strength used here is inadequate, or that higher terms, such as quadrupole pairing, are necessary to explain the even–even cases.

It is interesting to test the predictions for rotational bands in odd-Z nuclei which are known to have bandcrossings similar to those of their even–even neighbours. Calculated $\hbar\omega_c$'s and Δi_x's for the $\pi h_{11/2}[514]9/2^-$ configuration, in the Ta isotopes, are compared with the neighbouring even–even Hf and W isotopes in Fig. 17, (a) and (b), respectively.

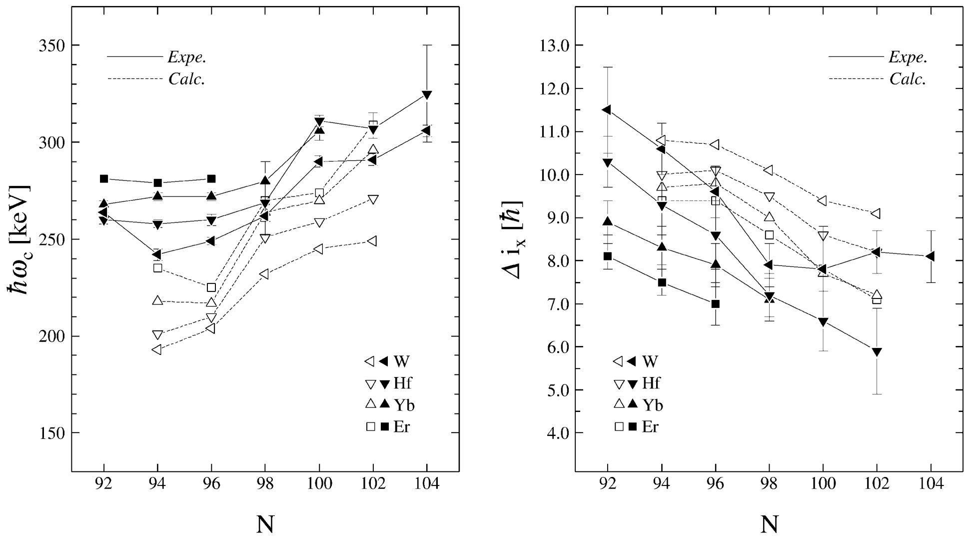

Fig. 16. Experimental (solid lines) and predicted (dashed lines) (a) frequency, $\hbar\omega_c$, and (b) gain in aligned angular momentum, Δi_x, at the crossing with the S-band for the $(0,+)$ yrast configuration in even-N isotopes of Er, Yb, Hf and W.

Table 8

Experimental rotational frequencies, $\hbar\omega_c$ (in keV), and gain in aligned angular momenta, Δi_x (in $\hbar$), at the AB-band crossing for the [541]1/2$^-$ band in isotopes of Ho, Tm, Lu, Ta, Re and Ir, and for the yrast band (g-band) in the neighbouring even–even isotopes of Er, Yb, Hf and W. Data for ^{157}Ho are from [51], $^{158–164}$Er from [34,52–54], ^{161,163}Tm from [3,55], ^{165,167}Tm from the present work and [14], $^{160–170}$Yb from [35,56–60], $^{165–171}$Lu from [8,10,61,62], $^{162–176}$Hf from [57,63–69], $^{167–177}$Ta from [4,70–73,103], $^{166–180}$W from [74–79], $^{171–181}$Re from [40,80–84] and $^{173–185}$Ir from [85–90]

Nucleus		$N=90$	$N=92$	$N=94$	$N=96$	$N=98$	$N=100$	$N=102$	$N=104$	$N=106$
Ir	$\hbar\omega_c$				263^{+4}_{-4}	274^{+6}_{-7}	300^{+5}_{-6}	305^{+5}_{-6}	300^{+7}_{-8}	280^{+10}_{-10}
	Δi_x				$9.4^{+0.7}_{-0.7}$	$\geqslant 7.5$	$7.5^{+0.6}_{-0.6}$	$7.3^{+0.6}_{-0.5}$	$7.0^{+0.4}_{-0.3}$	$6.5^{+0.7}_{-0.5}$
Re	$\hbar\omega_c$				274^{+3}_{-4}	288^{+10}_{-10}	314^{+4}_{-5}	329^{+5}_{-5}	335^{+8}_{-9}	325^{+11}_{-13}
	Δi_x				$7.9^{+0.5}_{-0.5}$	$6.1^{+0.4}_{-0.4}$	$6.0^{+0.5}_{-0.5}$	$6.3^{+0.4}_{-0.4}$	$\geqslant 4.0$	
W	$\hbar\omega_c$		264^{+4}_{-4}	242^{+3}_{-3}	249^{+2}_{-2}	262^{+10}_{-10}	290^{+3}_{-3}	291^{+3}_{-3}	306^{+3}_{-3}	290^{+2}_{-2}
	Δi_x		$11.5^{+1.0}_{-1.0}$	$10.6^{+0.6}_{-0.6}$	$9.6^{+0.6}_{-0.6}$	$7.9^{+0.5}_{-0.5}$	$7.8^{+1.0}_{-0.5}$	$8.2^{+0.5}_{-0.5}$	$8.1^{+0.6}_{-0.6}$	
Ta	$\hbar\omega_c$			292^{+5}_{-5}	303^{+3}_{-3}	300^{+11}_{-11}	350^{+2}_{-2}	373^{+2}_{-2}	333^{+17}_{-23}	
	Δi_x			$\geqslant 6.0$	$7.4^{+0.4}_{-0.4}$	$4.4^{+0.4}_{-0.4}$	$5.6^{+0.5}_{-0.5}$	$6.6^{+0.8}_{-0.8}$		
Hf	$\hbar\omega_c$	274^{+2}_{-2}	260^{+2}_{-2}	258^{+2}_{-2}	260^{+3}_{-3}	269^{+10}_{-10}	311^{+3}_{-3}	307^{+8}_{-5}	325^{+25}_{-25}	
	Δi_x	$11.4^{+0.6}_{-0.6}$	$10.3^{+0.6}_{-0.6}$	$9.3^{+0.7}_{-0.7}$	$8.6^{+0.8}_{-0.8}$	$7.2^{+0.5}_{-0.5}$	$6.6^{+0.7}_{-0.7}$	$5.9^{+1.0}_{-1.0}$		
Lu	$\hbar\omega_c$			318^{+5}_{-5}	337^{+4}_{-4}	306^{+11}_{-11}	350^{+5}_{-5}			
	Δi_x			$\geqslant 9.0$	$6.9^{+0.5}_{-0.4}$	$2.8^{+0.5}_{-0.5}$	$4.6^{+0.7}_{-0.5}$			
Yb	$\hbar\omega_c$	270^{+2}_{-2}	268^{+2}_{-2}	272^{+2}_{-2}	269^{+2}_{-2}	280^{+10}_{-10}	306^{+6}_{-6}			
	Δi_x	$10.4^{+0.6}_{-0.6}$	$8.9^{+0.5}_{-0.5}$	$8.3^{+0.5}_{-0.5}$	$7.9^{+0.5}_{-0.5}$	$7.1^{+0.5}_{-0.5}$	$\geqslant 6.0$			
Tm	$\hbar\omega_c$		340^{+2}_{-2}	350^{+10}_{-10}	355^{+15}_{-5}	321^{+12}_{-12}				
	Δi_x		$\geqslant 7.2$	$\geqslant 6.0$	$\geqslant 5.3$	$2.4^{+0.4}_{-0.4}$				
Er	$\hbar\omega_c$	271^{+2}_{-2}	281^{+2}_{-2}	279^{+2}_{-2}	281^{+2}_{-2}					
	Δi_x	$9.3^{+0.2}_{-0.3}$	$8.1^{+0.5}_{-0.3}$	$7.5^{+0.4}_{-0.3}$	$7.0^{+0.5}_{-0.5}$					
Ho	$\hbar\omega_c$	347^{+10}_{-13}								
	Δi_x	$5.2^{+0.9}_{-0.6}$								

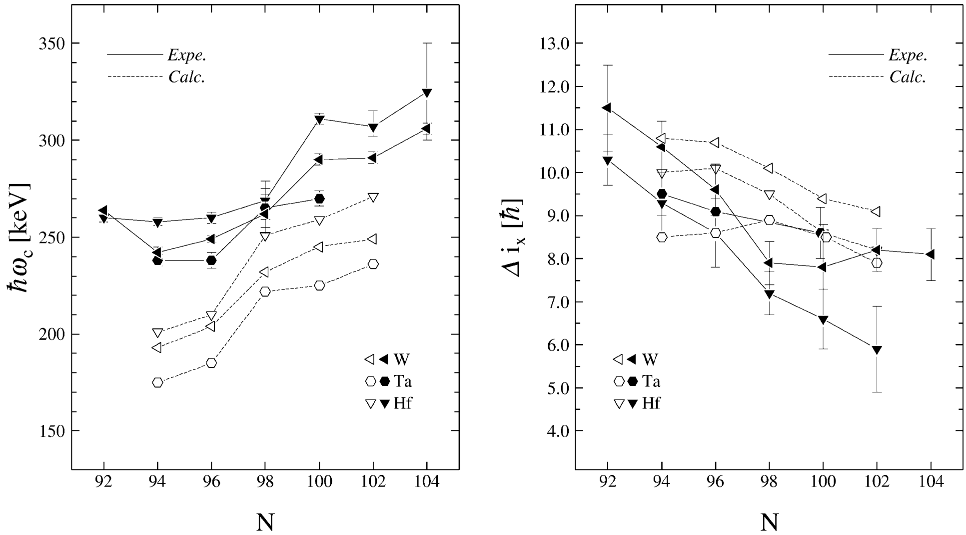

Fig. 17. Experimental (solid lines) and predicted (dashed lines) (a) frequency, $\hbar\omega_c$, and (b) gain in aligned angular momentum, Δi_x, at the crossing with the S-band for the $\pi h_{11/2}[514]9/2^-$ configuration in even-N isotopes of Ta, and for the $(0,+)$ yrast configuration in the neighbouring even–even Hf and W isotopes.

The deviation between experiment and theory for the $[514]9/2^-$ configuration is very similar to that of the even–even Hf and W isotones. The deformation parameters of the $[514]9/2^-$ configuration and the $(0,+)$ bands in the even–even nuclei are, in addition, predicted to be very similar. Thus we must conclude that the present CSM calculations systematically underestimate the crossing frequency by about 45 keV.

Attention is now turned to the $[541]1/2^-$ bands. Their crossing frequencies and alignments are listed in Table 8 and are compared with theory in Fig. 18. Although a modest shift in crossing frequency is predicted, in comparison to the $(0,+)$ bands in the even–even nuclei, and the $[514]9/2^-$ band, the calculations for the $[541]1/2^-$ bands are clearly at a larger discrepancy with the experimental values. Whereas the discrepancy in crossing frequency is around 45 keV for the even–even cases, the discrepancy for the $[541]1/2^-$ bands is as large as 100 keV, especially at low neutron numbers. For the gain in aligned angular momentum the discrepancy is typically 1–3 $\hbar$, with large fluctuations. Note that $N = 98$ stands out as being rather unique, with low crossing frequencies and alignment gains (see Fig. 18), as discussed in detail recently [14]. As in the even–even cases, part of the discrepancy might be due to pairing, but as pointed out in [3], an increase in deformation is accompanied by a *decrease* in pairing correlations, which would normally reduce the crossing frequency. If there are no systematic uncertainties in the measured Q_t's for the $[541]1/2^-$ bands due to stopping powers, the present calculations underestimate the deformation of the $[541]1/2^-$ band (see Section 3.2) by about 0.02 in ε_2, but such an increase in deformation would be insufficient to increase the crossing frequency by more than 20 keV [3]. The additional discrepancy between data and theory for the $[541]1/2^-$ remains unexplained in the present model.

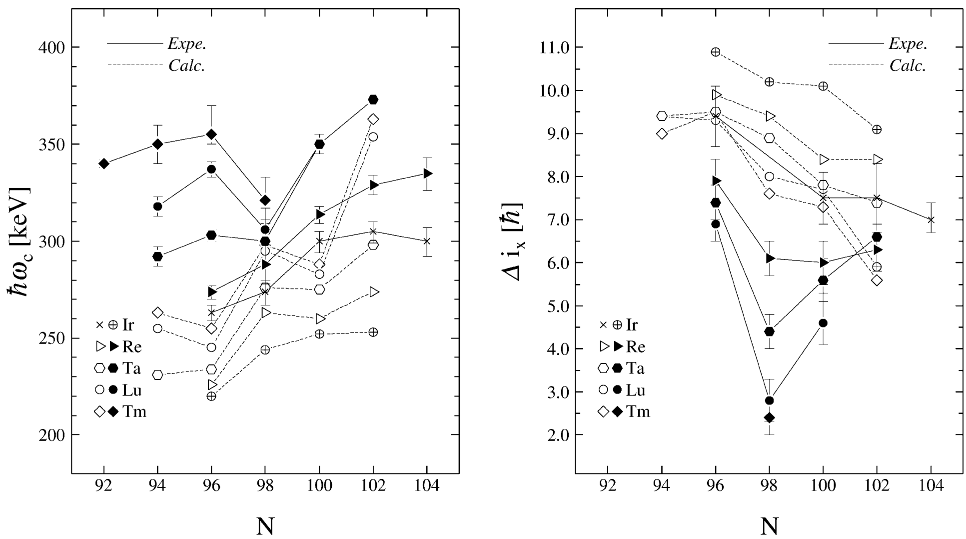

Fig. 18. Experimental (solid lines) and predicted (dashed lines) (a) frequency, $\hbar\omega_c$, and (b) gain in aligned angular momentum, Δi_x, at the crossing with the S-band for the $[541]1/2^-$ configuration in even-N isotopes of Tm, Lu, Ta, Re and Ir.

Another approach to the problem of the delayed crossing in the $[541]1/2^-$ bands has been the Projected Shell Model (PSM) [2,91–94]. Although this model has been claimed to be able to reproduce the systematic trends in the crossing frequency, the manner in which the results of these calculations have been presented [2,94] in the form of alignment curves rather than calculated crossing frequencies, makes it difficult to evaluate whether the PSM is any more accurate than the CSM.

Recently, empirical evidence has come in support of a suggestion that a residual proton–neutron interaction may contribute to the shift [7]. In odd–odd nuclei, a signature inversion has been reported in the $\pi h_{9/2} \otimes \nu i_{13/2}$ bands in a variety of odd-proton nuclei of the rare-earth region, see, e.g., [17,95–98]. Particle-rotor model calculations are only able to explain these inversions if a residual proton–neutron interaction is included [9,17,95,97]. These inversions were also analysed by transforming the data into the rotating frame and extracting an empirical proton–neutron interaction, V_{pn}, between the $\pi h_{9/2}$ proton, (e) and $i_{13/2}$ neutron, (A, B) by making use of the additivity of Routhians in the CSM. It can then be shown that the expected shift in crossing frequency due to V_{pn} is given by [9,99]

$$\delta\hbar\omega_c(eAB) = \frac{V_{eA} + V_{eB}}{i_{AB}}. \qquad (6)$$

Estimates [9,17] of V_{pn} in the neighbourhood of ^{164}Tm and ^{174}Ta give $V_{pn} \simeq 100$–200 keV, implying shifts of 15–40 keV. Therefore, up to 50% of the shift in crossing frequency may originate in a proton–neutron interaction, and the rest may be accounted for by deformation changes, as implied by the present systematic CSM investigations.

7. E1-transition probabilities

Interband $\Delta I = 1$ transitions have been observed between the bands built on the $[411]1/2^+$ and $[541]1/2^-$ configurations, in both directions, in the spin range between $I = 7/2$ and $31/2$, see Fig. 3. DCO ratios listed in Table 1 support the assignment of E1 character for these transitions. Decay between these two configurations have been observed and analysed in other odd-Z rare-earth nuclei [10,62,100–103] and the observed reduced E1 transition rates are considerably enhanced, by orders of magnitude, compared to the calculated single-particle E1 strength. Coupling to octupole vibrational degrees of freedom for the core may play an important role for the understanding of the observed enhancement.

The reduced B(E1) values for the observed E1 transitions between the bands built on the $[411]1/2^+$ and $[541]1/2^-$ configurations can be extracted from the experimental branching ratios, if the transition quadrupole moments Q_t for the bands are known.

$$B(\mathrm{E1}) = 7.63 \times 10^{-4} Q_t^2 \frac{1}{\lambda} \langle IK20 \mid I-2K\rangle^2 \frac{[E_\gamma(I \to I-2)]^5}{[E_\gamma(I \to I-1)]^3} \left[e^2\,\mathrm{fm}^2\right], \tag{7}$$

where E_γ is in MeV and Q_t in units of b. The branching ratio is defined as

$$\lambda = \frac{T_\gamma(\mathrm{E2}, I \to I-2)}{T_\gamma(\mathrm{E1}, I \to I-1)}.$$

The values of Q_t for the E2 transitions in the two bands used in the extraction are the measured values given in Table 6, originating from the DSAM analysis. The correction for the possible mixing of the wave-function with $\Omega \geqslant 3/2$ states, as in Section 5.2, was found to be negligible compared to the relative large uncertainties for the extracted B(E1) values.

The B(E1) values extracted from the data are presented in Fig. 19 as a function of $I_f(I_f+1) - I_i(I_i+1)$. There are in principle three different kinds of transitions

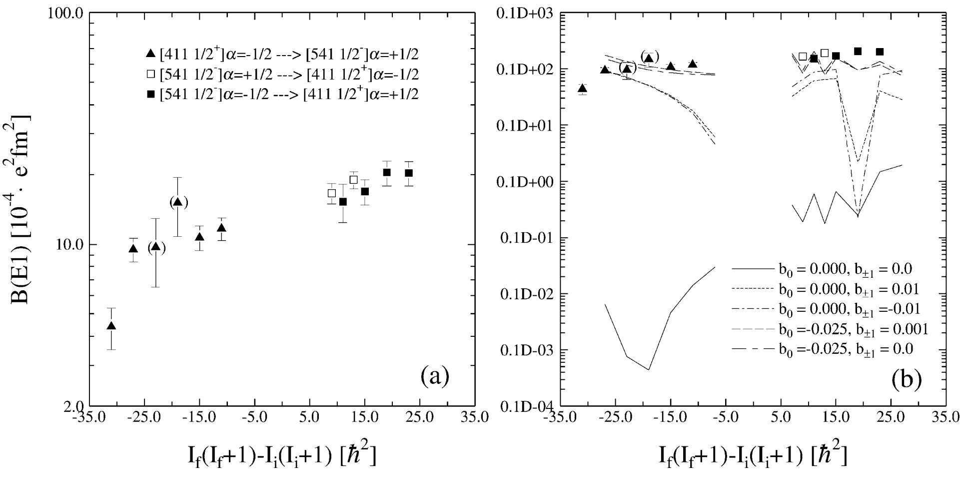

Fig. 19. (a) Experimental B(E1) values for transitions between band $[411]1/2^+$ and $[541]1/2^-$ plotted as a function of $I_f(I_f+1) - I_i(I_i+1)$. (b) Examples of calculations with different values of the parameters b_0 and $b_{\pm 1}$, which are given in units of fm^{-2}.

differing according to direction and signature. They are all shown in the figure converted to $B(\mathrm{E1}, I_i[411]1/2^+ \to I_f[541]1/2^-)$ by applying the statistical factor $(2I_f+1)/(2I_i+1)$ when necessary.

The analysis includes states in the $[411]1/2^+$ band which have admixed amplitudes of the $[404]7/2^+$ configuration in the wave-functions. It is assumed that the E1 decay does not involve these admixtures, since such transitions would be K-forbidden with $\Delta K = 3$. The branching ratios are in such cases corrected for the admixed amplitudes, which are determined from the mixing analysis (see Section 5.1 and Table 5). The influence of the mixing analysis on the extracted E1 strength has been investigated, and the error-bars include this extra uncertainty.

The data presented in Fig. 19 cover a broad spin range of transitions including both negative and positive values of $I_f(I_f+1) - I_i(I_i+1)$, which is rather unique. In the right-hand side, Fig. 19(b), the data are compared to particle-rotor calculations by I. Hamamoto [104]. The expected single-particle $B(\mathrm{E1})$ strength is based on an effective charge $e_{\mathrm{eff}} = 0.2\,e$ is shown in solid. Large deviations, 3 and 5 orders of magnitude, respectively, for positive and negative values of $I_f(I_f+1) - I_i(I_i+1)$ are seen. An attempt to explain this enhancement of the E1 strength by introducing a coupling to octupole–vibrational degrees of freedom of the core [104] is also shown in Fig. 19(b).

Assuming that the particle octupole–vibrational coupling can be treated as a perturbation, the E1 transition operator of the odd particle in the intrinsic system is [102]:

$$\mathcal{O}(\mathrm{E1},\nu) = e_{\mathrm{eff}}(\mathrm{E1}) r Y_{1\nu} + e b_\nu r^3 Y_{3\nu}, \tag{8}$$

where the parameters b_ν are expressed in terms of the sum over octupole vibrations (i) with frequencies $(\hbar\omega_i)$ of the core:

$$e\,b_\nu = x_3 \sum_i \left(\frac{-2}{\hbar\omega_i}\right) \langle i|r^3 Y^*_{3\nu}|0\rangle \langle 0|(\mathrm{E1})_\nu|i\rangle, \tag{9}$$

where x_3 expresses the strength of the octupole–octupole interaction. The dependence of b_ν on rotational frequency was ignored in the present calculation. More details of the calculations are found in [102]. A fit of the coupling parameters, b_0 and $b_{\pm 1}$ was not attempted as in [102], examples of calculated E1-strength for different combinations of b_0 and $b_{\pm 1}$ are shown in Fig. 19(b). The large irregularities in some of the curves are probably due to several components, which in some cases happen to partly cancel, close to a change of sign in the E1 operator of Eq. (8). It appears that a large overall improvement is obtained when the coupling to octupole vibrations is included, and the data and predictions are in qualitative agreement for $b_0 = -0.025\ \mathrm{fm}^2$ and $b_{\pm 1} = 0$, although the signature dependence is somewhat overestimated for $I_f(I_f+1) - I_i(I_i+1) > 0$, and the spin dependence at variance for $I_f(I_f+1) - I_i(I_i+1) < 0$.

8. Summary and conclusion

The level scheme of ^{165}Tm has been extended by the observation of several bands and high-spin states. Lifetimes obtained for the $[541]1/2^-$, $[523]7/2^-$, $[411]1/2^+$ and

[404]7/2$^+$ bands imply deformations which are in reasonable agreement with diabatic calculations performed with the code "Ultimate Cranker". The deformation driving properties of the $\pi h_{9/2}$ orbital are confirmed. However, in the model, the core-polarization effect is only able to reproduce part of the full shift in crossing frequency observed in the [541]1/2$^-$ band. Systematic calculations of crossing frequencies throughout the rare-earth region confirm the inadequacy of the model, requiring other effects, such as residual proton–neutron interactions, to make up the remainder of the shift. A comprehensive understanding of the role of p–n interactions in connection with intruder bands based on $\pi i_{13/2}$ and $\pi h_{9/2}$ orbitals in the rare-earth region is now required.

The E1 transitions observed here present a unique set of data, which allows both signature directions to be analysed in terms of coupling to octupole degrees of freedom.

Acknowledgements

This work was supported by the Danish Natural Science Research Council, the Swedish Natural Research Council, the Academy of Finland, the Nordic Committee for Accelerator Based Research, NorFa (Nordisk Forskerutdanningsakademi), the NORDBALL collaboration and the US Dept. of Energy under the grant DE-FG05-92ER40694.

R.A.B. gratefully acknowledges the support received from the Danish Natural Science Research Council, while visiting NBI.

References

[1] H.J. Jensen, R.A. Bark, Acta Phys. Pol. B 26 (1995) 271.
[2] D.E. Archer, M.A. Riley, T.B. Brown, J. Döring, D.J. Hartley, G.D. Johns, T.D. Johnson, R.A. Kaye, J. Pfohl, S.L. Tabor, J. Simpson, Yang Sun, Phys. Rev. C 52 (1995) 1326.
[3] H.J. Jensen, G.B. Hagemann, P.O. Tjøm, S. Frauendorf, A. Atac, M. Bergström, A. Bracco, A. Brockstedt, H. Carlsson, P. Ekström, J.M. Espino, B. Herskind, F. Ingebretsen, J. Jongman, S. Leoni, R.M. Lieder, T. Lönnroth, A. Maj, B. Million, A. Nordlund, J. Nyberg, M. Piiparinen, H. Ryde, M. Sugawara, A. Virtanen, Z. Phys. A 340 (1991) 351.
[4] Shu-Xian Wen, Hua Zheng, Sheng-Gang Li, Guang-Sheng Li, Guan-Jun Yuan, Peng-Fei Hua, Pei-Kun Weng, Lan-Kuan Zhang, Pan-Shui Yu, Chun-Xiang Yang, Hui-Bin Sun, Ya-Bo Lui, Yun-Zuo Lu, Yang Sun, Da Hsuan Feng, Phys. Rev. C 54 (1996) 1015.
[5] S. Frauendorf, Phys. Scr. 24 (1981) 349.
[6] R. Bengtsson, S. Frauendorf, Nucl. Phys. A 314 (1979) 27, Nucl. Phys. A 327 (1979) 139.
[7] W. Satula, R. Wyss, F. Dönau, Nucl. Phys. A 565 (1993) 573.
[8] C.-H. Yu, G.B. Hagemann, J.M. Espino, K. Furuno, J.D. Garrett, R. Chapman, D. Clarke, F. Khazaie, J.C. Lisle, J.N. Mo, M. Bergström, L. Carlen, L.P. Ekström, J. Lyttkens, H. Ryde, Nucl. Phys. A 511 (1990) 157.
[9] R.A. Bark, H. Carlsson, S.J. Freeman, G.B. Hagemann, F. Ingebretsen, H.J. Jensen, T. Lonnroth, M.J. Piiparinen, I. Ragnarsson, H. Ryde, H. Schnack-Petersen, P.B. Semmes, P.O. Tjøm, Nucl. Phys. A 630 (1998) 603.
[10] S. Ogaza, J. Kownacki, M.P. Carpenter, J. Gascon, G.B. Hagemann, I. Hamamoto, Y. Iwata, H.J. Jensen, T. Komatsubara, J. Nyberg, G. Sletten, P.O. Tjøm, W. Waluś, Nucl. Phys. A 559 (1993) 100.

[11] J. Gascon, C.-H. Yu, G.B. Hagemann, M.C. Carpenter, J.M. Espino, Y. Iwata, T. Komatsubara, J. Nyberg, S. Ogaza, G. Sletten, P.O. Tjøm, D.C. Radford, J. Simpson, A. Alderson, M.A. Bentley, P. Fallon, P.D. Forsyth, J.W. Roberts, J.F. Sharpey-Schafer, Nucl. Phys. A 513 (1990) 344.
[12] S.J. Warburton, R. Chapman, J. Copnell, F. Lidén, A.G. Smith, J.P. Sweeney, D.M. Thompson, S.J. Freeman, G.B. Hagemann, M. Piiparinen, Nucl. Phys. A 591 (1995) 323.
[13] R. Chapman, J.P. Sweeney, F. Liden, J.C. Lisle, S. Schwebel, A.G. Smith, D.M. Thompson, S.J. Warburton, R.A. Bark, G.B. Hagemann, in: Contr. Symp. on New Spectroscopy and Nuclear Structure 1997, Copenhagen, September 16–20, 1997.
[14] H.J. Jensen, R.A. Bark, R. Bengtsson, G.B. Hagemann, P.O. Tjøm, S.Y. Araddad, C.W. Beausang, R. Chapman, J. Copnell, A. Fitzpatrick, S.J. Freeman, S. Leoni, J.C. Lisle, J. Simpson, A.G. Smith, D.M. Thompson, S.J. Warburton, J. Wrzesinski, Z. Phys. A 359 (1997) 127.
[15] B. Herskind, Nucl. Phys. A 447 (1986) 395c.
[16] G. Sletten, J. Gascon, J. Nyberg, Proc. Int. Conf. on the Spectroscopy of Heavy Nuclei, Create, June 1989, Institute of Physics Conference Series, Vol. 105, IOP Publishing, Bristol, p. 125.
[17] W. Reviol, L.L. Riedinger, X.Z. Wang, J.-Y. Zhang, R.A. Bark, G.B. Hagemann, H.J. Jensen, S. Leoni, T. Lönnroth, H. Schnack-Petersen, P.B. Semmes, T. Shizuma, P.O. Tjøm, J. Wrzesinski, Phys. Rev. C 59 (1999) 1358.
[18] C.M. Lederer, V.S. Shirley, Table of Isotopes, Seventh edition, Wiley-Interscience, 1978.
[19] J. Wrzesinski, Report from EUROBALL Data Analysis Group, The Niels Bohr Institute, August 1995, and private communication.
[20] D.C. Radford, Nucl. Instrum. Methods A 361 (1995) 297.
[21] G. Palameta, J.C. Waddington, Nucl. Instrum. Methods A 234 (1985) 476.
[22] T. Yamazaki, Nucl. Data A 3 (1967) 1.
[23] R.M. Steffen, K. Alder, Angular distributions and correlations of gamma rays — I. Theory, in: W.D. Hamilton (Ed.), The Electromagnetic Interactions in Nuclear Physics, North-Holland, Amsterdam, 1972, Chapter XII.
[24] K.S. Krane, R.M. Steffen, R.M. Wheeler, Nucl. Data Tables 11 (1973) 351.
[25] J. Gizon, A. Gizon, S.A. Hjorth, D. Barneoud, S. André, J. Treherne, Nucl. Phys. A 193 (1972) 193.
[26] T. Tamura, I. Rezanka, S. Iwata, J.O. Rasmussen, J. Alonso, Phys. Rev. C 8 (1973) 2425.
[27] C. Foin, S. André, D. Barneoud, Phys. Rev. Lett. 35 (1975) 1697.
[28] W.M. Currie, Nucl. Instrum. Methods 73 (1969) 173.
[29] L.C. Northcliffe, R.F. Schilling, At. Data Nucl. Data Tables 7 (1970) 256.
[30] S.H. Sie, D. Ward, J.S. Geiger, R.L. Graham, H.R. Andrews, Nucl. Phys. A 291 (1977) 443.
[31] J.F. Ziegler, W.K. Chu, At. Data Nucl. Data Tables 13 (1974) 463.
[32] J. Lindhart, M. Scharff, H.E. Schiott, Mat. Fys. Medd. Dan. Vid. Selsk. 33 (14) (1963).
[33] J.C. Bacelar, R.M. Diamond, E.M. Beck, M.A. Deleplanque, J. Draper, F.S. Stephens, Phys. Rev. C 35 (1987) 1170.
[34] C.A. Fields, F.W.N. De Boer, K.H. Hicks, L.K. Peker, R.J. Peterson, R.A. Ristinen, P.M. Walker, Nucl. Phys. A 422 (1984) 215.
[35] W. Walús, N. Roy, S. Johnson, L. Carlén, H. Ryde, G.B. Hagemann, B. Herskind, J.D. Garrett, Y.S. Chen, J. Almberger, G. Leander, Phys. Scr. 24 (1981) 324.
[36] F. Dönau, S. Frauendorf, in: N.R. Johnson (Ed.), Proc. Conf. on High Angular Momentum Properties of Nuclei, Oak Ridge, TN, 1982, Harwood Academic, New York, 1983.
[37] F. Dönau, Nucl. Phys. A 471 (1987) 469.
[38] R. Bengtsson, J. Dudek, W. Nazarewicz, P. Olanders, Phys. Scr. 39 (1989) 196.
[39] S. Olbrich, V. Ionescu, J. Kern, C. Nordmann, W. Reichart, Nucl. Phys. A 342 (1980) 133.
[40] R.A. Bark, G.B. Hagemann, B. Herskind, H.J. Jensen, W. Korten, J. Wrzesinski, H. Carlsson, M. Bergström, A. Brockstedt, A. Nordlund, H. Ryde, P. Bosetti, S. Leoni, F. Ingebretsen, P.O. Tjøm, Nucl. Phys. A 591 (1995) 265.

[41] M.A.J. Mariscotti, G. Scharff-Goldhaber, B. Buck, Phys. Rev. 178 (1968) 1864.
[42] R. Bengtsson, S. Frauendorf, F.-R. May, At. Data Nucl. Data Tables 35 (1986) 15.
[43] W. Nazarewicz, M.A. Riley, J.D. Garrett, Nucl. Phys. A 512 (1990) 61.
[44] T. Bengtsson, Nucl. Phys. A 496 (1989) 56.
[45] R. Bengtsson, T. Bengtsson, M. Bergström, H. Ryde, G.B. Hagemann, Nucl. Phys. A 569 (1994) 469.
[46] T. Bengtsson, I. Ragnarsson, Nucl. Phys. A 436 (1984) 14.
[47] R.A. Bark, R. Bengtsson, H. Carlsson, Phys. Rev. Lett. B 339 (1994) 11.
[48] H.-B. Håkansson, R. Bengtsson, R.A. Bark, in preparation.
[49] D. Müller, A. Virtanen, R. Julin, S. Juutinen, A. Lampinen, M. Piiparinen, S. Törmänen, F. Christancho, A.P. Byrne, G.D. Dracoulis, B. Fabricius, C. Fahlander, A. Johnson, K.P. Lieb, J. Nyberg, I. Thorslund, R. Wyss, Phys. Lett. B 332 (1994) 265.
[50] G.D. Dracoulis, G.D. Sprouse, O.C. Kistner, M.H. Rafailovich, Phys. Rev. C 29 (1984) 1576.
[51] D.C. Radford, H.R. Andrews, G.C. Ball, D. Horn, D. Ward, F. Banville, S. Flibotte, S. Monaro, S. Pilotte, P. Taras, J.K. Johansson, D. Tucker, J.C. Waddington, M. Riley, G.B. Hagemann, I. Hamamoto, Nucl. Phys. A 545 (1992) 665.
[52] J. Simpson et al., J. Phys. G 10 (1984) 383.
[53] J. Simpson et al., J. Phys. G 13 (1987) 847.
[54] R.G. Helmer, Nucl. Data Sheets 64 (1991) 79.
[55] A.G. Smith, R. Chapman, D.C. Clarke, J. Copnell, S.J. Freeman, F. Khazaie, G.S. Li, J.C. Lisle, J.N. Mo, C. Tenreiro, D.M. Thompson, G.J. Yuan, J. Espino, G.B. Hagemann, Nucl. Phys. A 587 (1995) 150.
[56] L.L. Riedinger et al., Phys. Scr. T 5 (1983) 36.
[57] J.N. Mo et al., Nucl. Phys. A 472 (1987) 295.
[58] S. Jónsson, N. Roy, H. Ryde, W. Waluś, J. Kownacki, J.D. Garrett, G.B. Hagemann, B. Herskind, R. Bengtsson, S. Åberg, Nucl. Phys. A 449 (1986) 537.
[59] J.C. Bacelar, M. Diebel, C. Ellegaard, J.D. Garrett, G.B. Hagemann, B. Herskind, A. Holm, C.-X. Yang, J.-Y. Zhang, P.O. Tjøm, J.C. Lisle, Nucl. Phys. A 442 (1985) 509.
[60] P.M. Walker et al., Nucl. Phys. A 365 (1981) 61.
[61] P. Frandsen, R. Chapman, J.D. Garrett, J.J. Gaardhøje, G.B. Hagemann, B. Herskind, Nucl. Phys. A 489 (1988) 508.
[62] R.A. Bark, H. Carlsson, S.J. Freeman, G.B. Hagemann, F. Ingebretsen, H.J. Jensen, T. Lonnroth, S. Mitarai, M.J. Piiparinen, H. Ryde, H. Schnack-Petersen, P.O. Tjøm, Nucl. Phys. A 644 (1998) 29.
[63] H. Hübel et al., Z. Phys. A 329 (1988) 289.
[64] H. Hübel, K.P. Blume, K.H. Maier, A. Maj, H. Kluge, A. Kuhnert, J. Recht, M. Guttormsen, in: I. Iori (Ed.), XXIII Int. Winter Meeting on Nucl. Phys., Bormio, 1985, Ricerca Scientifica ed Educazione Permanente, Milano, 1985.
[65] R. Chapman, J.C. Lisle, J.N. Mo, E. Paul, A. Simcock, J.C. Willmott, J.R. Leslie, H.G. Price, P.M. Walker, J.C. Bacelar, J.D. Garrett, G.B. Hagemann, B. Herskind, A. Holm, P.J. Nolan, Phys. Rev. Lett. 51 (1983) 2265.
[66] J.C. Lisle, J.D. Garrett, G.B. Hagemann, B. Herskind, S. Ogaza, Nucl. Phys. A 366 (1981) 281.
[67] B. Singh, Nucl. Data Sheets 75 (1995) 199.
[68] P.M. Walker et al., Phys. Scr. T 5 (1983) 29.
[69] E. Browne, Nucl. Data Sheets 60 (1990) 227.
[70] R. Chapman et al., Manchester University Annual Report 1990, pp. 166–167;
K. Theine et al., Nucl. Phys. A 536 (1992) 418.
[71] S.G. Li, C.-X. Yang, R. Chapman, F. Khazaie, J.C. Lisle, J.N. Mo, J.D. Garrett, G.B. Hagemann, B. Herskind, H. Ryde, Nucl. Phys. A 555 (1993) 435.
[72] J.C. Bacelar, R. Chapman, J.R. Leslie, J.C. Lisle, J.N. Mo, E. Paul, A. Simcock, J.C. Willmott, J.D. Garrett, G.B. Hagemann, B. Herskind, A. Holm, P.M. Walker, Nucl. Phys. A 442 (1985) 547.

[73] M.A. Riley et al., Z. Phys. A 346 (1993) 319.
[74] J. Gerl et al., Nucl. Phys. A 443 (1985) 348.
[75] G.D. Dracoulis et al., Nucl. Phys. A 405 (1983) 363.
[76] J. Recht et al., Nucl. Phys. A 440 (1985) 366.
[77] G.D. Dracoulis et al., J. Phys. G 4 (1978) 713.
[78] E. Browne, Nucl. Data Sheets 54 (1988) 199.
[79] E. Browne, Nucl. Data Sheets 52 (1987) 127.
[80] R.A. Bark, G.D. Dracoulis, A.E. Stuchbery, A.P. Byrne, A.M. Baxter, F. Riess, P.K. Weng, Nucl. Phys. A 501 (1989) 157.
[81] L. Hildingsson, W. Klamra, Th. Lindblad, C.G. Linden, C.A. Kalfas, S. Kossionides, C.T. Papadopoulos, R. Vlastou, J. Gizon, D. Clarke, F. Khazaie, J.N. Mo, Nucl. Phys. A 513 (1990) 394.
[82] T. Kibédi, G.D. Dracoulis, B. Fabricius, A.P. Byrne, A.E. Stuchberry, Nucl. Phys. A 539 (1992) 137.
[83] Ts. Venkova, T. Morek, R.M. Lieder, W. Gast, G. Hebbinghaus, A. Krämer-Flecken, W. Urban, G. Sletten, K.H. Maier, Z. Phys. A 334 (1989) 385.
[84] R.B. Firestone, Nucl. Data Sheets 43 (1984) 289.
[85] S. Juutinen et al., Nucl. Phys. A 526 (1991) 346.
[86] B. Cederwall, B. Fant, R. Wyss, A. Johnson, J. Nyberg, J. Simpson, A.M. Bruce, J.N. Mo, Phys. Rev. C 43 (1991) 2031.
[87] G.D. Dracoulis, B. Fabricius, T. Kibédi, A.M. Baxter, A.P. Byrne, K.P. Lieb, A.E. Stuchbery, Nucl. Phys. A 534 (1991) 173.
[88] H.Q. Jin, C.R. Bingham, M.P. Carpenter, V.P. Janzen, L.L. Riedinger, L. Zhou, C. Baktash, M.L. Halbert, N.R. Johnson, I.Y. Lee, F.K. McGowan, M.A. Riley, Progress Report on Nuclear Spectroscopic Studies, University of Tennessee, 1989, p. 7;
H.Q. Jin et al., Phys. Rev. C, submitted.
[89] G.D. Dracoulis, B. Fabricius, T. Kibédi, A.P. Byrne, A.E. Stuchbery, Nucl. Phys. A 554 (1993) 439.
[90] S. Andrè, J. Genevey-Rivier, J. Treherne, R. Kaczarowski, J. Lukasiak, J. Jastrzebski, C. Schück, Nucl. Phys. A 325 (1979) 445.
[91] K. Hara, S. Iwasaki, Nucl. Phys. A 332 (1979) 61, Nucl. Phys. A 348 (1980) 200, Nucl. Phys. A 430 (1984) 174.
[92] S. Iwasaki, K. Hara, Prog. Theor. Phys. 68 (1982) 1782.
[93] Y. Sun, D.H. Feng, Preprint submitted to Elsevier Science and private communication.
[94] Y. Sun, S. Wen, D.H. Feng, Phys. Rev. Lett. 72 (1994) 3483.
[95] R.A. Bark, J.M. Espino, W. Reviol, P.B. Semmes, H. Carlsson, I.G. Bearden, G.B. Hagemann, H.J. Jensen, I. Ragnarsson, L.L. Riedinger, H. Ryde, P.O. Tjøm, Phys. Lett. B 406 (1997) 193; Erratum: Phys. Lett. B 416 (1998) 453.
[96] J.M. Espino, G.B. Hagemann, I.G. Bearden, R.A. Bark, M. Bergström, A. Bracco, B. Herskind, H.J. Jensen, S. Leoni, C. Martinez-Torre, B. Million, P.O. Tjøm, Nucl. Phys. A 640 (1998) 163.
[97] M.A. Cardona, A.J. Kreiner, D. Hojman, G. Levinton, M.E. Debray, M. Davidson, J. Davidson, R. Pirchio, H. Somacal, D.R. Napoli, D. Bazzacco, N. Blasi, R. Burch, D. De Acuna, S.M. Lenzi, G. Lo Bianco, J. Rico, C. Rossi Alvarez, Phys. Rev. C 59 (1999) 1298.
[98] G. Levinton, A.J. Kreiner, M.A. Cardona, M.E. Debray, D. Hojman, J. Davidson, G. Marti, A. Burlon, M. Davidson, D.R. Napoli, M. De Poli, D. Bazzacco, N. Blasi, S.M. Lenzi, G. Lo Bianco, C. Rossi Alvarez, V.R. Vanin, Phys. Rev. C 60 (1999) 044309.
[99] C.X. Yang, S.G. Li, X.A. Liu, Chinese J. Nucl. Phys. 16 (1994) 217.
[100] A. Bohr, B.R. Mottelson, Nuclear Structure, Vol. II, Benjamin, New York, 1975.
[101] I. Hamamoto, J. Höller, X.Z. Zhang, Phys. Lett. B 226 (1989) 17.
[102] G.B. Hagemann, I. Hamamoto, W. Satula, Phys. Rev. C 47 (1993) 2008.

[103] H. Carlsson, R.A. Bark, L.P. Ekström, S.J. Freeman, G.B. Hagemann, F. Ingebretsen, H.J. Jensen, T. Lönnroth, S. Miterai, A. Nordlund, M.J. Piiparinen, H. Ryde, H. Schnack-Petersen, P.O. Tjøm, Nucl. Phys. A 592 (1995) 89.
[104] I. Hamamoto, private communication, 1995.